NTNU – Trondheim
Norwegian University of
Science and Technology

Installation of large subsea structures

Lowering of suction anchors through the
splash zone

Torleif Ølund Bertelsen

Marine Technology
Submission date: June 2014
Supervisor: Marilena Greco, IMT

Norwegian University of Science and Technology
Department of Marine Technology

NTNU Trondheim
Norwegian University of Science and Technology
Faculty of Engineering Science and Technology
Department of MarineTechnology

MASTER THESIS IN MARINE TECHNOLOGY

SPRING 2014

FOR

Torleif Bertelsen

Installation of large subsea structures: Lowering of suction anchors through the splash zone

(Installasjon av store undervannsstrukturer: Låring av sugeankere gjennom skvalpesonen)

For installation of large subsea structures in harsh sea conditions, it is important to examine the different designs, the installation analyses and installation procedures in order to ensure safe operations for personnel and equipment. The challenges connected with installation when using large construction vessels, operating in the proximity of the crane capacity, need to be identified and quantified. This can guide toward a robust system design to a secure installation at the required operation time frame (and related sea state). A possible widening of the installation limits in terms of sea conditions is important also for a decrease of the waiting time due to limited weather windows to obtain cost effective operations. Different issues are associated to the different phases of the installation: (a) overboarding, (b) transition through the splash zone, (c) landing on seabed. The project examined them to provide an overview and state of the art of the problem and focused on (b) which in most cases is responsible for the largest forces in the crane wire. This is due to the wave-structure hydrodynamic interaction and also to air ventilation through hatch openings in the suction piles during lowering. A simplified 1D model for the hydrodynamic loads acting on one suction anchor of a subsea structure was developed and compared in terms of vertical force against experimental results at sea in nearly calm-water conditions. The model, say, Model A includes the effect of air presence in the anchor

and the impact of the water with the top of the anchor, the latter estimated within a strip theory approach.

Objective

The aim of the thesis is to investigate the transition through the splash zone for a subsea structure with suction anchors as foundation in regular and irregular waves so to carry on a statistical investigation of the critical loads conditions and provide contributions for design improvements.

The work should be carried out in steps as follows:

1. Summarize major findings/outcomes from the project thesis and compare the model developed during the project work with available experiments on a single cylindrical suction anchor in terms of pressure in the anchor. Use the developed method to perform a parameter investigation in terms of relevant variables associated with the problem.
2. Examine oscillation frequencies of the measured pressure from item 1 and assess importance of cavity oscillations inside the anchor and possible added-mass effects. Model A does not account for cavity oscillations: identify a simplified approach to estimate the added-mass associated with the cavity oscillations and validate the results against the experimental pressure. Study possible methods for performing a small-scale model tests able to scale the pressure correctly.
3. Examine state-of-the-art methods for calculating slamming loads in geometrical conditions relevant for impacts of water at the suction anchor top.
4. Examine a complete sub-sea structure with four suction anchors and use (possibly extended) Model A to estimate the loads in the four anchors in regular and irregular waves, using the superposition principle. Examine possible critical conditions for the whole structure. Compare the crane loads from this approach with those available from full-scale experiments during operations, once avoided from the measured loads effects from other sources.

5. Using existing safety criteria for this type of operations, try to identify possible design limitations, for example in terms of perforation area and diameter of the suction anchor.

The work may show to be more extensive than anticipated. Some topics may therefore be left out after discussion with the supervisor without any negative influence on the grading.

The candidate should in his report give a personal contribution to the solution of the problem formulated in this text. All assumptions and conclusions must be supported by mathematical models and/or references to physical effects in a logical manner.

The candidate should apply all available sources to find relevant literature and information on the actual problem.

The thesis should be organised in a rational manner to give a clear presentation of the work in terms of exposition of results, assessments, and conclusions. It is important that the text is well written and that tables and figures are used to support the verbal presentation. The thesis should be complete, but still as short as possible. In particular, the text should be brief and to the point, with a clear language. Telegraphic language should be avoided.

The thesis must contain the following elements: the text defining the scope (i.e. this text), preface (outlining project-work steps and acknowledgements), abstract (providing the summary), table of contents, main body of thesis, conclusions with recommendations for further work, list of symbols and acronyms, references and (optional) appendices. All figures, tables and equations shall be numerated.

The supervisor may require that the candidate, in an early stage of the work, present a written plan for the completion of the work. The plan should include budget for the use of computer and laboratory

resources that will be charged to the department. Overruns shall be reported to the supervisor.

From the thesis it should be possible to identify the work carried out by the candidate and what has been found in the available literature. It is important to give references to the original source for theories and experimental results.

The thesis shall be submitted in two copies:
- The copies must be signed by the candidate.
- This text, defining the scope, must be included.
- The report must appear in a bound volume or a binder.
- Drawings and/or computer prints that cannot be included in the main volume should be organised in a separate folder.
- The bound volume shall be accompanied by a CD or DVD containing the written thesis in World or PDF format. In case computer programs have been made as part of the thesis work, the source codes shall be included. In case of experimental work, the experimental results shall be included in a suitable electronic format.

Supervisor :Marilena Greco
Submitted :16 January 2013
Deadline :10 June 2013

Marilena Greco
Supervisor

Preface

This thesis represents the end of my Master's of Science Degree in Marine Technology with specialization in marine hydrodynamics at the Norwegian University of Science and Technology (NTNU). This thesis is a mandatory part of the Master of Science program and it has been performed with Professor Marilena Greco as supervisor.

I would like to make a special thanks to my supervisor Professor Marilena Greco for great inspiration, feedback and support through this process. I would also like to thank Halvard Larsen and Haavard Haaskjold at Det norske oljeselskap ASA who came up with the idea of the project, and has provided valuable experience and understanding of marine operations. Leiv Aspelund, Petter Moen, Tore Jacobsen and Øystein Døskeland in Subsea 7 for providing experimental data and assistance when needed. Tor Inge Tjelta in Statoil which has been the responsible person for the experimental data provided by Subsea 7. Per Magne Sparrevik, NGI, which has provided pressure measurements for my work. Peter Sandvik, MARINTEK for helpful discussions. Odd Magnus Faltinsen and Sverre Steen, NTNU for helpful discussions. Tormod Bøe and Arne Bøckmann, Det Norske Veritas who has made proposals for topics to be studied and provided assistance then needed. Peng Li, Ph.d candidate at NTNU for valuable help with the software WAMIT and helpful discussions. I also acknowledge the help of fellow student Hongtao Li who arranged access to the Vilje HPC and for helpful discussions during my thesis.

The process of writing the master thesis has been time consuming and challenging, but also very educational and interesting. It has overall been a valuable experience that I will take with me when I now enter the working life. I would like to thank my fellow students for good memories and valuable discussions during my five years at NTNU. Last, but not least, I would to thank my family for their support and my dear Cathrine B. Løvvig for her endless support these five years at NTNU in addition to patience and understanding during long nights in front of the computer.

Torleif Ølund Bertelsen.
Trondheim, June 24,2014.

Abstract

In this thesis the dynamic air cushion pressure inside suction anchors during lowering through the splash zone has been studied. A non-linear continuity equation for the air mass is used to establish a theoretical model for the dynamic air cushion pressure. Buoyancy forces due to dynamic air cushion pressure inside the suction anchors are calculated until the wave elevation inside the suction anchor reach the top. At impact Wagner's wedge method together with Von Karman's wetted length is used to calculate the impact force on the cone-shaped suction anchor top.

Important parameters affecting the dynamic air cushion pressure and thus the buoyancy forces have been investigated. Force measured in lifting wire during splash zone transition of a single suction anchor is used as basis for comparison. The parameters that are investigated are introduction of a time-varying lowering velocity, changing characteristics of the ventilation hatch outlet and introducing regular and irregular waves. By varying these parameters a best-fit comparison with 2.5 [%] deviation between calculations and measurements have been obtained.

Further, a comparison between theoretical calculations and force measurements from a lifting operation of a subsea structure with suction anchors as foundation has been performed. The buoyancy forces calculated prior to impact are due to the dynamic air cushion pressure alone. The total force in the lifting wire for this phase are corresponding well to the magnitude of the measured force.

During this comparison the effect of changing perforation ratio clearly show an increase of buoyancy forces for decreasing size of ventilation hatch. Including both inflow and outflow of air from the suction anchors when oscillating in large waves have also been studied. When comparing with force measurements the importance of including both inflow and outflow of air to account for both suction and compressive pressure has been shown. This lead to negative and positive buoyancy forces respectively.

Long crested waves accounting for wind and swell sea are calculated with the JONSWAP- and Torsethaugen-spectra. By using empirical formulas for the limiting case between wind and swell sea it is shown that wind sea is the dominating part for the sea state measured during splash zone transition of the suction anchors.

Using Wagner's wedge model together with Von Karman's wetted length for calculating impact force on a flat suction anchor top is also performed. Impact forces with impact angles in the range of 5-15 degrees between the wedge-shaped water and top overestimate the force compared with measurements. A best-fit for the impact forces with the measurements has been obtained with deadrise angle of 17.5 [deg] in addition to impact forces calculated with a time-varying

slamming coefficient.

Possible resonant phenomena connected with oscillations of suction anchor and pressure measurements at impact have been studied. Simplified models for calculating A) natural period of oscillating air cushion, B) piston mode of water column and C) coupled piston mode of air cushion and water column has been developed. These have been compared with oscillation-period of pressure measurements observed after impact of a single suction anchor. These calculations have also been compared with oscillations of the suction anchor observed from videos of experiment. Case B) proved to give the most similar results with the suction anchor oscillations while case A) and C) were not in the proximity of the observed oscillations. This showed that the air cushion were not causing any resonant motion.

Using a common safety criterion for avoiding slack in lifting wire, the calculation model have been used to give a recommendation for perforation ratios for the suction anchors used on the installation of the subsea structure studied here. Perforation ratios in the range 1-3[%] used on suction anchor with diameters in the range 3-6[m] proved to be well within the slack-wire limit.

When using the theoretical model developed in this thesis a design recommendation for using ventilation hatches with a certain height have been made. Also uniform hatches are advised to ensure as similar conditions as possible for outflow and inflow of air.

Sammendrag

Abstract in Norwegian

Denne masteroppgaven omhandler dynamisk luftputetrykk inne i sugeankre ved låring gjennom skvalpesonen. En ikke-lineær kontinuitetsligning brukes til å representere luftmassen inne i sugeankeret. Denne brukes så til å utvikle en teoretisk modell for det dynamiske luftputetrykket. Oppdriftskrefter beregnes med hensyn på dynamisk luftputetrykk i sugeankrene, helt til den indre bølgehevingen når toppen av sugeankrene. Ved kollisjon beregnes slammingkrefter ved bruk av Wagner's kiletilnærming sammed med Von Karman's modell for våt lengde. Oppdriftskrefter og slammingkrefter er verifisert med full-skala kraftmålinger i løftevaier når et enkelt sugeanker låres gjennom plaskesonen.

Hvordan det dynamiske luftputetrykket og de påfølgende oppdriftskreftene påvirkes ved variasjon av viktige parametre blir også utforsket. Dette undersøkes ved bruk av fullskala målinger som sammenlignings-grunnlag. Forskjellige sammenligninger utføres ved å variere låringshastigheten, endre karakteristikken på ventilasjonslukens utløp og tilføre regulære og irregulære bølger i beregningene. Ved å variere disse parameterne er det oppnådd en beste tilpasning med 2.5 [%] avvik mellom beregninger og målinger.

I tillegg utføres sammenlikninger mellom teoretiske beregninger og målinger av krefter fra en løfteoperasjon med en undervanns-beskyttelsesstruktur der sugeankre blir brukt som fundament. Før den indre overflatehevingen kolliderer mot toppen av sugeankeret er oppdriftskreftene på grunn av det dynamiske luftputetrykket i samsvar med målingene.

Effekten av å endre perforeringsandel viser at oppdriftskreftene øker vesentlig når størrelsen på ventilasjonsluken minskes. Inkludering av både tilførsel og utstrømming av luft fra sugeankrene når de oscillerer i store bølger har blitt studert. Ved å sammenligne med kraftmålingene vises viktigheten av å inkludere både tilførsel og utstrømming av luft for å ta ta både under- og overtrykk med i beregningene. Dette fører til henholdsvis, negative og positive oppdriftskrefter.

Langkammede bølger som tar hensyn til både vind- og dønning-sjø er beregnet fra JONSWAP-spekteret og Torsethaugen-spekteret. Ved bruk av empiriske formler er det vist at vind-sjø er dominerende for sjøtilstanden målt under plaskesonelåringen av sugeankrene på beskyttelsesstrukturen.

Wagner's kiletilnærming sammen med Von Karman's modell for våt lengde brukes også for kollisjon mellom vann og flat sugeanker-topp. Her er kontaktvinkler mellom 5 og 15 [grader] brukt mellom vannet (som nå er kileformet) og den flate toppen. Dette resulterer i overestimering av slamming kreftene. Slamming krefter beregnet med denne metoden med kontaktvinkel på 17.5 [grader] i tillegg

til slamming krefter ved bruk av en tidsvarierende slamming-koeffisient gir mer samsvar med målingene.

Potensielle resonans-fenomen knyttet til oscillerende trykkmålinger og sugeanker observert i videoer har blitt studert. Forenklede modeller til beregning av A) naturlig periode av oscillerende luftpute, B) stempelmodus av vannsøyle og C) koblet stempelmodus mellom luftpute og vannsøyle er utviklet. Resultater fra disse er sammenlignet med svingningsperioder observert fra trykkmålinger etter kollisjon mellom vann og sugeanker-topp. Disse resultatene er også sammenlignet med svingninger av det enkle sugeankeret ved å studere videoer fra eksperimentet. Tilstand B) viser samsvar med de observerte svingningene. Derimot viser tilfellene A) og C) ingen nærliggende resultater til de observerte svingningene. Dette viser at luftputen ikke forårsaker resonnerende svingning av sugeankeret eller trykkmålinger. De naturlige periodene fra tilfellene B) og C), er også sammenlignet med høyfrekvente svingninger observert etter kontakt mellom sugeanker og vannoverflate under installasjon til havs.

Ved bruk av sikkerhetskriterium for å unngå slakk løftevaier blir beregningsmodellen benyttet til å anbefale perforeringsandel til sugeankrene tilhørende den aktuelle beskyttelsesstrukturen. Perforeringsandeler mellom 1 og 3 [%] på sugeankre med diameter mellom 3 og 6 [m] gir tilstrekkelig sikkerhetsmargin.

For å kunne bruke den teoretiske modellen utviklet i denne oppgaven er det gjort en design-anbefaling for bruk av ventilasjonsluker med en viss høyde. I tillegg er det anbefalt at uniforme luker brukes for mest mulig lik inn- og utstrømming av luft til sugeankeret.

Abbreviations

1D	one dimensional
3D	Three dimensional
BATCH	name to a given type of script file to be run in the command prompt
BEM	Boundary Element Method
CFD	Computational Fluid Dynamics
CFS	Complete Froude Scaling
DP	Differential pressure measured between inner and outer pressure sensors [kPa]
FPS	fishing protection structures
GDF	Geometric Data File
JONSWAP	Joint North Sea Wave Project
LOA	length over all
MRU	Motion Reference Unit
NCS	Norwegian Continental Shelf
NE-SA	North-east-suction anchor
NGI	Norwegian Geotechnical Institute
NTNU	The Norwegian University of Science and Technology
NW-SA	North-west-suction anchor
ODE45	Numerical solver in MATLAB for non-stiff differential equations
perforation ratio	ratio between horizontal area of ventilation hatch and suction anchor top
PLEM	pipeline end-manifold
RAO	Response Amplitude Operator
RNG	Random Number Generator
ROV	Remote Operated Vehicle

SES	Surface Effect Ships
SE-SA	South-east-suction anchor
SIMO	Simulation of Marine Operations
SW-SA	South-west-suction anchor

Symbols

P_c	air cushion pressure
a	lower frequency limit
A_{33c}	three-dimensional added mass in heave of air cushion
$A_{33,disk}$	three-dimensional added mass in heave of a thin disk
$A_{33,sa}$	added mass in heave of fully submerged suction anchor
$A_{33,trappedwater}$	three-dimensional added mass in heave of entrapped water inside suction
A_{33w}	added mass in heave of the water column inside the suction anchor
Ac	circular area of suction anchor
a_f	factor depending on fetch length
$\eta_{3,anchor,i}$	total vertical motion of suction anchor 1-4
$\boldsymbol{\omega}$	angular motion vector
A_p	projected area in the horizontal plane for the submerged part of the suction anchor
A_{top}	area of suction anchor top
A_{wire}	cross sectional area of the lifting wire
b	upper frequency limit
β	impact- or deadrise-angle between the impacting body and water surface
F_{buoy}	buoyancy force on suction anchor
C_p	arbitrary function of time
$\eta_{3,const}$	constant part of the lowering velocity
C	contraction coefficient due to the shape of the ventilation hatch
Cs_{rp}	constant slamming coefficient
Cs_{var}	time varying slamming coefficient
ρ_c	density of the air cushion mass

c	wetted length of suction anchor top during impact
D_{anchor}	diameter of suction anchors on FPS
Δt	duration of impulse at impact
D_{hatch1}	diameter of smallest ventilation hatch on FPS-anchors
D_{hatch2}	diameter of largest ventilation hatch on FPS-anchors
E	Young's modulus of elasticity
ϵ	random, independent and uniformly distributed phase angles between 0 and 2π
ϵ_{ij}	random and uniformly distributed phase angles between 0 and 2π in longitudinal and transverse direction
$\eta_{1,mru}$	surge motion at MRU
$\eta_{2,mru}$	sway motion at MRU
$\eta_{3,mru}$	heave motion at MRU
$\eta_{4,mru}$	roll motion at MRU
$\eta_{5,mru}$	pitch motion at MRU
$\eta_{6,mru}$	yaw motion at MRU
η_{3s}	vertical motion of the suction anchor. Positive upwards
$\mathbf{V}(x, y, z, t)$	fluid velocity vector
F_{slam}	slamming force
γ_a	ratio of specific heat for air
A_l	area of ventilation hatch
h_{hatch}	height of ventilation hatch
H_s	height of cylinder
H_{fs}	wave height of regular waves measured from lowering videos
h_e	water depth measured at full scale tests
h_w	height of well
Hs	significant wave height or average of the 1/3 of the highest waves

h	time step used in forward differentiation
h_c	the instantaneous vertical position of the water surface
I	pressure impulse at impact
r_{inner}	radius of air cushion at impact from full-scale experiments
Ω_{inner}	volume of air cushion at impact from full-scale experiments
$\boldsymbol{i}$	vector along x-axis
$\boldsymbol{j}$	vector along y-axis
K	stiffness of the total hoisting system
k_i	wave number in deep water and short crested waves
δ	kronecker delta function
k_{tip}	stiffness of crane tip
$\boldsymbol{k}$	vector along z-axis
k	wave number
λ_{fs}	wave length of the first waves generated after impact from lowering videos
λ_{rp}	heave added mass parameter for suction anchor
λ_{scale}	scaling factor between model- and full-scale
L_{fs}	length at full-scale
L_{ms}	length at model-scale
L_{wire}	length of the wire from the crane tip to the lifting hook
M	mass of the suction anchor in air
$\mu(t)$	dynamic variation of air cushion pressure
m_{top}	mass of flat suction anchor top
$\dot{\mu}(t)$	time derivative of dynamic air cushion pressure
$P_1 e^{i\omega t}$	dynamic part of the air cushion pressure
n	number of frequency intervals
N_2	Nitrogen dioxide

ω_c	natural frequency of air cushion
T_c	natural period of air cushion
n_s	spreading parameter
$\omega_{coupled}$	coupled natural frequency between piston mode of air cushion and water column
ω_w	natural frequency of the liquid inside one well
$\omega_{coupled,A33}$	natural frequency of coupled piston mode between air cushion and water column in terms of heave added mass
ω_P	peak frequency
P_{atm}	atmospheric pressure
p	total water-pressure defined by Bernoulli's equation
γ	peak parameter for JONSWAP spectrum
P_{out}	outer pressure at impact measured during full-scale experiments
p^{fs}	pressure at full-scale
ϕ_p	piston mode velocity potential
ϕ_{slam}	velocity potential during impact
P_{in}	inner pressure measured at impact during full-scale experiments
p^{ms}	pressure at model-scale
P_{peak}	peak pressure at impact
P_{slam}	instantaneous local slamming pressure
R	radius of suction anchor
$\zeta_{A,fs}$	amplitude of waves measured from lowering videos
$\eta_{3,rel}$	relative vertical motion between the suction anchor and the inner wave elevation
ρ_{atm}	density of air
$s_{3,anchor,i}$	vertical motion of suction anchors due to vessel motions
$\boldsymbol{r}$	translational motion vector

Sf_6	Sulphur hexafluoride
σ	spectrum shape parameter
$sign$	signum function
Cs	non-dimensional slamming coefficient
F_{slam}	slamming load acting on top of suction anchor
$S(\omega)$	uni-directional Torsethaugen spectrum
$S(\omega, \theta)$	directional spectrum
$D(\theta, \omega)$	directional spreading function
F_{stat}	static weight of structure in air
θ_{hoist}	correction factor accounting for the cable mass
θ_s	relative direction between wind and swell sea
Δz	deflection of crane tip
$s_{3,tip}$	vertical crane tip motion
$\dot{\eta}_{3,tip}$	vertical crane tip velocity
Tp	peak period
t_s	time step used in slamming calculation starting from zero at impact
P_0	initial pressure in the air cushion
ρ_0	density of the air cushion at the initial time of creation of the air pocket
Va	velocity of plate after impact
$\eta_{3,varying}$	time varying part of the lowering velocity
ϕ	velocity potential
Ω_0	initial air cushion volume
V_{rel}	relative velocity between body and waves
P_{ζ_s}	pressure in water inside air cushion
$\dot{\eta}_{3,winch}$	lowering velocity of the crane winch
F_{wire}	force in lifting wire

x_{tip}	longitudinal location of crane tip relative to MRU
y_{tip}	transverse location of tip relative to MRU
Tz	zero crossing wave period
ζ_A	wave amplitude calculated from spectrum
ζ_{inc}	wave elevation of incident waves
ζ_{tw}	height between suction anchor top and wave elevation at impact from full-scale experiments
z_{tip}	vertical location of tip relative to MRU

Contents

List of Figures

List of Tables

1 Introduction

1.1 Background and motivation

Before installation of large subsea structures at the Norwegian Continental Shelf (NCS) it is important that the installation is well planned. This is in order to perform a safe lifting operation with respect to human safety, lifting equipment and installation vessel. The lifting process can be defined as lift-off from deck, over-boarding, lowering through splash zone and finally landing on seabed. During a lifting process at a given sea state it is important to assess the most critical loads that can occur on the structure and lifting equipment in the lifting process. To be on the safe side conservative calculation methods are utilized by contractors, class societies and companies performing 3^{rd} party verification work.

Optimization of sea states is a term widely used when planning operations. According to Jacobsen et al. (2012) it is known that the forces acting on a subsea structure during splash zone transition are often the largest during a lifting process on the Norwegian Continental Shelf (NCS). Therefore this phase is given much attention when determining the design sea state for installation. Hydrodynamic analyzes like time-domain simulations, Computational Fluid Dynamics and model testing are used to optimize the design sea state during this phase. However, each of these methods have their limitations in addition to being time consuming and costly for model testing.

The recommended practise Det Norske Veritas (2011) suggests a simplified and conservative calculation method for hydrodynamic forces acting on subsea structures during splash zone transition. Det Norske Veritas (2011) is used actively together with environmental conditions given in Det Norske Veritas (2010) by contractors all around the world according to Arunjyoti and Gudmestad (2010). According to Tormod Bøe (2013) the intention of these recommended practises are to give a conservative estimate in a preliminary phase when planning installation of subsea structures and to see how large forces can occur during installation. However, contractors and design companies may tend to use the loads estimated with this approach as design criteria without performing thorough hydrodynamic analyzes. This may result in too conservative estimates for the design sea state which again lead to larger installation costs with requirement of larger installation vessels and more strict weather windows.

Deployment of subsea structures with suction anchors as foundation through splash zone are well described in Det Norske Veritas (2011). If large buoyancy forces occur that impose a risk of slack lifting wire, this may be the limiting factor when determining the design sea state for the installation. For this case Det Norske Veritas (2011) suggests methods for calculating added mass, drag- and impact-forces on the suction anchors.

However, the effect of dynamic air cushion pressure on the buoyancy forces inside the suction anchor is not described. It is only mentioned that sufficient ventilation of air during splash zone transition shall be accounted for to avoid large buoyancy forces. For ensuring that the air is sufficiently evacuated a ventilation hatch must be installed at the top of the suction anchor. To avoid large buoyancy forces which may lead to risk of slack in the lifting wire or slings, the ratio between horizontal area of ventilation hatch and suction anchor top (perforation ratio) must be of a certain size.

Known to the author a recommendation for this is not given in any literature. However, Ølund Bertelsen (2013) has made some observations by studying videos of lowering of suction anchors with very small perforation ratios through splash zone. There it was observed that too small perforation ratio will induce large buoyancy forces which may lead to tilting of the suction anchor and then slack in lifting wire. Therefore the present thesis will investigate the influence of air cushion pressure on buoyancy forces acting on suction anchors during splash zone transition. This will be performed with theoretical calculations that will be compared with measurements from full-scale experiments and offshore installations.

1.2 Scoope of thesis

The present thesis will quantify the effect of dynamic air cushion pressure on the buoyancy forces with respect to various lowering velocities, outlets of ventilation hatches, perforation ratios and air flow conditions. For this case full-scale force and pressure measurements will be used for comparison.

Impact loads will also be investigated due to findings in Ølund Bertelsen (2013) showing that slamming is more critical with respect to slack in the lifting wire when sufficient ventilation of air is present.

The influence including both swell and wind sea on long crested waves should be studied. The effect of this on the calculation of the buoyancy forces forces due to the dynamic air cushion pressure should be compared with measured forces from offshore installation.

Further, natural periods connected with oscillation of the air cushion and water column inside suction anchor should be evaluated post impact. This is in order to evaluate if resonant motion of the air cushion can affect oscillations of suction anchors.

Finally a method for performing a design recommendation for suction anchors and required ventilation hatch sizes with respect to avoiding slack in lifting wire should be proposed.

1.3 Structure of thesis

This thesis is mainly divided into four parts.

The first part summarize a comparison between theoretical calculations and full-scale force measurements performed by Ølund Bertelsen (2013). The effect of varying lowering velocity, regular and irregular waves and characteristics of ventilation hatch outlet on the dynamic air cushion pressure will also be studied. This is performed in chapter 2.

The second part is shown in chapter 3 where pressure measurements from the same full-scale experiment as in the first part of this thesis will be investigated. Different phenomena connected with oscillations observed in measurements will be investigated. Of particular importance is the study of resonant motion of the air cushion in order to quantify the effect of air cushion oscillations on suction anchors after impact. Also the piston mode of a coupled air cushion and water column will be evaluated to see if the oscillating air cushion influence the piston motion of water column. This is performed

The third part will be conducted in chapter 4 where an installation of a subsea protection structure with suction anchors as foundation is studied. Measurements from this installation will be extracted and used in theoretical calculations to calculate forces in lifting wire during submergence of suction anchors. Force measurements in lifting wire will be used for comparison with the theoretical model. Buoyancy forces due to dynamic air cushion pressure in addition to impact forces are calculated for all suction anchors.

The last part conducted in chapter 5.1 perform a statistical analysis for investigating important parameters in the design of suction anchors. Theoretical calculations are compared with a slack-wire criterion for different perforation ratios will used on the suction anchors.

Finally, a proposal for further work for expanding the calculation model developed during this thesis in addition to proposal for a small-scale impact test able to scale the impact pressure to full-scale will be performed.

2 Comparison between full scale measurements and theoretical calculations

In this chapter major findings from project work performed by Ølund Bertelsen (2013) in 2013 at The Norwegian University of Science and Technology (NTNU), Department of Marine Technology, will be summarized. During Ølund Bertelsen (2013) has compared force measurements from a full scale test of a single suction anchor with theoretical calculations.

A short description of the full scale test will be given in chapter 2.1. The theoretical calculations will be summarized in chapter 2.2 and a parameter-study where different effects that influence the air cushion is varied is performed in chapter 2.5.

2.1 Full-scale test

In this chapter a full scale test performed by Aspelund,Leiv (2014) of a single suction anchor lowered into the sea will be described. The test was performed at 16^{th} of August, 2013 at the Hinna base in Stavanger. The test was performed in cooperation with the Norwegian Geotechnical Institute (NGI) on behalf of Statoil. The goal of the test was to measure pressure inside and outside the suction anchor during lowering to the seabed. However, the force in the lifting wire and pressure in the suction anchor were also measured during splash zone transition for different perforation ratio. A sketch of the test set-up for the experiment is shown in figure 2.1:

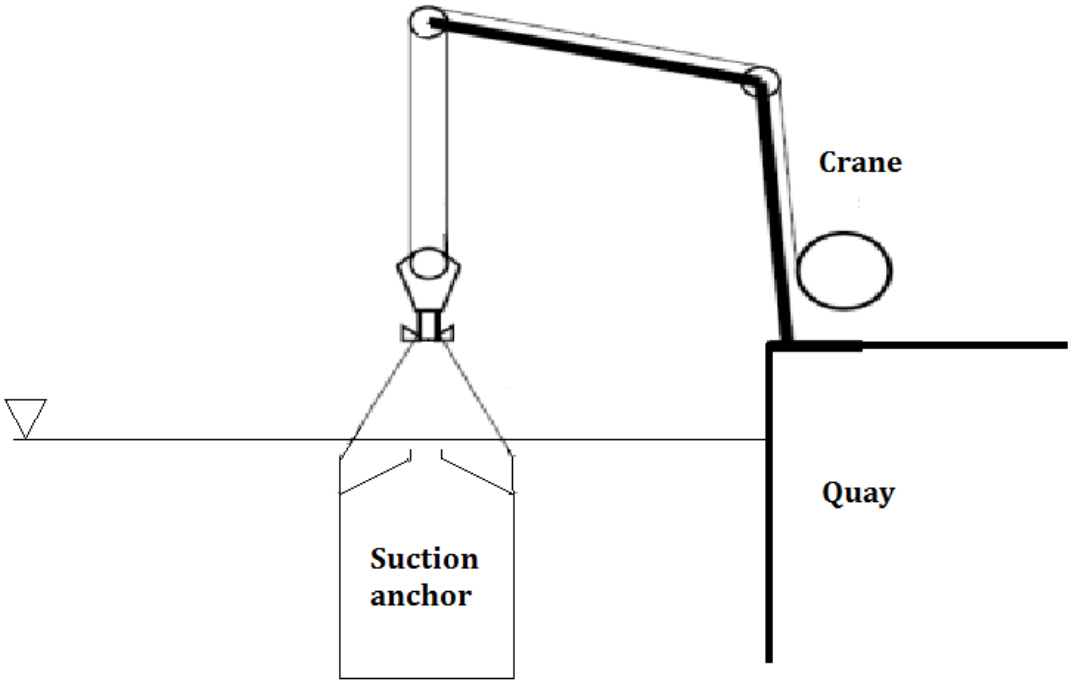

Figure 2.1: Test set-up for full scale test of suction anchor

The top of the suction anchor is shaped like a cone with the ventilation hatch located in the center of the top. The part underneath the conical top is cylindrical. The suction anchor is made of steel and is hollow inside. The main data for the suction anchor are shown in table 2.1:

Full-scale suction anchor	
Mass	12900 [kg]
Diameter	3.4 [m]
Height	5.96 [m]
Perforation	1.98 [%]

Table 2.1: Data for comparison suction anchor.

A detailed drawing of the suction anchor used in the experiment is shown in appendix B.1, figure B.1.

2.1.1 Operational concerns

The test was performed inshore with no significant waves present. However, the recordings show some small waves which might contribute to increasing the dynamic air cushion pressure and also oscillation of the pressure during transition through the splash zone. To prevent resonant effects it is important that the wave period is far away from the natural period of the air cushion or water inside the suction anchor. This will be investigated in chapter 3.2 and 3.6.

There is no measurement of the lowering velocity, but it has been estimated from video recordings. The recordings show that the velocity increases from start of lowering until the suction anchor enters the water. However, Ølund Bertelsen (2013) estimated the lowering velocity as constant equal to 0.98 $[\frac{m}{s}]$ from water entry until fully submergence of the suction anchor. A varying lowering velocity will be investigated in chapter 2.5.2.

2.1.2 Uncertainties

According to Aspelund,Leiv (2014) there are large uncertainty connected with the measurements from this test which must be taken into account when comparing with the theoretical calculations. The uncertainties are found by studying videos of the lowering provided by Aspelund,Leiv (2014) and are listed below:

- The lowering velocity is not measured and must be read off the video
- The lowering is stopped right after the suction anchor becomes submerged, which might be too early to capture the effect of slamming properly in addition to creating an oscillation of the anchor due to inertia forces from the motion of the anchor.
- From videos there are small waves present which may influence the results. This may lead to oscillation of the air cushion
- The videos also show some inclination of the anchor when the submergence level is increasing.

The most relevant uncertainties will be investigated in chapter 2.5.

2.2 Simplified analysis of air cushion inside suction anchor

In this chapter a theoretical model developed by Ølund Bertelsen (2013) will be presented which has reproduced the force measurements obtained from the full scale tests described in chapter 2 in a decent way. The calculations in Ølund Bertelsen (2013) are based on air cushion theory used for evaluating the performance of Surface Effect Ships presented in O.M. Faltinsen (2005). The calculation model is shown in figure 2.2 and the main hydrodynamic assumptions for the calculation model is listed below:

- Quasi static conditions apply, where equilibrium between water surface and air cushion is considered
- Surface tension on the water surface is neglected
- Buoyancy forces acting on the wall of the suction anchor are neglected due to thin-walled cross section

- The incident waves are assumed long relative to the characteristic length of the suction anchor
- No waves are generated during submergence
- The water is assumed incompressible and isothermal
- Due to immersion of anchor wall only, drag forces on the wall are assumed negligible
- Slamming forces are active when inner wave elevation impacts against top of suction anchor
- The wave elevation inside the suction anchor is assumed uniform and that it rises like a piston during lowering

The main assumptions for the air cushion are listed as follows:

- Pressure distribution in the air cushion is assumed uniform
- The air is adiabatic, which means that it will have constant entropy and constant gain or loss of heat
- Ideal gas conditions apply for the air, compressibility is considered
- The air-flux is only allowed out of the air cushion

All the assumptions listed here except the last one will be used throughout the present thesis.

2.2.1 Equilibrium between air cushion and water

For deriving an expression for the dynamic air cushion pressure, Ølund Bertelsen (2013) used the calculation model shown in figure 2.2:

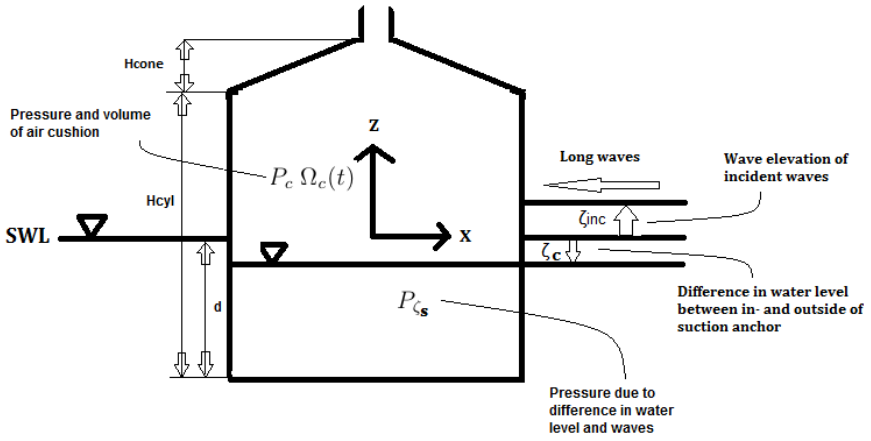

Figure 2.2: Calculation model of the suction anchor

In order to describe the air cushion pressure at each submergence level equilibrium between the air cushion pressure and the water pressure is introduced. First, an expression for the total pressure for the air cushion inside the suction anchor is established in equation 2.1:

$$P_c = P_{atm} + \mu(t) \tag{2.1}$$

Where:

- P_c is the air cushion pressure
- P_{atm} is the atmospheric pressure
- $\mu(t)$ is the dynamic variation of air cushion pressure

The total pressure on the water surface inside the suction anchor can be written as:

$$P_{\zeta_s} = P_{atm} + \rho_w g \zeta_{inc}(t) - \rho_w g \zeta_c(t) \tag{2.2}$$

Where:

- P_{ζ_s} is the pressure in water inside air cushion.
- ρ_w is the density of seawater.
- g is the gravitational acceleration.

- $\zeta_{inc}(t)$ is the wave elevation of incident waves. Positive upwards.
- $\zeta_c(t)$ is the water elevation inside the suction anchor. Positive upwards.

This is seen from figure 2.2.
By setting equation 2.1 equal to equation 2.2 equilibrium is applied on the surface inside the suction anchor. This results in the following expression for ζ_c:

$$\zeta_c = \zeta_{inc} - \frac{\mu(t)}{\rho_w g} \tag{2.3}$$

By geometrical considerations of figure 2.2 the vertical motion and volume the air cushion can now be calculated for all time instants.

2.2.2 Continuity equation for air mass inside suction anchor

The continuity equation for the air mass inside the suction anchor will be used to develop an equation for finding the dynamic air cushion pressure. This can be written as:

$$-\rho_c Q_{out} = \frac{d\rho_c}{dt}\Omega_c(t) + \rho_c \frac{d\Omega_c}{dt} \tag{2.4}$$

Where:

- ρ_c is the density of the air inside the air cushion $[\frac{kg}{m^3}]$
- Q_{out} is the volume flow of air flowing out of the suction anchor through the ventilation hatch $[\frac{m^3}{s}]$
- $\Omega_c(t)$ is the instantaneous volume of the air cushion $[m^3]$

According to Ølund Bertelsen (2013) the volume flow of air out of the ventilation hatch can be calculated with equation 2.5:

$$Q_{out} = C A_l \sqrt{\frac{2\mu(t)}{\rho_{atm}}} \tag{2.5}$$

Where:

- A_l is the area of ventilation hatch
- ρ_{atm} is the density of air
- C is the contraction coefficient due to the shape of the ventilation hatch.

C is found from Blevins (1984) to be 0.61 [-] for the ventilation hatch in study.

2.2.3 Resulting expression the dynamic air cushion pressure

By applying the assumptions stated in chapter 2.2 together with the main equations 2.1 and 2.4 the following non-linear expression for the time derivative of the dynamic air cushion pressure is obtained from Ølund Bertelsen (2013):

$$\dot{\mu}(t) = \frac{\dot{\zeta}_{inc} - \dot{\eta}_{3s} - C\frac{A_l}{Ac}\sqrt{\frac{2\mu(t)}{\rho_{atm}}}}{\frac{1}{\gamma_a P_{atm}}\left(1+\frac{\mu(t)}{P_{atm}}\right)^{-1}\left(H_s + \frac{\mu(t)}{\rho_w g} - \zeta_{inc} - \eta_{3s}\right) + \frac{1}{\rho_w g}} \tag{2.6}$$

Where:

- $\dot{\mu}(t)$ is the time derivative of dynamic air cushion pressure
- Ac is the circular area of suction anchor
- η_{3s} is the vertical motion of the suction anchor. Positive upwards
- $\dot{\zeta}_{inc}$ is the velocity of the incident wave elevation. Positive upwards.
- γ_a is the ratio of specific heat for air
- H_s is the height of cylinder

Equation 2.6 is solved numerically for $\mu(t)$ by a time integration method. The solution method is described in chapter 2.3.

2.3 Numerical calculation of the dynamic pressure

Equation 2.6 is on the form $\dot{\mu}(t) = f(t, \mu)$ and Ølund Bertelsen (2013) has solved this by a time integration with an explicit Runge Kutta 4 method. According to Kreyzig (2006) this method is exact to the fourth order and is well suited for computational calculations since it needs no special starting procedure, require little storage capacity and is numerically stable.

In Ølund Bertelsen (2013) the initial condition for the dynamic pressure is when the suction anchor is hanging right above the water surface, and letting this be the starting time for the calculations. Then $\mu(0) = 0$ because no pressure due to difference in wave elevation inside and outside of the suction is present. A simplification in Ølund Bertelsen (2013) is that the dynamic pressure is calculated up to the top of the suction anchor by simplifying the cone-shaped top as cylindrical. The result for the time integration of $\mu(t)$ is shown in figure 2.3 where a step size of 1000 is used.

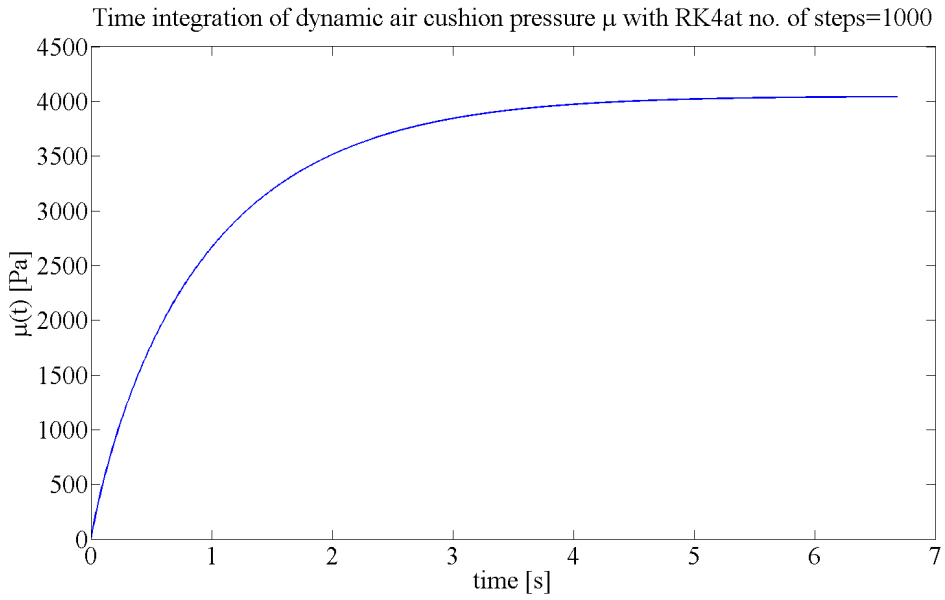

Figure 2.3: Time integration of dynamic air cushion pressure μ

From a convergence study it is seen that the curve for μ becomes more smooth for increasing step size up to 1000. MATLAB is used for calculating $\mu(t)$ with the script CalcRK.m which can be seen in appendix G.1.

When calculating the dynamic air cushion pressure in Ølund Bertelsen (2013) the following limitations should be kept in mind:

- lowering velocity $\dot{\eta}_3$ is assumed constant during lowering
- wave elevation ζ_{inc} is also assumed constant or equal to zero.
- air-flux out of the suction anchor is only considered

2.4 Force calculations

During submergence the air inside the suction anchor will be compressed by the water pressure which acts upwards on the air cushion. As observed in figure 2.3 the dynamic air cushion pressure increase during submergence which means that there are an increasing buoyancy force acting on the air cushion. This may lead to risk of slack in the lifting wire if it exceeds the total weight of the submerged suction anchor. Especially if the anchor oscillates this may result in snap loads that are critical for the capacity of the lifting equipment as mentioned in chapter 1.1.

Regarding force calculations performed by Ølund Bertelsen (2013) the total force in the wire is calculated taking the static weight of the suction anchor in air minus the buoyancy due to water pressure acting on the air cushion only. This is

correct for the cylindrical part of the suction anchor. However, when the inner wave elevation impacts against the conical shaped top impact forces occur.

Assuming potential theory the slamming load occurring at impact is calculated by a strip theory approach where the pressure from Bernoulli's equation is integrated over the wetted area of each strip. This is performed using both von Karman (1929)'s and Wagner (1932)'s method for calculating the wetted length for a wedge-impact. The calculation of wetted length with these two approaches are performed by assuming that the water rise up during impact is included versus neglecting it respectively.

The total load in the lifting wire due to the buoyancy forces from to the dynamic air cushion pressure and impact force with the two methods described above can now be calculated. This will be compared with 3 full-scale force measurements performed by Aspelund,Leiv (2014). This is shown in figure 2.4.

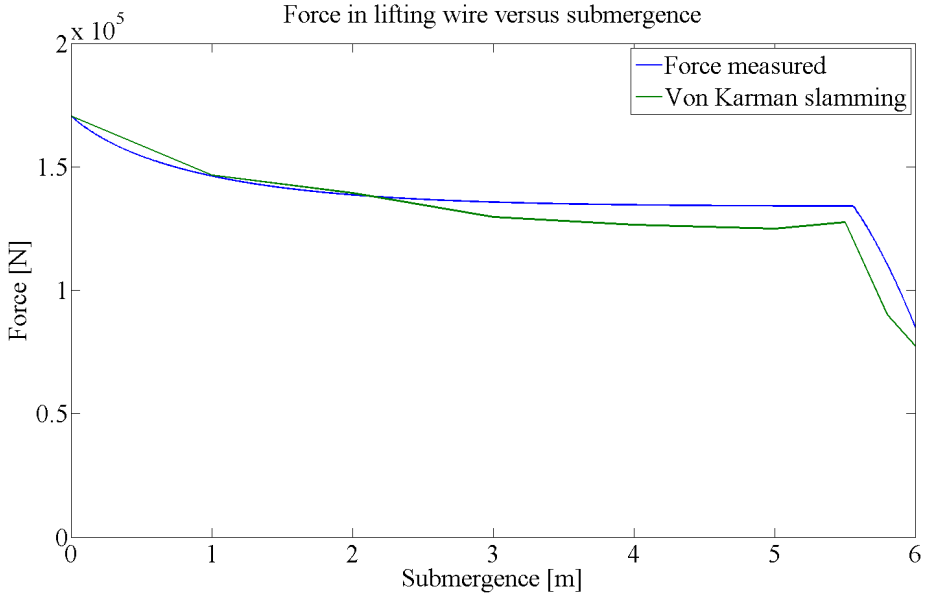

Figure 2.4: Comparison of wire load between theoretical force calculations and experimental force measurements

From figure 2.4 it is seen that the calculated buoyancy force after a submergence of 2.5 [m] are underestimated compared with the measured force. This will be investigated by varying different parameters in the calculations in chapter 2.5. From figure 2.4 it is seen that von Karman (1929)'s approach is more similar to the measurements and that Wagner (1932)'s approach overestimates the slamming force. The maximum deviation between the calculated and measured force is 7.5 [%].

2.5 Parameter study

In this chapter the most significant uncertainties discussed in chapter 2.1.2 will be studied. The following parameter-study will be performed:

- Changing the contraction coefficient
- Introducing a varying lowering velocity
- Varying impact area
- Introducing regular waves
- Introducing irregular waves

The change of contraction coefficient and introduction of regular waves are repeated from Ølund Bertelsen (2013).

2.5.1 Changing the contraction coefficient

Considering Blevins (1984) the contraction coefficients for different nozzle types are based on empirical data which may not be quite similar to the case studied in the present thesis. By looking at similar nozzle types and after discussion with the supervisor for the present thesis, Greco (2014) a contraction coefficient of 0.59 was proposed as an alternative. This resulted in larger correspondence with the measurements. The result with this contraction coefficient for the comparison of force calculated and measured is shown in figure C.1 in appendix C.1.

The maximum deviation is now 5.6 [%] before slamming compared to the original case with a maximum deviation of 7.5 [%]. The physical effect of decreasing the contraction coefficient means that the outflow of air through the ventilation hatch is more contracted leading to increased dynamic air cushion pressure and thus larger buoyancy forces. However, even if a smaller contraction coefficient will result in more correspondence it is according to the recommended values in Blevins (1984) not likely that the contraction will be smaller than 0.59.

2.5.2 Introducing varying lowering velocity

By introducing a time dependent velocity component it is possible to investigate lowering of the suction anchor in a more realistic way since the velocity of the crane-winch is not known. Since it takes some time before the crane winch has reached the desired lowering velocity it can be seen from the videos by Aspelund,Leiv (2014) that the lowering velocity is increasing slightly as the anchor is lowered into the sea. Then, mathematically the total lowering velocity can be stated as:

$$\dot{\eta}_{3,s} = (\dot{\eta}_{3,const} + \dot{\eta}_{3,varying}) \tag{2.7}$$

Where:

- $\eta_{3,const}$ is the constant part of the lowering velocity
- $\eta_{3,varying}$ is the time varying part of the lowering velocity

There are some uncertainties connected with reading off the velocity from video recordings. Therefore a uncertainty of $\pm 5[\%]$ for the estimated lowering velocity should be accounted for. Then the maximum velocity limit during submergence is approximately $1.03[\frac{m}{s}]$. By using the velocity $\dot{\eta}_{3,tot} = -(0.97 + 0.01t)$ the wire force and impact-depth becomes more similar to the measurements compared to a constant velocity of $-0.98[\frac{m}{s}]$ as shown in figure C.2, appendix C.2. This will also influence the vertical motion of the suction anchor which can be represented by equation 2.8:

$$\eta_3 = \int_{t'} \dot{\eta}_{3,tot}(t')dt' \tag{2.8}$$

This results in a maximum deviation of 5 [%] which is highly improved compared to the case with constant lowering velocity. In addition the impact-depth corresponds more to the one in the measurements. A parameter study of different deadrise angles will be performed in chapter 2.5.3.

2.5.3 Varying impact area

Depending on the lowering velocity the calculated impact is occurring both after and at the same stage as than the measurements. Therefore it is necessary to investigate the area where the impact occurs. In Ølund Bertelsen (2013) it was assumed that the slope of the top started at a height of 5.2 [m]. However, considering figure 2.5 the curvature of the conical top can be assumed to start at a height of 5 [m]:

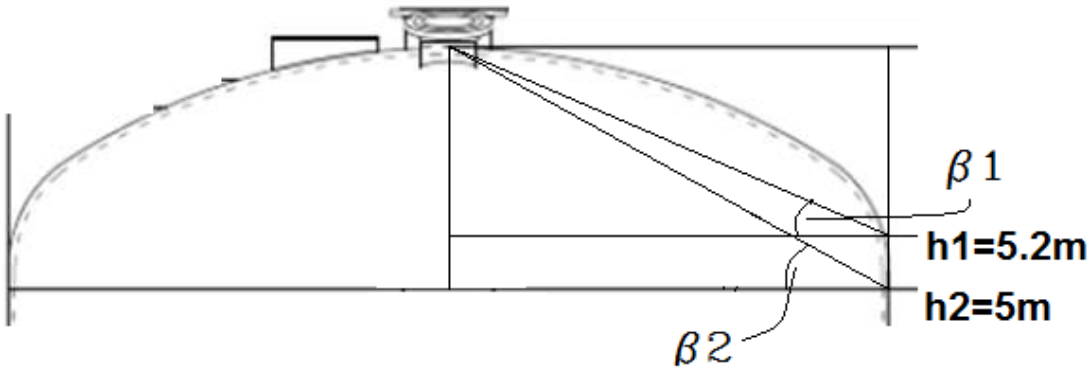

Figure 2.5: Study of conical top with different deadrise angles

The results using the slope corresponding to β_2 is shown in appendix C.3, figure C.3. However, considering figure 2.5 the slope corresponding to β_2 is not similar to the actual conical top, and therefore the impact will occur earlier than what is calculated with β_1. This discussion concludes that an impact with deadrise

angle β_1 corresponds more to the measured results compared with deadrise angle β_2. However, there are still some uncertainty regarding the influence of waves on the force measurements, and this will be discussed in chapter 2.5.4.

2.5.4 Including regular waves in the calculations

Considering the videos provided by Aspelund,Leiv (2014) there are some small waves present during the tests. These wave heights can be estimated

Wave realizations with regular waves at the center of the suction anchor can be calculated with equation 2.9:

$$\zeta_{inc} = \zeta_{A,fs} sin(\omega t) = \zeta_{A,fs} sin\left(\frac{2\pi}{T_z} t\right) \tag{2.9}$$

Where:

- $\zeta_{A,fs}$ is the amplitude of waves measured from lowering videos
- Tz is the zero crossing wave period

Where Tz is defined from the minimum zero crossing period defined as 3.4 [s] from Det Norske Veritas (2011). $\zeta_{A,fs}$=$\frac{H_{fs}}{2}$ where wave height of regular waves measured from lowering videos (H_{fs}) is estimated to 0.1 [m] from the lowering videos. Now the dynamic air cushion pressure and thus the buoyancy force will start to oscillate as shown in figure C.4 in appendix C.4. Due to low sampling rate of the force measurements, oscillations are not captured. However, when including regular waves in the calculations the results show some correspondence with the results from measurements obtained at the third run in the experiments.

A comparison of the calculations calculations with irregular waves is conducted in chapter 2.5.5.

2.5.5 Irregular wave calculations

To investigate the effect of irregular waves, the Joint North Sea Wave Project (JONSWAP) spectrum is used. This spectrum is created from a series of wave measurements in the North Sea. According to Myrhaug (2007) the waves are based on the assumption of unlimited fetch and duration which is not be the case for the measurement at the Hinna quay. However, since the waves are small, it is assumed that this spectrum is sufficient for the comparison analysis. According to Myrhaug (2007) the wave spectrum can be calculated with equation 2.10:

$$S_n(\omega) = \frac{5}{32\pi} Hs^2 Tp \left(\frac{\omega_p}{\omega}\right)^5 e^{-\frac{5}{4}\left(\frac{\omega_p}{\omega}\right)^4} (1 - 0.287 \ln\gamma) \gamma^{e^{-\frac{\left(\frac{\omega}{\omega_p}-1\right)^2}{2\sigma^2}}} \tag{2.10}$$

Where:

- ω_P is the peak frequency
- γ is the peak parameter for JONSWAP spectrum
- Tp is the peak period
- Hs is the significant wave height or average of the 1/3 of the highest waves

σ is the spectrum shape parameter and must satisfy the following requirements:

$$\sigma = \begin{cases} 0.07\omega \leq \omega_P \\ 0.09\omega_P < \omega \end{cases}$$

Tp is estimated from Myrhaug (2007), (figure 2.9) to be $4\sqrt{Hs}$. The wave frequency ω is calculated with the midpoint formula shown in equation 2.11:

$$\bar{\omega_i} = a + (b-a)\frac{(i-\frac{1}{2})}{n} \tag{2.11}$$

Where:

- b is the upper frequency limit defined as $\frac{33}{Tp}$ in WAFO-group (2000)
- a is the lower frequency limit
- n is the number of frequency intervals

According to Holm (2013) when approximating the wave frequencies with the midpoint formula the wave spectrum must be integrated over the frequency intervals. The integral for the wave spectrum can then be approximated by dividing the integration area into equal size of intervals and calculate the spectral value for the midpoint in each interval. The wave spectrum will then be calculated with equation 2.12:

$$S_n(\omega) = \frac{b-a}{n}\sum_{i=1}^{n} S(\bar{\omega_i}) \tag{2.12}$$

A convergence study show that number of wave intervals n=10000 is required for obtaining a smooth peak of the JONSWAP-spectrum.

The JONSWAP-spectrum is shown in figure 2.6 for $Hs = 0.1[m]$, $Tp = 1.27[s]$ and $\gamma = 3.3$ which is the average value of the peak parameter in the North sea found in Myrhaug (2007).

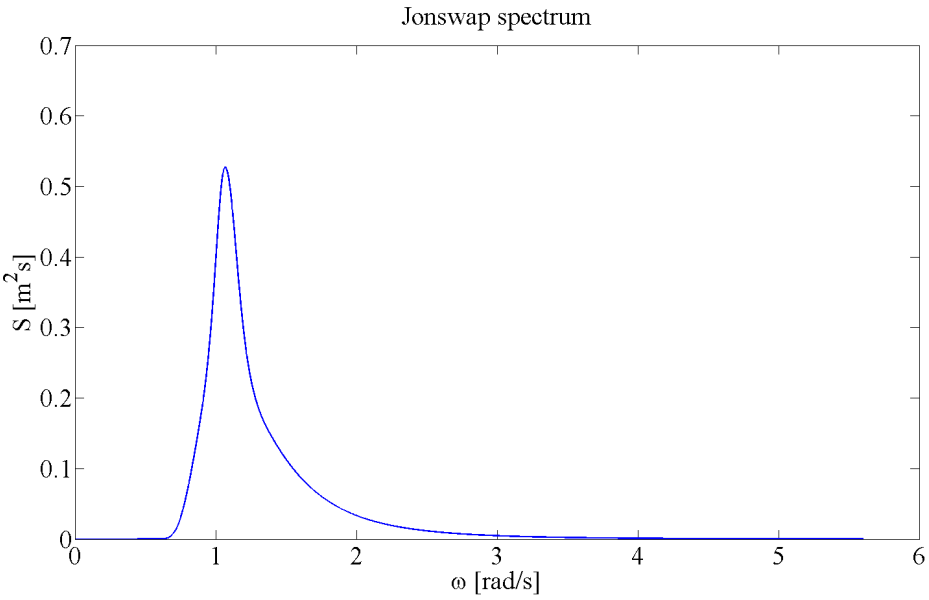

Figure 2.6: JONSWAP wave spectrum

By assuming Gaussian sea the wave elevation of incident waves ζ_{inc} can be calculated as:

$$\zeta_{inc}(x,t) = \sum_{n=1}^{N} \zeta_{An} sin(\omega_n t - k_n x + \epsilon_n) \tag{2.13}$$

Where the wave amplitude ζ_A is found by setting the area within a small frequency interval $\Delta\omega$ equal to the energy of all the wave components within this interval as shown in equation 2.14:

$$\frac{1}{2}\zeta_{An}^2 = S(\omega_n)\Delta\omega \tag{2.14}$$

The resulting wave elevation for linear and long crested waves propagating in the positive x-direction can be calculated with equation 2.15:

$$\zeta_{inc}(x,t) = \sum_{n=1}^{N} \sqrt{2S(\omega_n)\Delta\omega} sin(\omega_n t - k_n x + \epsilon_n) \tag{2.15}$$

Where ϵ are random, independent and uniformly distributed phase angles between 0 and 2π. A realization of the wave elevation used in the analyzes and the resulting force in the lifting wire subject to these waves is shown in figure C.5 and C.6 respectively in appendix C.5.

2.6 Summary of parameter-study

A comparison between the average of three force measurements versus a best-fit parameter variation of the parameters discussed in chapter 2.5 are shown in figure 2.7.

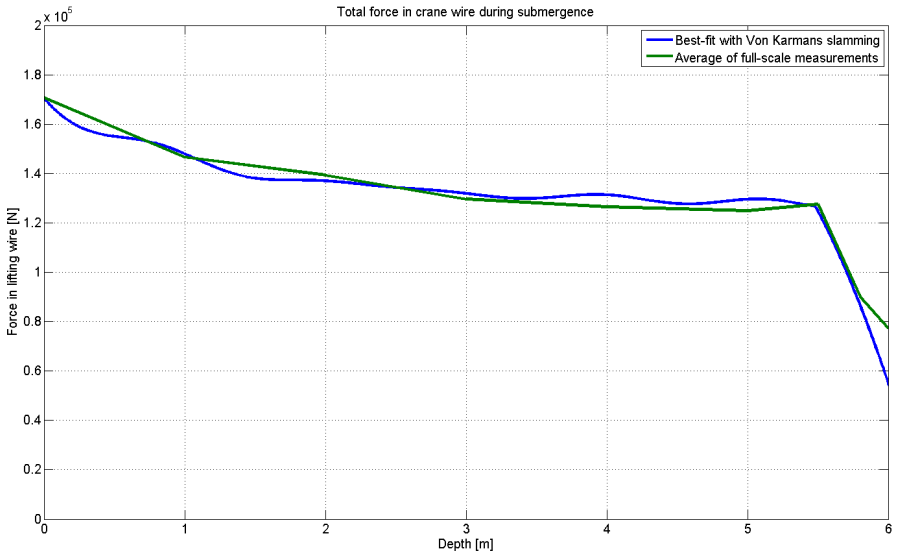

Figure 2.7: Best fit parameter study

The maximum deviation due to varying parameters discussed in chapter 2.5 are shown in table 2.2:

Effect	Max deviation %
1. Changing contraction coefficient	7.5
2. Varying velocity	5
3. Combination of 1 and 2	2.5

Table 2.2: Summary of parameter study

It can be seen that changing the contraction coefficient, vary the lowering velocity and introduce irregular waves with small amplitude in the calculations gives a good estimate for reproducing the actual data from the force measurements.

The remaining deviation of 2.5 [%] may be due to viscous effects, low sampling rate in the measurements or three dimensional (3D) effects that are not taken into account in the simplified theoretical calculations.

By varying the incoming wave heights it is seen that the dynamic air cushion pressure and thus buoyancy force is very sensitive to change in wave height and period. The results are therefore deviating from the measurements with increasing Hs above 0.1 [m]. For wave heights smaller than this, the pressure and thus force in the lifting wire is not changing much, and it is therefore concluded that the wave heights present in the measurements is $\leq 0.1[m]$ and that the JONSWAP-spectrum gives a good estimate for the measurements.

Also, since the sampling ratio of the force measurements is low, it is hard to say

if the force in the experiments is oscillating as the results obtained in figure C.6. Therefore it will be necessary to investigate pressure measurements to see if the pressure inside the suction anchor is oscillating. This is performed in chapter 3.

Due to the comparison-study Ølund Bertelsen (2013)'s model can be used in a preliminary installation analysis if the suction anchors are not subjected to large waves that will require inflow and outflow of air to the suction anchors. However, for subsea installations at the NCS it is important to evaluate the effect of waves and vessel motions on the calculations. Therefore a modification of the inflow and outflow of air through the ventilation hatch will be discussed in chapter 4.4.

3 Full-scale pressure measurements

This chapter will investigate pressure measurements performed by Sparrevik (2014) for the same suction anchor studied in chapter 2. This investigation consist of comparing pressure oscillations observed in the measurements with theoretical calculations of natural periods for systems that might have their resonant motion excited during lowering through splash zone. Oscillations of suction anchor observed in videos will also be investigated.

First the pressure measurements will be described. A sketch of the measurement equipment located on the suction anchor is shown in figure 3.1:

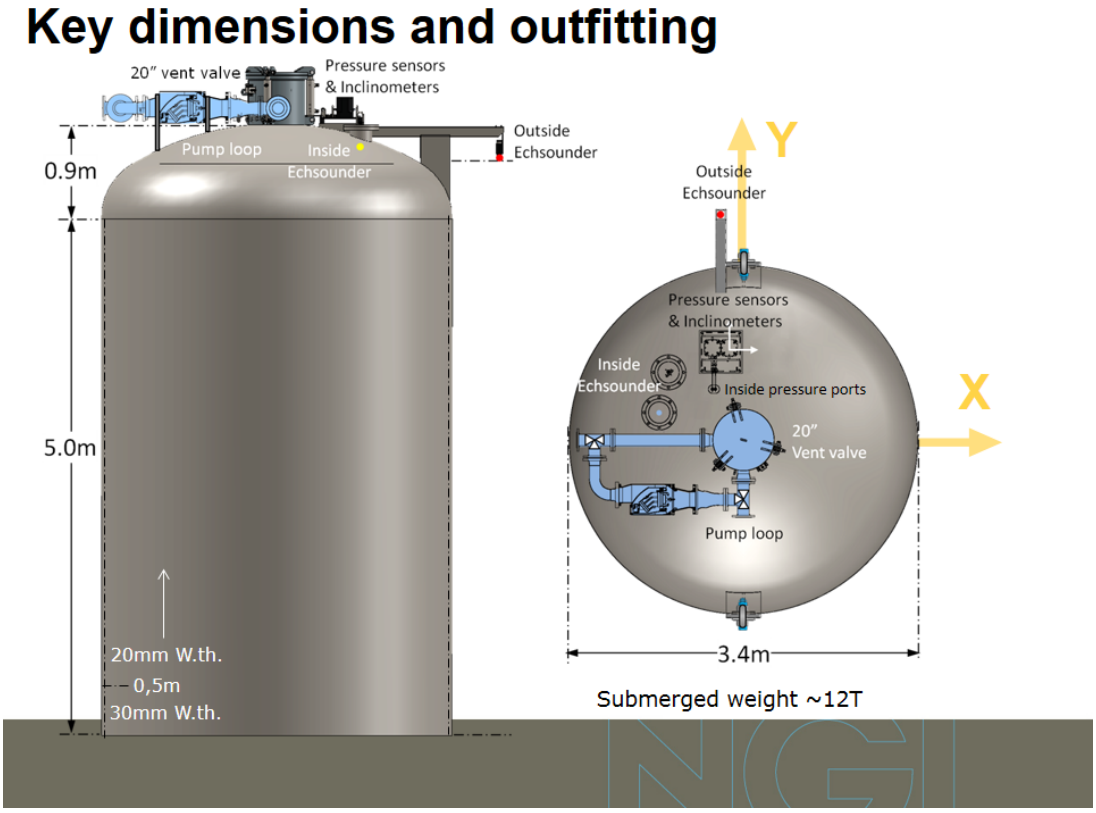

Figure 3.1: Suction anchor and equipment for pressure measurements from full-scale tests, courtesy of Sparrevik (2014)

From figure 3.1 it can be seen that pressure- and echosounder-sensors are located both inside and outside the suction anchor.
The measurements that will be studied during submergence are:

- Inner pressure
- External pressure
- Echosounder depth

These measurements are logged with a 5 [Hz] sampling frequency

3.1 Pressure oscillations

The measured pressure during splash zone transition of the suction anchor is shown in figure 3.2:

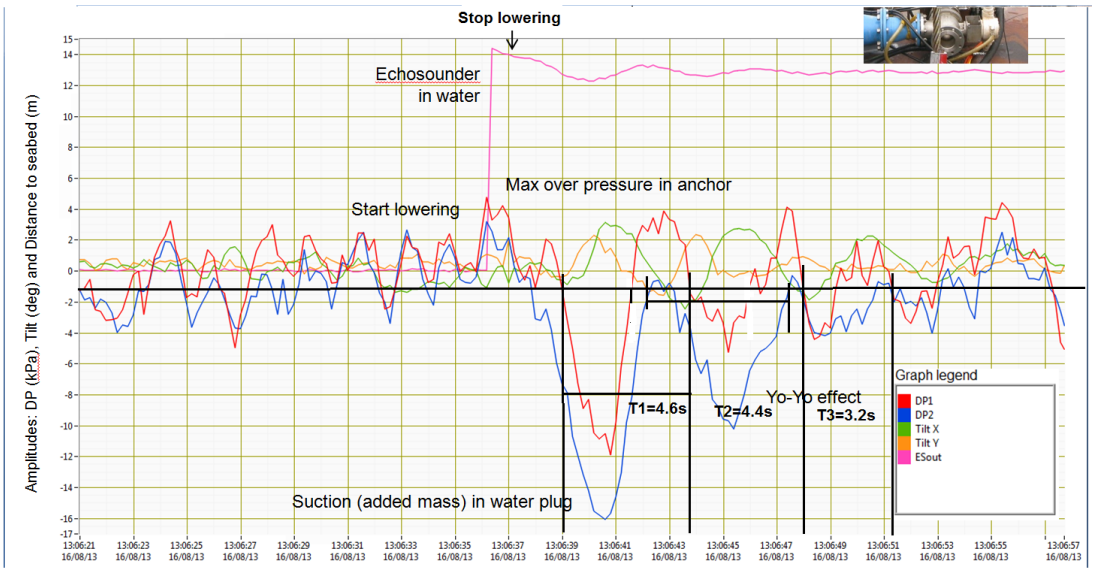

Figure 3.2: Pressure measurements from full-scale tests, courtesy of Sparrevik (2014)

In figure 3.2 the red and blue lines are of most interest. These represent the differential pressure measured between the inner and outer sensors 1 (DP-1) and 2 (DP-2) respectively. The sensors measured the absolute pressure inside and outside of the suction anchor to get the total difference in pressure. Also tilting of the anchor is shown, which is corresponding to visual observations in the videos provided by Aspelund,Leiv (2014). The tilting of the anchor is most probably due to dynamic air cushion pressure and thus buoyancy forces.

It is also seen that the pressure oscillates slightly about -1.5 [kPa] before the submergence of the suction anchor commences. This indicates that the pressure sensors have a calibration error of $\approx -1.5[kPa]$. This oscillation may also indicate that the sensors are sensitive to environmental conditions like wind fluctuations or oscillation of crane wire. However, according to Sparrevik (2014) the sensors have negligible mass and thus it should not be possible to excite resonant motion of the sensors. The oscillation periods after impact are indicated on the figure.

From figure 3.2 it is seen that the suction pressure has the largest oscillation amplitude. Large suction pressure may result in a large and downwards force contribution in the lifting wire which may be critical for the capacity of the lifting equipment.

3.1.1 Interpretation of pressure oscillations

The oscillation of the pressure after impact may indicate that resonant motion of a system is excited. To see if the pressure oscillations observed in figure 3.2 is affecting oscillation of the suction anchor videos from the lowering provided by Aspelund,Leiv (2014) will be studied.

Prior to total submergence of the suction anchor the videos show that the water inside the suction anchor impacts against the top of the suction anchor where a mixture of air and water sprays out of the ventilation hatch located on the top of the anchor. A snapshot of this phenomena is shown in figure D.1,appendix D.1.

There is also a whizzing sound from the ventilation hatch during submergence indicating that the air-flow velocity out of the ventilation hatch is large.

After impact the suction anchor starts to oscillate with a period of approximately 5 [s]. This is consistent with the measured pressure in figure 3.2 where the first oscillation period of the pressure is 4.6 [s]. In the figure this is referred to as a yo-yo motion. The observed and measured periods for one run are summarized in table 3.1:

Method	Oscillation period [s]
Visual observation	5.0
Measurements	4.6

Table 3.1: Visual and measured oscillation periods

The large oscillations after impact may indicate that the fluid inside the suction anchor starts to oscillate which again force the suction anchor to oscillate. Therefore it is interesting to investigate if the resonant motion of the oscillating fluid is excited. Here the oscillating fluid is considered to be A) the air cushion alone and B) coupled air cushion and water column or the water column alone. Two theoretical methods for calculating the natural periods of A) and B) will be performed in chapter 3.2 and 3.6 respectively.

3.2 Natural period of oscillating air cushion

An air pocket may be trapped between the water and suction anchor top at impact. If this is present resonant motion of the air cushion may be excited due to large impulse pressure from the impact.

Large oscillations are often connected with resonant motion. Faltinsen and Timokha (2009) state that "*Excitation with frequencies in the vicinity of the lowest natural frequencies of the liquid motion is of primary practical interest*". Large

oscillations due to resonant motion of air cushion may therefore influence the motion of the suction anchor. This may therefore be a possible reason for the oscillation of the suction anchor observed in the videos in addition to the large compressive (positive) and suction (negative) pressure oscillations observed in figure 3.2.

This chapter will make a theoretical investigation if resonant motion of the air cushion is excited at impact. The natural period of the air cushion will then be calculated based on an approach using theory for sloshing and oscillating air pockets inside a liquid cargo tank as described in Faltinsen and Timokha (2009). This will then be compared with the oscillation period of the pressure measured in figure 3.2.

When using the approach with the oscillating air pockets inside a liquid cargo tank a description of phenomena related to sloshing must be given. According to Braeunig et al. (2009) these phenomena can be described as shown in table 3.2:

• Evacuation of air from the air cushion through the ventilation hatch which will lead to a momentum transfer between the water and the air.
• If the air is not evacuated sufficiently the air may be partially entrapped as bubbles or pockets.
• At impact there will be a rapid change of momentum of the water which is forced to adapt its shape to avoid the obstacle.
• Creation of shock waves due to pressure waves within the water and strain waves within the top. This happens when the density ratio is low or when the compressibility modulus of the gas is low.

Table 3.2: Description of impact phenomena

These different phenomena can occur when the inner wave elevation impacts against the suction anchor top during splash zone transition.

Adopting the approach from Faltinsen and Timokha (2009) for calculating the natural period of the air cushion the following assumptions are made:

- it is assumed that the water compressing the air cushion is incompressible
- the air cushion is a perfect gas
- the air cushion is to be compressed in quasi equilibrium
- the air cushion pressure is uniform
- the air cushion moves with a constant velocity

Due to these assumptions the air-water surface is uniform and the motion of the air cushion can be simplified as a one dimensional (1D) piston mode according

to Faltinsen and Timokha (2009).

This piston mode of air pockets was first studied by Bagnold (1939) during impact between a breaking wave and a vertical wall. The "Bagnold" model is shown in figure 3.3:

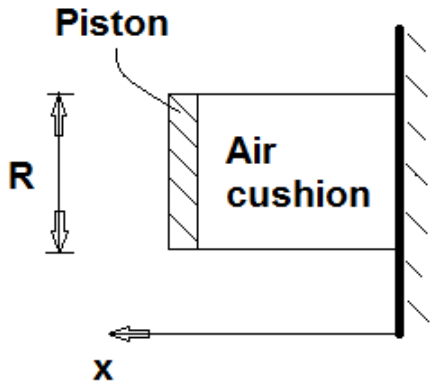

Figure 3.3: Definitions in a Bagnold-type air cushion model

This model will be used by rotating it 90 degrees so that the one dimensional vertical motion of the air cushion during splash zone transition is represented. The procedure of calculating the natural period of the oscillating air cushion will be derived in chapter 3.3.

3.3 Continuity equation for the air cushion

Similar to the approach for calculating the dynamic air cushion pressure as summarized in chapter 2.2 the continuity equation defined in equation 2.4 will be used to describe the behaviour of the air cushion pressure during splash zone transition. Since it is the natural period which is of interest, damping is neglected, such that the air leakage term on the left hand side in equation 2.4 can be removed. The continuity equation is then represented by equation 3.1:

$$\rho_c \dot{\Omega}_c + \dot{\rho}_c \Omega_c(t) = 0 \tag{3.1}$$

By assuming small oscillations for the air cushion steady state conditions apply. Then a harmonic time dependence can be applied such that all time varying terms can be represented in terms of $e^{i\omega t}$. Then the air cushion pressure can be expressed by equation 3.2:

$$P_c = P_0 + P_1 e^{i\omega t} \tag{3.2}$$

Similar to theory for oscillating air pockets inside a liquid cargo tank studied in Faltinsen and Timokha (2009) P_0 is the initial pressure in the air cushion. In this way the initial pressure in the air cushion can be studied at different time instants. $P_1 e^{i\omega t}$ is the dynamic part of the air cushion pressure.

For finding the density of the air cushion it is assumed that no heat is exchanged during the splash zone transition. The relationship between the air cushion pressure and density will then be adiabatic as shown in equation 3.3:

$$\frac{P_c}{P_0} = \left(\frac{\rho_c}{\rho_0}\right)^{\gamma_a} \tag{3.3}$$

Where

- ρ_0 is the density of the air cushion at the initial time of creation of the air pocket
- ρ_c is the density of the air cushion mass

By rearranging equation 3.3 in terms of the densities the adiabatic expression is represented with equation 3.4:

$$\left(\frac{\rho_c}{\rho_0}\right) = \left(\frac{P_c}{P_0}\right)^{\frac{1}{\gamma_a}} \tag{3.4}$$

By assuming small oscillations of the air cushion this equation can be linearized. Using the expression for P_c in equation 3.2 the linearization is performed by setting $x = P_1 e^{i\omega t}$ and $F(x) = \left(\frac{P_c}{P_0}\right)^{\frac{1}{\gamma_a}} = \left(1 + \frac{x}{P_0}\right)^{\frac{1}{\gamma_a}}$ and differentiate with respect to x such that F'(x) can be expressed with equation 3.5:

$$F'(x) = \frac{1}{\gamma_a P_0}\left(1 + \frac{x}{P_0}\right)^{\frac{1}{\gamma_a}-1} \tag{3.5}$$

Further a Taylor-series expansion is performed where higher order terms are neglected and F(x) will be determined by equation 3.6:

$$F(x) = F(0) + F'(x)|_{x=0}(x - 0) \tag{3.6}$$

By inserting equation 3.5 into equation 3.6 the linearized adiabatic relationship between the density and pressure of the air cushion can be represented by equation 3.7:

$$\frac{\rho_c}{\rho_0} = 1 + \frac{P_1 e^{i\omega t}}{\gamma_a P_0} \tag{3.7}$$

By differentiating with respect to time the following expression for the rate of change of time of the air cushion density is obtained in equation 3.8:

$$\dot{\rho_c} \approx \frac{\rho_0}{\gamma_a}\frac{i\omega P_1 e^{i\omega t}}{P_0} \tag{3.8}$$

For finding the volume rate of change of time it the piston motion assumes that the air cushion inside the suction anchor moves like thin disk with uniform velocity $Ve^{i\omega t}$ bounded by the radial extension of the suction anchor. This results in a simplified rate of change of time of the volume shown in equation 3.9:

$$\dot{\Omega}_c \sim A_c V e^{i\omega t} \tag{3.9}$$

Where three-dimensional added mass in heave of air cushion (A_{33c}). Then the continuity equation can be written as shown in equation 3.10:

$$\rho_0 V A_c + \frac{\rho_0}{\gamma_a} \frac{i\omega P_1}{P_0} \Omega_0 = 0 \tag{3.10}$$

Where Ω_0 is the initial air cushion volume.

According to Faltinsen and Timokha (2009) a forced oscillation of the disk with velocity $Ve^{i\omega t}$ cause a vertical force $A_{33c} i\omega \dot{V} e^{i\omega t}$ acting on the disk. This force is found by integrating the dynamic pressure on the wetted part of the disk. Applying equilibrium on the surface of the disk, requires that the dynamic water pressure is the same as $P_1 e^{i\omega t}$ which can be approximated as a uniform pressure due to the force as shown in equation 3.11:

$$P_1 e^{i\omega t} = \frac{A_{33c} i\omega \dot{V} e^{i\omega t}}{\pi \left(\frac{D}{2}\right)^2} = \frac{A_{33c} i\omega \dot{V} e^{i\omega t}}{A_c} \tag{3.11}$$

By differentiating equation 3.11 with respect to time and inserting into equation 3.10 the continuity equation is finally shown in equation 3.12:

$$\rho_0 V A_c - \frac{\rho_0}{\gamma_a} \frac{A_{33c}\omega^2}{A_c P_0} \Omega_0 = 0 \tag{3.12}$$

By rearranging equation 3.12 the natural frequency of the oscillating air cushion can be calculated with equation 3.13:

$$\omega_c = A_c \sqrt{\frac{\gamma_a P_0}{A_{33c}\Omega_0}} \tag{3.13}$$

P_0 is the sum of the atmospheric pressure and the dynamic air cushion pressure found from numerical integration of equation 2.6. The MATLAB-code developed by Ølund Bertelsen (2013) will be further modified and used for calculating the natural frequency of the air cushion and can be seen in appendix G.1.

A_{33c} can be calculated with the sink-source software WAMIT. This is described in chapter 3.4.

3.4 Heave added mass of air cushion with WAMIT

A simplified calculation of the added mass of the air cushion can be made by modelling the intersection between the air cushion and inner wave elevation as a

disk inside the suction anchor. After impact this disk will oscillate close to the surface. Due to only small waves present at the full-scale test, the added mass of the disk can be evaluated at infinite wave frequency. Then the added mass can be evaluated by solving the radiation problem in heave. This will be performed with WAMIT and the theory used in WAMIT will be briefly described in chapter 3.4.1.

3.4.1 WAMIT-theory

WAMIT is based on potential theory and calculates hydrodynamic coefficients for floating and submerged objects subjected to ocean waves. This will be explained in chapter 3.4. WAMIT is based on linear and second order potential theory for floating and submerged bodies subject to waves. For evaluating the natural period of the air cushion with equation 3.13 A_{33c} must be calculated with no incident waves present. Then there will be no disturbance from diffracted waves such that only the radiation problem in heave needs to be solved in infinite fluid. This means that the added mass is found at the boundary where $\omega \to \infty$.

Of special importance for the calculations of the added mass of the air cushion is the appropriate free surface condition. As mentioned the fluid is assumed infinite with the top of the suction anchor being surrounded by a free surface with the velocity potential $\phi = 0$ as boundary condition. According to *WAMIT user manual* (2006), chapter 12 the Green function, which is used for solving inhomogeneous boundary value problems, will ensure that this boundary condition is automatically satisfied. The integral equations used for the boundary conditions are also described in *WAMIT user manual* (2006).

WAMIT must be run either in terminal window with a command prompt or by utilizing a BATCH file.

According to Li (2014) it is assumed that WAMIT's low-order method is sufficient for calculating the added mass of the disk inside the suction anchor. Then according to *WAMIT user manual* (2006) the geometry of the suction anchor should represented by flat quadrilateral panels. The geometry file used to model a mesh of the suction anchor and air cushion are described in chapter 3.4.2.

3.4.2 Suction anchor geometry file

A three dimensional (3D) model of the suction anchor is created with the 3D-modelling software Multisurf. According to Aerohydro (2014) a built-in function in Multisurf for exporting the 3D-coordinates of the corner points of the panels can be used to transform the model to a low-order Geometrical Data File (GDF) file. This is required for WAMIT to be able to do a low-order analysis of the model.

The mesh used in the calculations are quadrilateral panels and the Multisurf-model of the suction anchor is shown in figure 3.4:

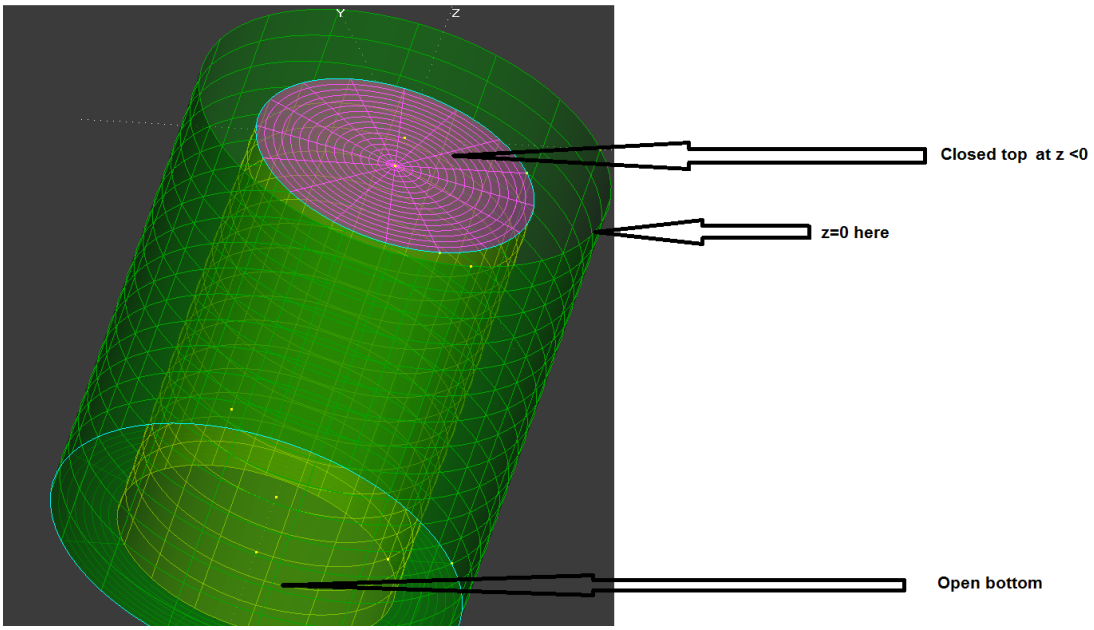

Figure 3.4: Suction anchor geometry used in WAMIT

In figure 3.4 the origin of the coordinate system is located in the center of the top of the suction anchor at the free surface. Also, in this figure the thickness between the inner and outer cylinder is exaggerated for visualisation purposes. In the calculations the thickness is $<< 1$, and will not contribute to the results. It is only defined for proper modelling of water inside the suction anchor.

The green outer surface of the anchor representing the suction anchor walls is defined with the normal vector pointing outwards into the surrounding fluid. The yellow inner surface representing the water inside the suction anchor is defined with the normal vector pointing inwards. The water surface is bounded above by the air cushion. The interface between the water and air cushion is defined as a pink disk and has a normal vector pointing downwards into the fluid.

For saving calculation time the x- and y-symmetry of the suction anchor is exploited requiring only one quarter of the model shown in figure 3.4 to be defined.

The remaining input files for running WAMIT are described in chapter 3.4.3.

3.4.3 Input files for WAMIT

According to *WAMIT user manual* (2006) the calculations in WAMIT are performed with the two subprograms POTEN and FORCE. POTEN will solve the radiation problem in heave by approximating the solution for the velocity potential by piecewise constant values on each of the panels. FORCE will use the

radiation velocity solved found by POTEN to calculate the added mass in heave of the interface between the air cushion and water.

A short description of the necessary input files for running POTEN and FORCE correctly are listed below. The complete files are attached in appendix D.3.

- aircushion.gdf - Geometry Data File. Describes the mesh-geometry of the suction anchor and air cushion surface to be analyzed in WAMIT.
- anchor.ms2 - Multisurf geometry file. This is described in chapter 3.4.2.
- aircushion.pot - Potential Control File. Inputs different parameters to POTEN. According to *WAMIT user manual* (2006) two alternative forms are available for this file where the second alternative form is used in this file. Here the IRAD-option is set to 1 while the IDIFF-option is set to -1 due to only solving the problem for the radiation velocity potential. This file also define the periods in which the velocity potential shall be evaluated for.
- aircushion.frc - Force Control File. Controls the parameters to FORCE. Similar to the Potential Control File two alternative forms exist for this file, where the first alternative form is used for this file.
- aircushion.cfg - Configuration file. Specifies various parameters and options to be used in the analysis.
- fnames.wam - Contains a list of all files that shall be used in the WAMIT-analysis.
- aircushion.out - Stores the output data. Here the normalized added mass values with respect to density are saved for the specified periods defined in the Potential Control File.

A more extensive description of how the input files are set up can be found in *WAMIT user manual* (2006).

The added mass calculations with WAMIT will first be verified against analytical results for a thin disk oscillating in the surface. The added mass results for the thin disk and suction anchor with air cushion are discussed in chapter 3.4.4.

3.4.4 Added mass-results from WAMIT-calculations

For a thin disk oscillating far from the surface the added mass in heave is found from Newman (1977), figure 4.8 to be:

$$A_{33,disk} = \frac{8}{3}\rho r^3 \tag{3.14}$$

Where $A_{33,disk}$ is the three-dimensional added mass in heave of a thin disk. When the disk is oscillating in the free surface $A_{33,disk}$ is only half of the value in equation 3.14 due to only the bottom of the disk being wet. This value will be used as reference value to verify the calculations in WAMIT. This will also verify that all the input files to WAMIT are properly made.

A comparison of the added mass of the disk calculated with WAMIT is shown in figure 3.5 where the added mass is normalized as $\frac{A_{33}}{A_{33,disk}/2}$:

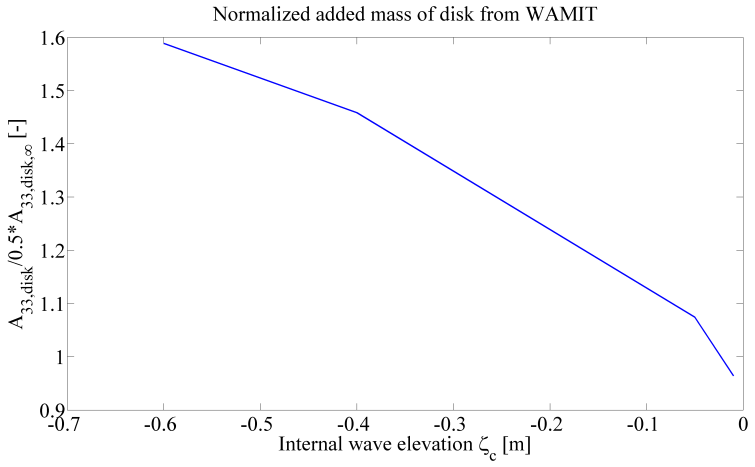

Figure 3.5: Normalized added mass of disk close to surface

Now the added mass for the circular disk has been verified and the model of the suction anchor shown in figure 3.4 can be analyzed. The distance between the air cushion and the free surface at impact must be specified when calculating the added mass of the air cushion.

3.5 Results for calculation of natural period of air cushion

From figure 2.4 the impact occurs at a draught of 5.6 [m] corresponding to ζ_c=-0.42 [m]. The added mass found from WAMIT corresponding to the air cushion and suction anchor at impact is equal to $7.8\frac{A_{33,disk}}{2} = 52.5[tonnes]$. This value seems very high for the air cushion alone. The added mass calculated with this approach will also have influence from the suction anchor when integrating the dynamic pressure around the wetted surface of the suction anchor. This can be explained by considering the oscillation of the air cushion with no waves present. Then intuitively the suction anchor should also be oscillating. Therefore the added mass calculations will not be for the oscillating air cushion alone, but also including a contribution from the suction anchor.

However, when knowing the added mass for the air cushion all the terms in

equation 3.13 are known such that ω_c can be calculated for any submergence level. By using the values for the pressure and added mass at impact as discussed in chapter 3.4.4 and using equation 3.15 the natural period of the air cushion (T_c) can be found:

$$T_c = \frac{2\pi}{\omega_c} \tag{3.15}$$

Where ω_c is the natural frequency of air cushion. The resulting natural period for the oscillating air cushion is found to be T_c=1.1 [s].

This is much lower than the period measured from the pressure oscillations and visual observations after impact shown in table 3.1. Comparing the mass of the air cushion with the weight of the suction anchor one could also argue if the air cushion will be able to excite a yo-yo motion of the suction anchor. From Ølund Bertelsen (2013), equation 8 the air cushion volume at impact is 7.2 [m^3] which corresponds to a mass of 8.8 [kg]. Since the mass of the suction anchor in air is 12900 [kg] it is unrealistic that the oscillating air cushion will be able to excite the observed yo-yo motion of the suction anchor after impact.

To evaluate the added mass calculated with WAMIT a comparison with the added mass corresponding to trapped water inside the suction anchor can be performed. The three-dimensional added mass in heave of entrapped water inside suction ($A_{33,trappedwater}$) can be calculated with equation 3.16:

$$A_{33,trappedwater} = \rho_w g A_c H \tag{3.16}$$

$A_{33,trappedwater}$ is found to be 54.9 [tonnes] which is close the value for the suction anchor and inner water surface obtained from WAMIT. Therefore, it is doubtful if the added mass found for the model shown in figure 3.4 can be used when calculating the natural period for the air cushion in equation 3.13. However, this added mass might be used for piston mode of an oscillating water column.

Since it has been shown that resonant motion of air cushion most likely is not excited at impact it will be interesting to see if a piston mode of the water column inside the suction anchor is oscillating and if this is the source for the oscillations shown in figure 3.2. However, the air cushion might have some influence on the piston mode of the water column. Therefore the natural period of the oscillating water column in addition to the natural period of the coupled oscillating water column and air cushion after impact will be calculated in chapter 3.6.

3.6 Natural period of oscillating liquid inside suction anchor

In the previous chapter it was shown that the natural period of the oscillating air cushion was much lower than the period of the yo-yo motion of the pressure

measurements given by Sparrevik (2014). This shows that oscillation of the air cushion alone cannot cause this yo-yo motion. It is therefore necessary to evaluate if the water column together with the air cushion or water column alone inside the suction anchor can start to oscillate and cause oscillation of the suction anchor.

To investigate the oscillation of the water column an approach similar to the eigenvalue problem for slow oscillations of water in a cylindrical well analyzed by Miles (2002) will be performed. Miles (2002) use a linearized potential theory for solving the problem in a vertical well with boundary conditions as follows:

- The top of the water is a free surface with atmospheric pressure.
- The bottom is a semi infinite reservoir formulated such that the depth of the well is large compared with its width.

The calculation-model can be seen in figure 3.6:

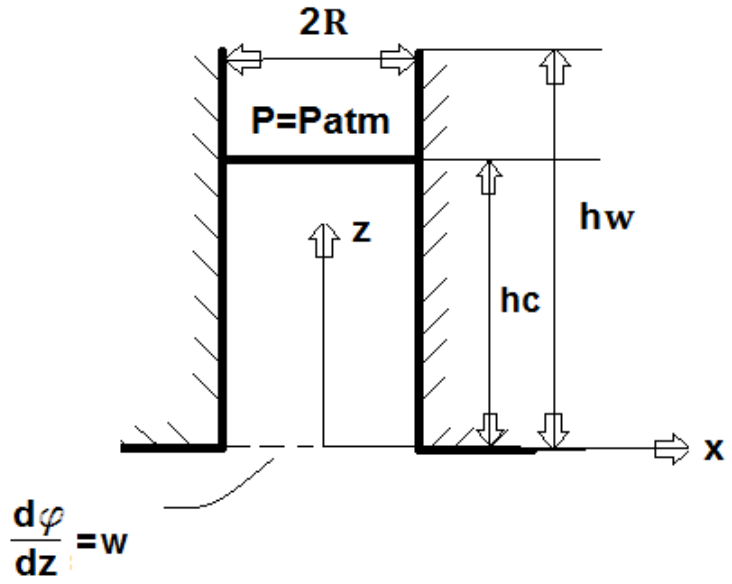

Figure 3.6: Calculation model for piston mode of water column inside suction anchor

In figure 3.6:

- h_w is the height of well
- h_c is the the instantaneous vertical position of the water surface

Here slow oscillations is considered such that the natural frequency of the liquid inside one well $\omega_w^2 << \frac{g}{R}$. This requires that $h_w >> R$ such that the fluid motion

is well described by the dominant rigid body motion according to Miles (2002). This means that the water in the well will move like a piston vertically.

For the suction anchor and the inner water column some difference from the model shown in 3.6 must be stated:

- the coordinate system is defined with the origin at the top of the water surface
- the radius of suction anchor is not $<< h_w$
- the water is bounded above by the air cushion pressure

Therefore the method developed by Miles (2002) will be a simplification of the water column inside the suction anchor, and it is assumed that using this approach will be able to describe the dominant rigid body motion of the water column.

A derivation of the appropriate boundary conditions for the suction anchor and water column will be performed in chapter 3.6.1.

3.6.1 Boundary conditions for water motion inside suction anchor

For the model shown in figure 3.6 potential theory will be used to describe the water motion within the boundaries. For water fluid velocity vector $\mathbf{V}(x, y, z, t)$ to be completely described by potential theory the water is assumed incompressible such that $\nabla \mathbf{V} = 0$ according to Faltinsen (1990). The water is also assumed irrotational and inviscid. Expressing $\mathbf{V}$ by a velocity potential (ϕ) at time t and in the Cartesian coordinates x,y,z can be shown in equation 3.17:

$$\mathbf{V} = \nabla\phi = \mathbf{i}\frac{\partial\phi}{\partial x} + \mathbf{j}\frac{\partial\phi}{\partial y} + \mathbf{k}\frac{\partial\phi}{\partial z} \tag{3.17}$$

The governing equation for finding a velocity potential which satisfies these conditions is the Laplace equation shown in equation 3.18:

$$\nabla^2\phi = \frac{\partial^2\phi}{\partial x^2} + \frac{\partial^2\phi}{\partial y^2} + \frac{\partial^2\phi}{\partial z^2} = 0 \tag{3.18}$$

Since 1D vertical piston motion of the water column is assumed, the Laplace equation is reduced to equation 3.19:

$$\nabla^2\phi = \frac{\partial^2\phi}{\partial z^2} = 0 \tag{3.19}$$

The pressure is found from the Bernoulli equation given in equation 3.20:

$$p = -\rho\frac{\partial\phi}{\partial t} - \rho g z - \frac{\rho}{2}\mathbf{V}\mathbf{V} + C_p \tag{3.20}$$

Where:

- p is the total water-pressure defined by Bernoulli's equation
- C_p is an arbitrary function of time

The water in the suction anchor is bounded above by the air cushion pressure. According to Faltinsen (1990) the dynamic free-surface condition can be found by setting the water pressure equal to the air cushion pressure defined in equation 3.2. Now steady state conditions is applied similar to chapter 3.2 such that a harmonic time dependence can be assumed. Then the static pressure expressed with Bernoulli's equation can be written as shown in equation 3.21:

$$\frac{p}{\rho_w} = -\frac{\partial\phi}{\partial t} - gz - \frac{1}{2}\underbrace{\mathbf{V}\mathbf{V}}_{=\nabla^2\phi} + \frac{P_0}{\rho_w} = \frac{P_0}{\rho_w} + \frac{P_1 e^{i\omega t}}{\rho_w} \tag{3.21}$$

Here $z = h_c$ and by using the result obtained in equation 3.19 the expression for the dynamic free surface condition is obtained in equation 3.22:

$$g h_c + \frac{\partial\phi}{\partial t} + \frac{P_1 e^{i\omega t}}{\rho_w} = 0 \tag{3.22}$$

According to Faltinsen (1990) the water particles on the surface always stays on the surface, resulting in the kinematic free surface condition in equation 3.23:

$$\frac{\partial h_c}{\partial t} = \frac{\partial\phi}{\partial z} \tag{3.23}$$

To find an expression for the velocity potential the dynamic free surface condition in equation 3.22 must be differentiated with respect to time and inserted into the expression for $\frac{\partial h_c}{\partial t}$ into the kinematic free surface condition in equation 3.23 such that the combined free surface condition can be written as shown in equation 3.24:

$$\frac{\partial^2\phi}{\partial t^2} = -\frac{1}{g}\left[\frac{i\omega P_1 e^{i\omega t}}{\rho_w} + \frac{\partial\phi}{\partial z}\right] \tag{3.24}$$

On the instantaneous wetted body surface the body boundary condition is satisfied and can be written as shown in equation 3.25:

$$\frac{\partial\phi}{\partial z} = V e^{i\omega t} \tag{3.25}$$

Where $V e^{i\omega t}$ is the body velocity in the vertical direction. The velocity potential can be expressed by an imaginary exponential as shown in equation 3.26:

$$\phi = \phi_p e^{i\omega t} \tag{3.26}$$

Where ϕ_p is the piston mode velocity potential. By differentiating equation 3.26 with respect to time and inserting this together with equation 3.25 into equation 3.24 the velocity potential at the surface can be represented by equation 3.27:

$$\phi_p = \frac{1}{\omega^2}\left[g\dot{\eta}_3 + \frac{i\omega P_1 e^{i\omega t}}{\rho_w}\right] \tag{3.27}$$

The bottom boundary condition is the same as in equation 3.25, so the total velocity potential satisfying the boundary conditions given in equation 3.22 and 3.25 can be expressed with equation 3.28:

$$\phi_p = V\left(z - h_c + \frac{g}{\omega^2}\right) + \frac{1}{\omega^2}\frac{i\omega P_1 e^{i\omega t}}{\rho_w} \tag{3.28}$$

When finding the natural frequency the dynamic part of the air cushion pressure $P_1 e^{i\omega t}$ must be linearized. This can be done by using an adiabatic relationship between pressure and volume as shown in equation 3.29:

$$\frac{\Omega_0}{\Omega_c} = \left(\frac{P_c}{P_0}\right)^{\frac{1}{\gamma_a}} = \left(1 + \frac{P_1 e^{i\omega t}}{P_0}\right)^{\frac{1}{\gamma_a}} \tag{3.29}$$

A Taylor-series expansion for $P_1 e^{i\omega t}$ can be performed similar to that for the mass density of the air cushion shown in the equations 3.5 to 3.7. Then the linearized adiabatic relationship between the dynamic air cushion pressure and air cushion volume is represented by equation 3.30:

$$\frac{\Omega_0}{\Omega_c} = 1 + \frac{P_1 e^{i\omega t}}{\gamma_a P_0} \tag{3.30}$$

By taking the time derivative of equation 3.30 the expression for linearized the dynamic air cushion pressure can be written as shown in equation 3.31:

$$i\omega P_1 e^{i\omega t} = -\frac{\gamma_a P_0 \Omega_0 \dot{\Omega}_c}{\Omega_c^2} \simeq -\frac{\gamma_a P_0 \dot{\Omega}_c}{\Omega_0} \tag{3.31}$$

Here the air cushion is assumed to be studied at impact, therefore $\Omega_c \simeq \Omega_0$. For a constant lowering velocity the time rate of change of the air cushion volume can be approximated as $\dot{\Omega}_c \simeq -A_c V e^{i\omega t}$. Now the linearized dynamic air cushion pressure can be written as shown in equation 3.32:

$$i\omega P_1 = \frac{\gamma_a P_0 A_c V}{\Omega_0} \tag{3.32}$$

By inserting equation 3.32 into equation 3.28 the velocity potential is obtained in equation3.33:

$$\phi = V\left(z - h_c + \frac{g}{\omega^2}\right) + \frac{1}{\omega^2}\frac{\gamma_a P_0 A_c V}{\Omega_0 \rho_w} \tag{3.33}$$

According to Miles (2002) this equation is valid for a circular cylinder where the radial and vertical extension for the fluid is limited by $0 < r < \frac{D}{2}$ and $0 \leq z \leq h_c$ respectively.

3.6.2 Derivation of piston mode-natural frequencies

Miles (2002) integrated the total impulse $\int\int \phi dS$ and obtained a linear and homogeneous equation for the frequency. By integrating equation 3.33 and using the expression obtained by Miles (2002) the following linear and homogeneous equation is obtained as shown in equation 3.34:

$$\left[\delta\left(h_c - \frac{g}{\omega^2} - \frac{\gamma_a P_0 A_c}{\rho_w \omega^2 V_0}\right) + \frac{4D}{3\pi}\right]\frac{D}{2}V = 0 \tag{3.34}$$

Where δ is the kronecker delta function and is equal to 1 for a single cylinder which is the case in this thesis. By rearranging this equation the natural frequency of the coupled piston mode between air cushion and water column, $\omega_{coupled}$ is obtained in equation 3.35:

$$\omega^2_{coupled} = \frac{g + \frac{\gamma_a P_0 A_c}{\rho_w \Omega_0}}{\frac{4D}{3\pi} + h_c} \tag{3.35}$$

The natural frequency for the piston mode of the water column alone is found by setting $P_0 = 0$.

The dynamic air cushion pressure can also be linearized in terms of the added mass in heave of the water column inside the suction anchor, A_{33w}. This can be done by differentiating the added mass for the air cushion found in equation 3.11 with respect to time. By replacing $A33_c$ with $A33_w$ the dynamic air cushion pressure can be expressed with equation 3.36:

$$i\omega P_1 e^{i\omega t} = \frac{A33_w \ddot{V}}{A_c} = -\omega^2 \frac{A33_w V e^{i\omega t}}{A_c} \tag{3.36}$$

By inserting equation 3.36 into equation 3.32 and using this in equation 3.33 to equation 3.34 the natural frequency of coupled piston mode between air cushion and water column in terms of heave added mass, can be calculated with equation 3.37:

$$\omega^2_{coupled,A33} = \frac{g}{\frac{4D}{3\pi} + h_c - \frac{A33_w}{\rho_w A_c}} \tag{3.37}$$

It can be shown that equation 3.37 is equivalent with 3.35. This is performed by expressing the added mass from equation 3.13. By substituting $A33_w$ for the added mass of the air cushion, the following expression is obtained:

$$A33_w = \frac{A_c^2 \gamma_a P_0}{\omega^2_{coupled} \Omega_0} \tag{3.38}$$

By inserting equation 3.38 into equation 3.37 the same expression for the natural frequency as shown in equation 3.35 is obtained. This result shows that the calculation of the natural frequency with the method in Miles (2002) and the method by Faltinsen and Timokha (2009) described in chapter 3.2 are equivalent for the coupled piston mode of the air cushion and water column. It is therefore assumed that natural frequency calculated with 3.35 will give a good estimate for this simplified case. The results for the natural frequency calculated with the different approaches discussed in this chapter are shown in chapter 3.6.3.

3.6.3 Results for natural period calculations of water inside suction anchor

In this chapter the results for the natural period of the following three approaches described in chapter 3.6 will be presented:

- I) piston mode of the coupled air cushion and water column in terms of dynamic air cushion pressure
- II) the same as I) calculated in terms of added mass
- III) piston mode of water column alone

Case I) investigate how much the presence of air cushion above the water surface will affect the results compared with case III) where the water is bounded above by the atmospheric pressure. The result for case III) is found by setting the second term in the numerator in equation 3.35 equal to zero. For case II) the heave added mass for the coupled piston mode calculated with WAMIT will be used. The added mass calculated with WAMIT in chapter 3.4.4 will be used for this purpose.

The natural periods for case I) and III) calculated with equation 3.35 are plotted versus depth in figure 3.7:

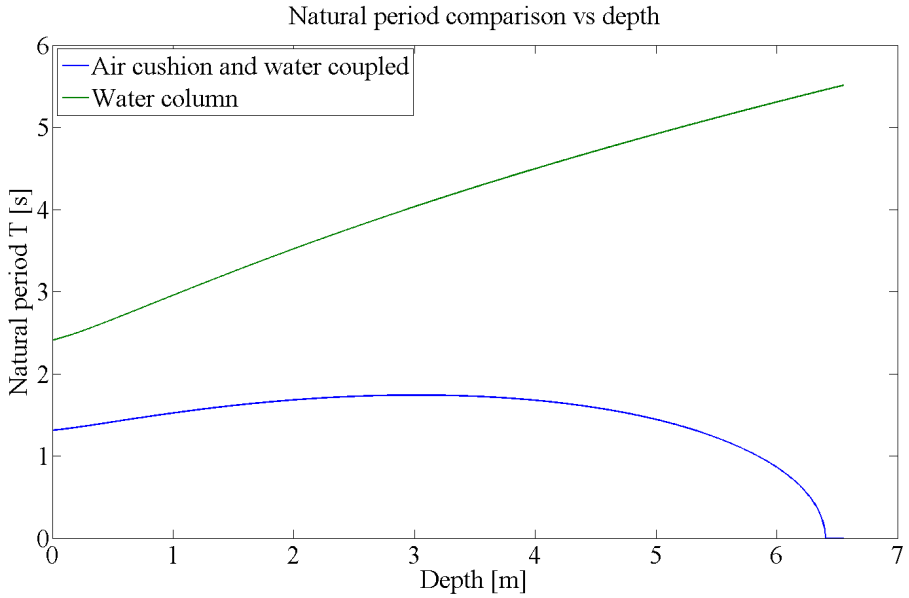

Figure 3.7: Calculation of natural periods with Miles (2002)' approach for piston mode of fluid inside suction anchor

From figure 3.7 it is seen that the air cushion pressure affect the natural period significantly. The results for case I) - III) are shown in table 3.3:

Piston modes	Natural period [s]
Coupled air cushion and water column	1.2
Water column (No coupling)	5.2
Coupled air cushion and water with added mass	2.0

Table 3.3: Natural periods of oscillating air-water surface

For case III) the added mass is calculated in infinite fluid with WAMIT. Then it is assumed that the coupled inner fluid is oscillating while the water surrounding the suction anchor is assumed still with no waves as $T \to 0$. To check the validity of this assumption an iteration process using the obtained natural period as input of the wave period to the added mass calculations in WAMIT. Then the new added mass corresponding to this period can be used to calculate the natural period with equation 3.37. The converged natural period should then go towards zero.

The obtained natural period from the convergence study is 1.96 [s], thus the assumption of infinite fluid does not seem to be correct. By considering the lowering videos and waves generated post impact, it is seen that the waves are very small with periods lower than the converged period. Therefore the calculation of added mass of the piston mode of the coupled fluid inside the suction anchor as $T \to 0$ with the linear theory applied in WAMIT may not be sufficient.

A discussion of damping mechanisms that may be relevant for the simplified piston mode models developed in this chapter and for the air cushion in chapter 3.2 will be described in chapter 8.2.

3.7 Comparison between inner pressure measurements and theoretical calculations

In a later stage during this thesis work, additional results from the lowering of the full scale suction anchor as described in chapter 2 have been made available. With respect to oscillation of the air cushion it will be more relevant to study the inner pressure than the differential pressure shown in figure 3.2. This will therefore be analysed in this chapter.

To investigate if the air cushion or water inside the suction anchor will start to oscillate after impact, measurements of the inner pressure provided by Sparrevik (2014) will be studied. The inner pressure measured for one run is shown in figure 3.8:

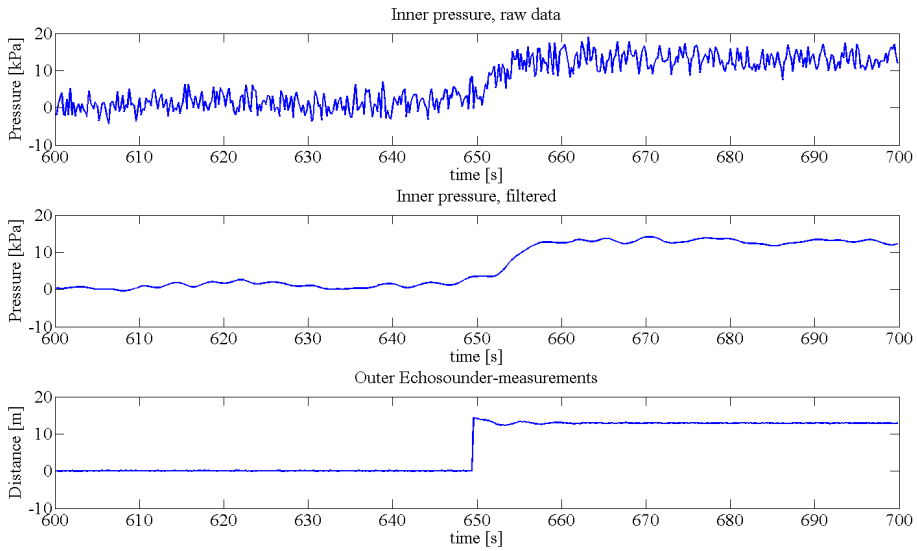

Figure 3.8: Measurements of inner pressure and echo-sounder from full-scale tests, courtesy of Sparrevik (2014)

In the upper figure it is seen that there are some high frequency noise in the raw-data measurements that should be filtered out to better read off the pressure characteristics. This is filtered out with a low-pass 4^{th} order Butterworth-filter as shown in the middle part of figure 3.8. To avoid down-folding the cut-off frequency must be atleast two times the sampling frequency according to Sverre Steen (2013). Here a normalized cut-off frequency of 0.2 according guidelines given in Mathworks (2014a) has been used. To be able to capture the largest

peaks when the noise is filtered out a sensitivity study with different cut-off frequencies has been performed.

The lowest part of figure 3.8 shows the measurements from the outer echo-sounder which measures the water depth by sending out sound waves towards the bottom. When the echo-sounders are in air the depth measured is zero. The figure also shows that the outer echo-sounder starts measuring when it touches the water at just before 650 [s]. This is indicated by the large peak when the depth increases.

The videos provided by Aspelund,Leiv (2014) show that the lowering of the suction anchor is stopped almost right after total submergence. Also the distance from the echo-sounders to the top of the suction anchor is very small as shown in figure 3.1. Therefore the time from when the echo-sounder touches the water until impact is very small. Considering the oscillations in the echo-sounder measurements right after the peak in the depth it is indicated that the anchor has stopped and is oscillating. However, the exact time of stopping is not given from this graph.

3.7.1 Investigation of inner and outer pressure oscillations

The measured inner and outer pressure will now be plotted together to see how the amplitude of the pressures are relative to each other and to investigate their oscillations as shown in figure 3.9. Also the signal from the echo-sounder is included to show when the lowering has stopped.

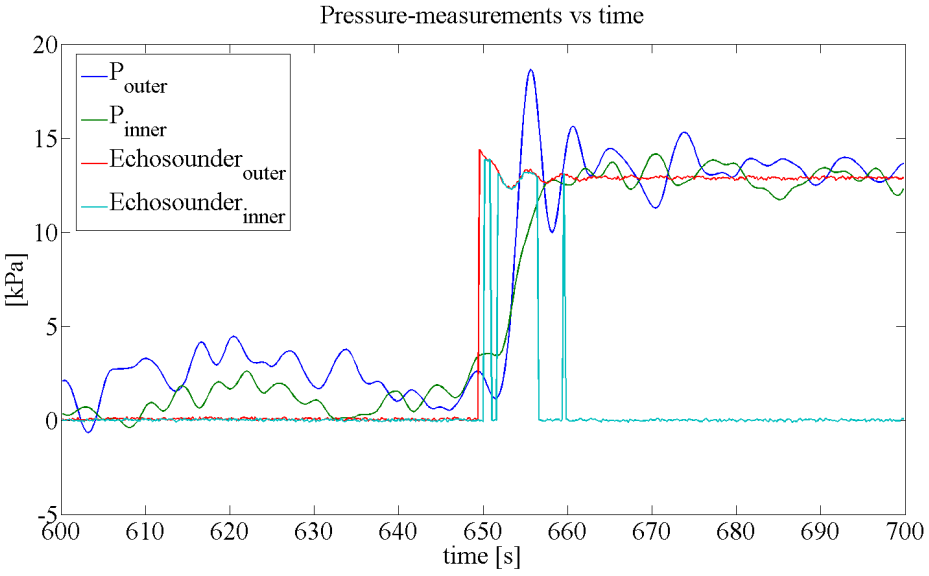

Figure 3.9: Pressure measurements from full-scale tests, courtesy of Sparrevik (2014)

After impact it can be seen from figure 3.9 that the outer pressure has the dominating oscillation-amplitude and a oscillation-period of approximately 4.8 [s]. This is in the proximity of the oscillation period observed in the videos in chapter 3.1.1. The inner pressure oscillates with the same period, but in 180 degrees out-of phase with the outer pressure. Also the inner pressure oscillations have much lower amplitude than the outer pressure. This shows that the oscillations of the pressure shown in figure 3.2, which were the differential pressure, are not due to oscillation of the inner fluid.

In order to conclude that the suction anchor oscillations are not affected by the coupled oscillating air cushion and water column after impact an estimate of the air cushion volume at impact should be made. This can be done by investigating the lowering videos provided by Aspelund,Leiv (2014) and make a judgement of the time between impact and when the echo-sounders enters into water. Then it is seen that the impact occurs around the time the echo-sounders enters into water. The time in the pressure measurements corresponding to this observation is approximately at 650 [s].

Considering figure 3.9 the inner pressure is larger than the outer pressure at the estimated time of impact. Then the height between the suction anchor top and the inner wave elevation can be calculated with equation 3.39:

$$\zeta_{tw} = \frac{P_{in} - P_{out}}{\rho_w g} \tag{3.39}$$

Where:

- ζ_{tw} is the height between suction anchor top and wave elevation at impact from full-scale experiments
- P_{in} is the inner pressure measured at impact during full-scale experiments
- P_{out} is the outer pressure at impact measured during full-scale experiments

Now the corresponding radius of the surface can be found by physical measurement of the lengths in figure 2.5. Then the volume of the air cushion is found by approximating the top as a cone such that the volume can be calculated with equation 3.40:

$$\Omega_{inner} = 1.5 * \frac{1}{3}\pi r_{inner}^2 \zeta_{tw} \tag{3.40}$$

Where:

- Ω_{inner} is the volume of air cushion at impact from full-scale experiments
- r_{inner} is the radius of air cushion at impact from full-scale experiments

Here the volume is multiplied with 1.5 due to the cone-volume is ≈ 0.5 times smaller than the real volume of the suction anchor top. This results in an air cushion volume of 0.09 $[m^3]$ which corresponds to an air-mass of 0.1 [kg]. This small mass of air confirms that the air cushion is not able to influence the oscillations shown in figure 3.2.

For investigating if the outer pressure oscillations are affected by waves generated after the impact, the wave period of the generated waves must be found. This is performed in chapter 3.7.2.

3.7.2 Effect of generated waves on pressure oscillation

The oscillation of the outer pressure may be due small waves created post impact. The period of these waves should therefore be investigated. This is done by estimating the wave length of the first wave generated after the impact. Considering the videos of the lowering this can be estimated to 0.7 [m].

An expression for the wave frequency is found by using the dispersion relationship in shallow water shown in equation 3.41:

$$\tanh kh_e = \frac{\omega^2}{g} \tag{3.41}$$

Where:

- k is the wave number
- λ_{fs} is the wave length of the first waves generated after impact from lowering videos
- h_e is the water depth measured at full scale tests

The wave number can be calculated with equation 3.42:

$$k = \frac{2\pi}{\lambda_{fs}} \tag{3.42}$$

By inserting equation 3.42 into equation 3.41 and replacing the wave frequency with the period, the wave period can be calculated with equation 3.43:

$$T = \frac{2\pi}{\sqrt{g \tanh(\frac{2\pi h_e}{\lambda})}} \tag{3.43}$$

By using equation 3.43 this results in a wave period of 1.13 [s]. This is much lower than the oscillation period of the suction anchor and therefore generated waves from impact are not assumed to affect the oscillation of the outer pressure.

To summarize the findings in chapter 3.2 to the present chapter, more recent pressure measurements show that the inner pressure is not oscillating in addition

that the generated waves do not affect the outer pressure oscillations. Therefore the source of the oscillation is still unknown and a further resonance study of the natural period of hoisting system will therefore be performed in chapter 3.8.

3.8 Natural period of hoisting system

For the calculation of the natural period of the hoisting system a derivation based on a pendulum system will be used. Since there are no information about the crane in the full-scale experiment described in chapter 2 , the properties of the hoisting system are approximated based on personal communication with Aspelund,Leiv (2014), Sandvik (2014) and from the videos of the lowering. A sketch of the hoisting system is shown in figure 2.1.

According to Det Norske Veritas (2011) chapter 4.3.3.3 the natural period of the hoisting system can be calculated with equation 3.44:

$$T_0 = 2\pi\sqrt{\frac{M + A_{33,sa} + \theta_{hoist} \cdot mL}{K}} \tag{3.44}$$

Where:

- M is the mass of the suction anchor in air
- $A_{33,sa}$ is the added mass in heave of fully submerged suction anchor
- K is the stiffness of the total hoisting system
- θ_{hoist} is the correction factor accounting for the cable mass

The mass is given in table 2.1 and from Det Norske Veritas (2011), chapter 4.6.3.3 the added mass in heave for the suction anchor can be calculated with equation 3.45:

$$A_{33,sa} = \left[1 + \sqrt{\frac{1 - \lambda_{rp}^2}{2(1 + \lambda_{rp}^2)}}\right] \frac{A_{33,disk}}{2} \tag{3.45}$$

In equation 3.45 the added mass of the disk is divided by 2 since only the bottom is wet when the suction anchors is oscillating in the surface. λ_{rp} is the heave added mass parameter for suction anchor and is calculated with equation 3.46:

$$\lambda_{rp} = \frac{\sqrt{A_p}}{H + \sqrt{A_p}} \tag{3.46}$$

Where A_p is the projected area in the horizontal plane for the submerged part of the suction anchor. The stiffness contributions included in K are listed below:

- Elastic stiffness of the crane wire

- Crane tip deflection

The elastic stiffness of the crane wire is calculated with equation 3.47:

$$k_{el} = \frac{EA}{L} \tag{3.47}$$

Where:

- E is the Young's modulus of elasticity $\left[\frac{N}{m^2}\right]$
- A_{wire} is the cross sectional area of the lifting wire
- L_{wire} is the length of the wire from the crane tip to the lifting hook

By estimating the diameter of the lifting wire from the videos provided by Aspelund,Leiv (2014) the cross sectional area is found, and the corresponding E is found from *Lankhorst Ropes* (2014). The wire length from the crane tip to the lifting hook is estimated to be 15 [m] according to Aspelund,Leiv (2014).

The stiffness due to deflection of the crane tip Δz is calculated with Hooke's law as shown in equation 3.48:

$$F_3 = Mg = k_{tip}\Delta z \tag{3.48}$$

Where:

- k_{tip} is the stiffness of crane tip
- Δz is the deflection of crane tip

According to Sandvik (2014) an estimate for $\Delta z = 0.3[m]$ is reasonable for an onshore-crane with this load. Since the stiffness contributions are coupled in series the total stiffness of the hoisting system is calculated with equation 3.49:

$$\frac{1}{K} = \frac{1}{k_{el}} + \frac{1}{k_{tip}} \tag{3.49}$$

The values for the different contributions to equation 3.44 are shown in table 3.4:

Parameters for hoisting system	
Suction anchor	
Mass	12900 [kg]
A33	13430 [kg]
Diameter	3.4 [m]
Height	5.96 [m]
Perforation	1.98 [%]
Lifting wire	
Length	15 [m]
D	0.041 [m]
$\frac{Weight}{m}$	6.54 $\left[\frac{kg}{m}\right]$
E	$8.54 \cdot 10^8$ $\left[\frac{N}{m^2}\right]$
θ	1 [-]
Crane	
Crane tip deflection	0.3 [m]

Table 3.4: Input-data for calculation of natural period of hoisting system

3.8.1 Results for natural period of hoisting system

This results in a natural period of the hoisting system equal to $T_{n,hoist} = 0.5[s]$. This is far from the oscillation period for the outer pressure and thus the suction anchor. This result show that the resonance of the hoisting system can be ruled out as a source for the observed oscillation of the suction anchor.

The stiffness due to the slings are neglected which is assumed conservative with respect to the calculation of the natural period. The buoyancy forces acting on the submerged suction anchor are also small, and neglecting this will not influence the results significantly. Due to the aforementioned the natural period calculated here will be conservative and can be taken as a maximum. However, according to Larsen (2014) it should be noted that the flexibility of the crane is important when the wire length is small. Hence the crane flexibility might affect the natural period of the present hoisting system. However, due to lack of information about the hoisting system it is not possible to investigate this.

The calculation of this natural period can be found in appendix D.2.

3.9 Summary of resonance-study

The results from the resonance study of the different systems presented in chapter 3.2 to 3.8 are summarized in table 3.5. The different periods are shown versus the oscillation period of the suction anchor observed in the videos provided by Aspelund,Leiv (2014).

Case	Natural period [s]
Air cushion with added mass from WAMIT	1.1
Coupled piston mode of air cushion and water column	1.2
Piston mode of water column (No coupling)	5.2
Coupled piston mode of air cushion and water with added mass	2.0
Entrapped waves	1.1
Lifting system	0.5
Suction anchor from videos	5.0

Table 3.5: Natural periods compared with observed oscillation period

When more recent pressure oscillations were obtained it was discovered that the pressure oscillations shown in the old measurements were due to difference in the pressure measured by a pressure-sensor inside and outside the suction anchor. By examining more recent measurements of the inner and outer pressure measurements it was discovered that the large amplitude of the observed oscillations shown in figure 3.2 were due to oscillation of the outer pressure. Further it was discovered that the outer pressure oscillations are due to the oscillation of the suction anchor after impact.

It was also shown that generated waves did not influence the oscillation of the outer pressure.

Considering the natural period of the lifting system with the suction anchor hanging in the crane as a pendulum, this was also ruled out as a possible source for the oscillations. However, some uncertainty in the crane characteristics are still present.

By considering the oscillation period of the inner and outer pressure in figure 3.9 the sensors may be erroneous since they are oscillating with a period of 5 [s] both before and after the impact. Then the measurements with regards to resonance-analysis are useless if the sensors measure the same oscillation period everywhere.

From the lowering videos it is seen that right after the inner wave elevation impacts against the top of the suction anchor the lowering is suddenly stopped. Slack lifting wire is then caused by the large impact force. After the slack, snapping in the lifting wire occurs due to the sudden stop of lowering. A possible source of the oscillation after impact may be due to the impulse in the lifting wire caused by snapping after slack wire. However, for performing a modal-analysis due to this impulse the velocity of the suction anchor at this time instant must be known. This is hard to determine from the videos and have not been performed in this thesis.

4 Installation of subsea protection structures on the Jette field

The installation of a subsea protection structure on the Jette-field will be described in this chapter. Then a comparison between force measured in the lifting wire during this installation with theoretical calculations will be performed.

4.1 Jette-installation

On behalf of Det norske Oljeselskap three subsea protection structures were installed by Subsea 7 on the subsea oil-field Jette in the North Sea at the 16^{th} of February 2013. According to Ølund Bertelsen (2013) the main task of a subsea protection structure is to protect underlying equipment against hitting objects, with the most important being fishing trawls. According to Larsen (2013) the subsea protection structures can therefore be referred to as fishing protection structures (FPS). The installation of the protection structure for the pipeline end-manifold PLEM will be described in this chapter. The FPS-PLEM is shown in figure 4.1:

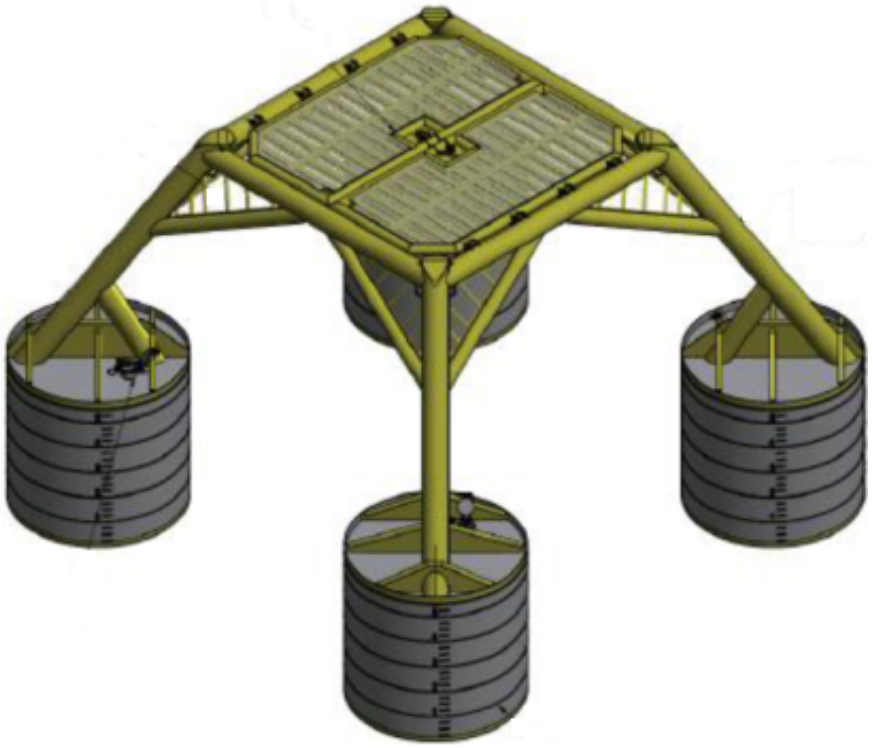

Figure 4.1: Fishing Protection Structure, courtesy of Storvik (2012)

As seen in figure 4.1 the legs of the FPS consists of four suction anchors with two ventilation hatches on top of each suction anchor. The reason for two ventilation hatches were that the initial design of the suction anchors were specified

with smaller diameter for the suction anchor requiring a perforation of 1 [%]. However, the diameter of the suction anchor was increased when manufactured. New installation analyses were then performed by Subsea 7 and DNV where CFD-calculations showed that the installation sea state would be limited to an unacceptable level according to Det norskes requirements if the perforation was not increased. Based on experience from previous operations an additional ventilation hatch was installed to ensure sufficient evacuation of the air. This resulted in a perforation rate of 3 [%]. The data for the FPS-PLEM are shown in table 4.1:

Fishing protection structure	
Dry Weight	200 [tonnes]
Footprint	$21.8 \times 21.8[m^2]$
Height	14.3 [m]
Suction anchors	
D_{anchor}	6 [m]
H_{anchor}	5.5 [m]
$D_{hatch,1}$	0.61 [m]
$D_{hatch,2}$	1.02 [m]

Table 4.1: FPS-Data.

Where:

- D_{anchor} is the diameter of suction anchors on FPS
- D_{hatch1} is the diameter of smallest ventilation hatch on FPS-anchors
- D_{hatch2} is the diameter of largest ventilation hatch on FPS-anchors

A snapshot of the installation of the FPS with the construction vessel Normand Oceanic is shown in figure 4.2. Normand Oceanic can be seen in figure E.1.

Figure 4.2: Installation of Fishing Protection Structure, courtesy of Storvik (2012)

The vessel-data are shown in table 4.2:

Vessel-characteristics	
length over all (LOA)	156.9 [m]
Breadth	27 [m]
Main deck crane	400 [tonnes] at 15 [m]

Table 4.2: Normand Oceanic-data.

The installation-method used during the FPS-installation and challenges related to this are described in chapter E.2.

4.2 Measurements from installation

Øystein Døskeland (2014) has provided measurements for the crane and vessel from this operation in addition to weather data from a wave buoy at the Jette field. The measurements are shown in table 4.3:

Crane measurements	
Load in lifting wire	[tonnes]
Lowering velocity of lifting wire	[m/s]
Crane tip velocity	[m/s]
Vessel motion-data	
Roll motion	[deg]
Pitch motion	[deg]
Weather data	
Significant wave height	[m]
Peak period	[s]

Table 4.3: Data measured at installation of FPS at the Jette field.

A description of the planning of the Jette-operation and weather data measured with a wave buoy at the Jette-field is given in appendix F.2.

The measurements given in table 4.3 will be used to calculate vertical motion, wave elevation and vertical velocity and will be used in the calculations of the dynamic air cushion pressure inside the suction anchors in chapter 4.4. The buoyancy forces due to this will be calculated and compared with force measured in lifting wire in chapter 4.7.

4.2.1 Measurement of vessel motions

The vessel motions are measured with a Motion Reference Unit (MRU) located just forward of the crane pedestal. This measures roll and pitch motion at this location with a frequency of 5 [Hz]. To achieve correct measurements it is important that the MRU is properly calibrated. According to Seatex (n.d.) to ensure that the MRU-measurements are sufficient, the MRU-axes and especially the yaw axis must not have a an alignment error smaller than 0.5 degrees.

In the present thesis it is assumed that the MRU is calibrated properly to ensure sufficient accuracy of the measured vessel-motions.

4.2.2 Force measurements in the lifting wire

According to Øystein Døskeland (2014) the force in the lifting wire is measured with a load-cell that are connected with the wire going through the crane tip. This measures the force independently of the crane tip motion with sampling

frequency of 5 [Hz]. The interaction between waves and FPS is assumed to be captured with this measuring-method.

Øystein Døskeland (2014) has provided a video displaying the lowering of the protection structure through the splash zone. From this video the time when the suction anchors first touches the water until all four suction anchors are totally submerged is found. The force-measurements from the installation are shown in figure 4.3:

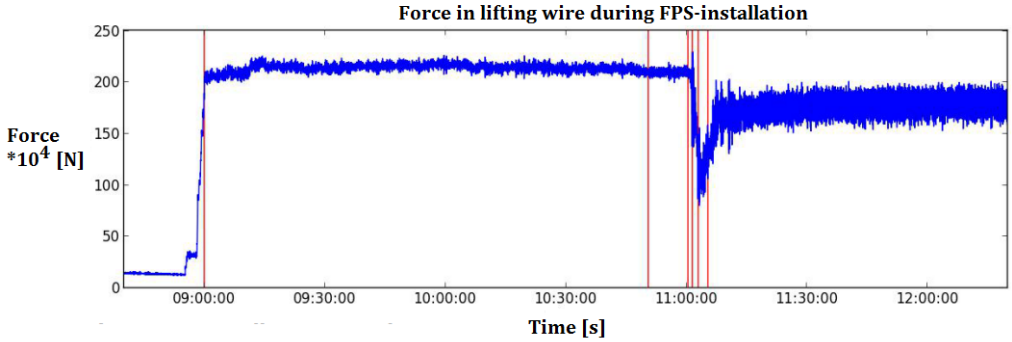

Figure 4.3: Force in lifting wire during installation of FPS, courtesy of Øystein Døskeland (2014)

In figure 4.3 the different phases during the total lifting process are indicated and can according to Øystein Døskeland (2014) be explained as shown in table 4.4:

1	Lift-off
2	Fully overboarded
3	First contact with water
4	First impact on anchor roof
5	Impact on structure roof
6	Fully submerged

Table 4.4: Description of phases during FPS-installation

Considering figure 4.3 and the phases described in table 4.4 the most critical load with respect to crane capacity is when the suction anchors are in the splash zone. This is indicated by the largest peak-load after the suction anchors starts to immerse. This may be due to resonant motion of a system excited by the impulse from slamming against top of the suction anchors.

Considering the minimum load observed in figure 4.3 it is seen that the phase when the roof of the FPS is lowered through the splash zone is the most critical with respect to large buoyancy or impact forces and thus slack in the lifting wire. The buoyancy forces when the suction anchors are lowered through the are not

large compared with the transition of the roof. This is due to the ventilation of air inside the suction anchors most likely is sufficient for this installation as discussed in chapter 4.1.

Since the present thesis is studying splash zone transition of the suction anchors the data described in table 4.3 will only be extracted and used for the time interval relevant to this phase. The post processing of this data will be discussed in chapter 4.3.

4.3 Analysis of FPS-installation

In this chapter the part of the FPS-installation where the suction anchors are lowered through the splash zone will be analysed. The objective of this analysis is to calculate the force in the lifting wire due to buoyancy forces on suction anchors during splash zone transition. In order to do this relevant measurements of vessel motion and weather data must be extracted and post processed.

Further, these data must be post processed and used to calculate important parameters needed for the calculation of dynamic air cushion pressure and buoyancy forces in each suction anchor with the code developed by Ølund Bertelsen (2013). In order to use this code for calculating the total force in lifting wire during suction anchors submergence the following modifications must be made:

- Use time-series measured during operation directly in the calculation of important parameters.
- Calculate vertical motion and velocity of suction anchor due to vessel motion and lowering speed.
- Calculate wave elevation inside each of the suction anchors.
- Allow air-flux in and out of the ventilation hatch.
- Calculate buoyancy forces in four suction anchors.
- Calculate slamming forces on the flat suction anchor top.

All the calculations and comparisons performed in this chapter are performed with the same random phase angles unless otherwise stated.

4.3.1 Time series used during splash zone transition of suction anchors

Since the measurements and the videos of the lowering are not synchronized a good-engineering judgement for choosing the relevant time-interval to extract the time-series from the measurements have been performed. From figure 4.3

and table 4.4 the time when the first suction anchor, here denoted as North-east suction anchor (NE-SA), touches the water is 11:00:21. The wave elevation inside the NE-SA impacts against the top 55 [s] later, and 25 [s] after this all suction anchors are submerged which is the end-time of the calculations. The time instants corresponding to start and stop of the calculations are shown in table 4.5:

	Time
Start of immersion	11:00:31
All suction anchors submerged	11:01:45

Table 4.5: Time start and stop for calculations during suction anchor transition through splash zone.

The time-series corresponding to the time interval shown in table 4.5 are extracted from the file cranedata.xlsx provided by Øystein Døskeland (2014). The measured force in the lifting wire during this interval are shown in figure 4.4:

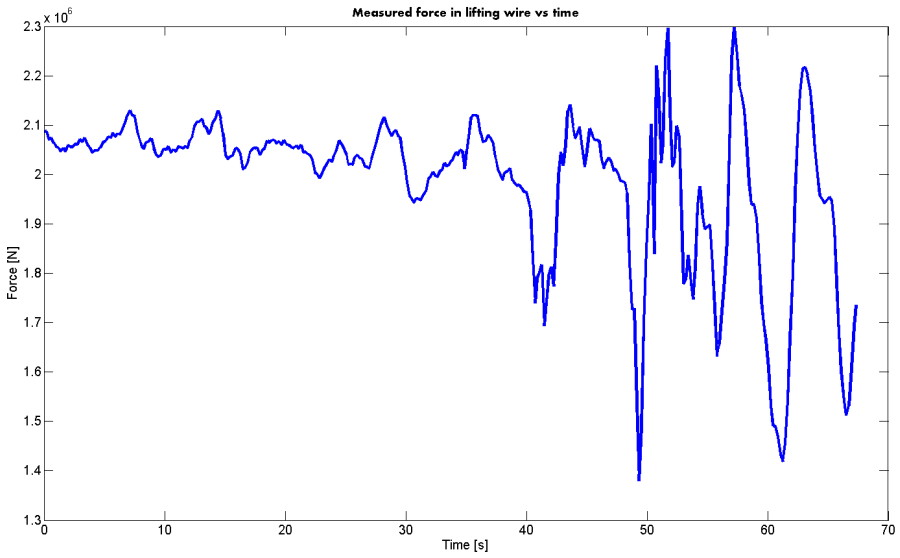

Figure 4.4: Force measurements during splash zone transition of suction anchors

Around t=30 [s] the first impact occurs where it is seen from videos provided by Øystein Døskeland (2014) that it is the North-east-suction anchor (NE-SA) that is immersed first and also experience slamming first. At 40 [s] a larger impact is recorded where both the NE-SA and North-west-suction anchor (NW-SA) experience slamming almost simultaneously. At 50 [s] the South-east-suction anchor (SE-SA) in addition to NE-SA and NW-SA experience impact almost at the same time and cause the structure and lifting slings to vibrate after the impact. This is most likely the reason for the high-frequency oscillations after this impact. The first two oscillation-periods of the high freq oscillations are 0.41

[s] and 0. 95 [s]. A method to account for this vibration due to an impulse from impact will be discussed further in chapter 8.1.1. The location of the suction anchors can be seen in figure 4.5.

4.3.2 Time-delay between water crossing

As mentioned above the first anchor that touches the water is the (NE-SA). However the initiation of the calculation of the dynamic air pressure will not commence at this time since the continuous immersion of the anchor does not start until 10 seconds later. This is because the suction anchor oscillates in and out of the water which again is due to small lowering velocity compared with wave velocity. When the continuous immersion has commenced this time-instant corresponds to the starting time t=0 [s] in figure 4.4.

From the videos it is seen that the FPS is tilted while the suction anchors are lowered through the splash zone. It is assumed that this is due to tension in the tugger wires that are used to constrain the pendulum motion of the FPS. This can be seen in figure E.2 and leads to immersion of the suction anchors at different time instants. The time of immersion for each of the suction anchors are estimated from the videos and are shown in table 4.6

	Time
NE-SA	11:00:31
NW-SA	11:01:33
SE-SA	11:00:37
SW-SA	11:01:38

Table 4.6: Time of water entry initiating calculations for each suction anchor.

4.3.3 Vertical velocity and motion of suction anchors

The vertical motion of the suction anchor will be a result of crane tip motion, vessel motion and lowering velocity. When using the measurements obtained by the MRU to find the resulting vertical motion of the suction anchor it is assumed that the suction anchors are rigidly connected with the with the vessel. However, the vertical motion at the MRU is unknown. This can be found by assuming the crane tip to be rigidly connected with the vessel. The crane tip motion must therefore be found first. Since the vertical crane tip velocity, $\dot{\eta}_{3,tip}$ is known, the vertical crane tip motion, $s_{3,tip}$ can be found by integrating the measured crane tip velocity with respect to time as shown in equation 4.5:

$$s_{3,tip} = \int_{t'} \dot{\eta}_{3,tip} dt' \tag{4.1}$$

Due to the assumption of rigid connection between crane tip and MRU-location the vertical motion of the MRU can be calculated with equation 3.9 in Faltinsen (1990) as shown in equation 4.2:

$$s_{3,tip} = \eta_{1,mru}\boldsymbol{i} + \eta_{2,mru}\boldsymbol{j} + \eta_{3,mru}\boldsymbol{k} + \boldsymbol{\omega} \times \boldsymbol{r} \tag{4.2}$$

- $\eta_{1,mru}$ is the surge motion at MRU
- $\eta_{2,mru}$ is the sway motion at MRU
- $\eta_{3,mru}$ is the heave motion at MRU
- $\boldsymbol{\omega}$ is the angular motion vector
- $\boldsymbol{r}$ is the translational motion vector
- $\boldsymbol{i}$ is the vector along x-axis
- $\boldsymbol{j}$ is the vector along y-axis
- $\boldsymbol{k}$ is the vector along z-axis

Here the bold letters represent vectors. The angular motion vector can be calculated as:

$$\boldsymbol{\omega} = \eta_{4,mru}\boldsymbol{i} + \eta_{5,mru}\boldsymbol{j} + \eta_{6,mru}\boldsymbol{k} \tag{4.3}$$

- $\eta_{4,mru}$ is the roll motion at MRU
- $\eta_{5,mru}$ is the pitch motion at MRU
- $\eta_{6,mru}$ is the yaw motion at MRU

The translational motion vector can be calculated as:

$$\boldsymbol{r} = x_{tip}\boldsymbol{i} + y_{tip}\boldsymbol{j} + z_{tip}\boldsymbol{k} \tag{4.4}$$

Where:

- x_{tip} is the longitudinal location of crane tip relative to MRU
- y_{tip} is the transverse location of tip relative to MRU
- z_{tip} is the vertical location of tip relative to MRU

To find the vertical motion at the MRU equation 4.2 is rearranged in terms of $\eta_{3,mru}$. Then by evaluating the cross product between $\boldsymbol{\omega}$ and $\boldsymbol{r}$ and only consider the terms connected with $\boldsymbol{k}$, the vertical motion at the MRU is found by equation 4.5:

$$\eta_{3,mru} = s_{3,tip} + \eta_{5,mru}x_{tip} - \eta_{4,mru}y_{tip} \tag{4.5}$$

The location of the MRU is provided by Øystein Døskeland (2014) and operational data as crane lifting radius and vessel heeling is found in Øystein Døskeland (2012). The x- and y- coordinates of the crane tip relative to the MRU together with an overview of relevant distances between FPS and vessel are shown in figure 4.5:

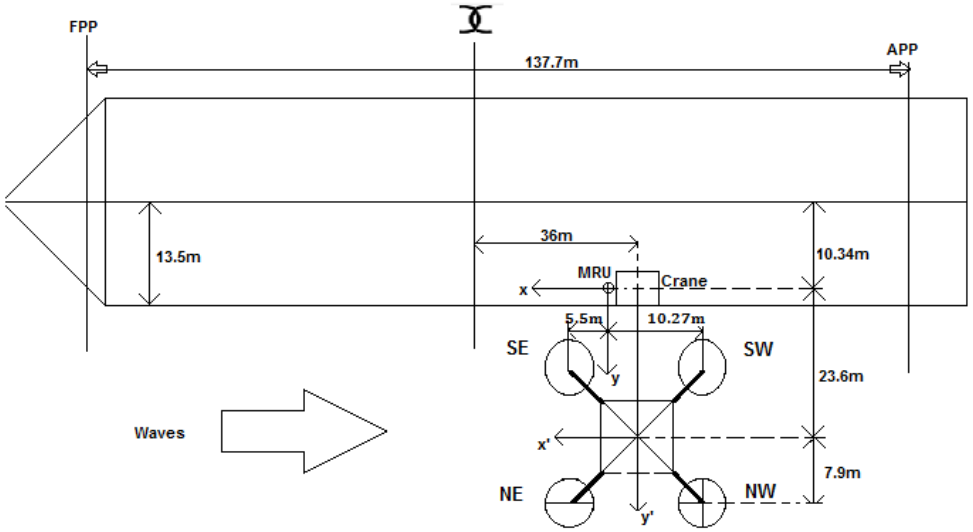

Figure 4.5: Calculation model for vessel and FPS

In figure 4.5 the global coordinate system is defined with origo at the MRU-location.

The total vertical motion of the suction anchors will be a sum of the vertical motion induced by the lowering speed of the winch and the vertical motion due to the vessel motions. The former can be found by integrating the lowering speed with respect to time in the same manner as for the crane tip in equation 4.1. The latter can be found by using equation 4.2 assuming that the vessel and suction anchors are rigidly connected through the connection between the FPS and crane tip. Then the total vertical motion of each of the suction anchors can be written as shown in equation 4.6:

$$\eta_{3,anchor,i} = \int_{t'} \dot{\eta}_{3,winch} dt' + s_{3,anchor,i} \tag{4.6}$$

Where:

- $\eta_{3,anchor,i}$ is the vertical motion of each of the suction anchors.
- $\dot{\eta}_{3,winch}$ is the lowering speed of the crane winch.
- $s_{3,anchor,i}$ is the vertical motion of the suction anchors due to vessel motion.

The resulting motion of the suction anchors is shown in figure 4.6:

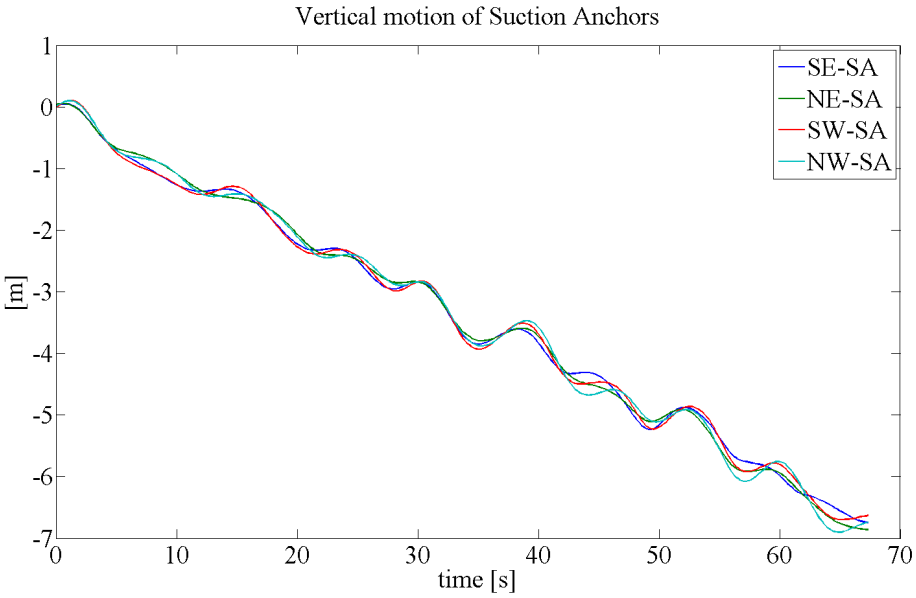

Figure 4.6: Vertical motion of suction anchors

From figure 4.6 it is seen that the roll and pitch motion of the vessel introduce some oscillations in the vertical motion of the suction anchors. However, the main contribution to the vertical motion is the lowering velocity. The vertical motion of the suction anchors are calculated with the MATLAB-routine `motion.m` shown in appendix G.4.

4.3.4 Generating wave realizations with Torsethaugen-spectrum

In this chapter a description on how to calculate the wave realizations during splash zone transition of suction anchors will be given. The two-peak Torsethaugen spectrum will be used for this purpose. According to Torsethaugen and Haver (2004) the Torsethaugen spectrum is developed from measured spectra at Haltenbanken and Statfjord and the only inputs that are needed for calculating the spectral values are Hs for the total sea and Tp for the dominating sea. The dominating sea is either wind or swell which are dominating for different Tp-ranges. The Tp-limits can be found by considering the actual peak period at the Jette-field and assuming fully developed sea which implies unlimited fetch and sea state duration.

The sea state for the FPS-installation is extracted from the weather buoy described in appendix F.2. The sea state for the time when the suction anchor is lowered through the splash zone can be seen in table 4.7:

Hs	1.94 [m]
Tp	5.89 [s]

Table 4.7: Sea state during suction anchor transition through splash zone.

According to Torsethaugen and Haver (2004) the sea state is wind-dominated if Tp measured at the Jette-field is less than $a_f Hs^{1/3}$ and swell-dominated for the opposite. a_f is the factor depending on fetch length. From Det Norske Veritas (2010) a_f is recommended to be 6.6 for a fetch larger than 370 [km]. The distance from the shore to the Jette-field is approximately 180 km] according to www.subseaworldnews.com (2013), therefore the required fetch for using the recommendation in Det Norske Veritas (2010) is not fulfilled. However, it is assumed to be sufficient for the purpose of the comparison study in the present thesis.

Then by using the recommendation from Det Norske Veritas (2010) and the values for Hs and Tp given in table 4.7 the sea state at the Jette-field when the suction anchors are lowered through the splash zone can be denoted as wind-dominated.

The spectral formulation for the Torsethaugen-spectrum can be found in Torsethaugen and Haver (2004), equation (43-46). To calculate the spectral values with the given sea state in table 4.7 the software WAFO developed by WAFO-group (2000) is used which is a freely distributed toolbox using Matlab routines.

The Torsethaugen-spectrum can be seen in figure 4.7 including both energy distribution of wind- and swell-sea:

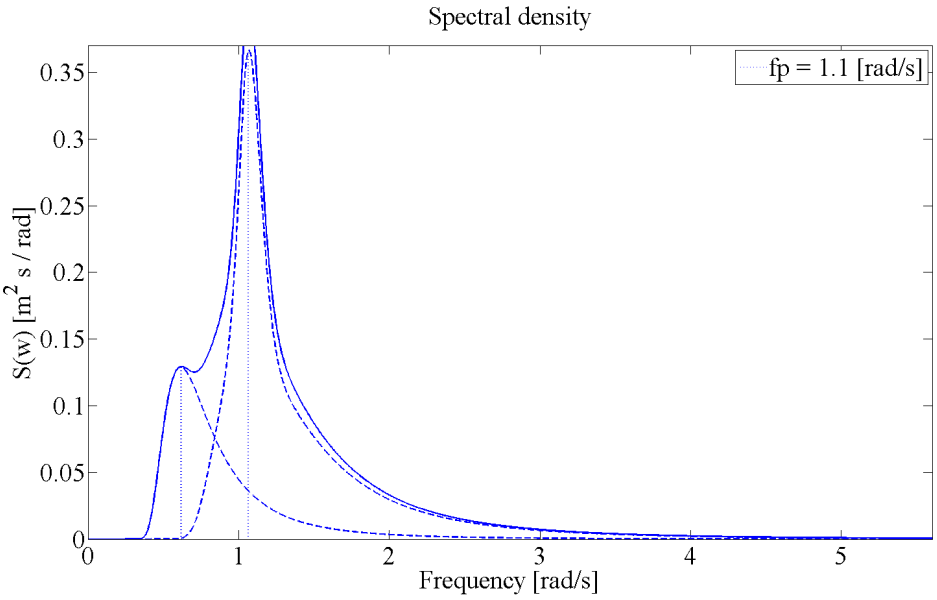

Figure 4.7: Torsethaugen spectrum

From figure 4.7 the wind-part is dominating which is in accordance with the above discussion. Comparing the energy distribution in figure 4.7 with the JONSWAP-spectrum in figure 2.6 it is seen that the JONSWAP-spectrum created previously has a larger energy distribution. The wave realizations between the two spectra should be compared. The wave realizations can be calculated with equation 2.15 using the same phase angles and similar direction of propagation for wind and swell sea. The comparison between the wave realizations created with the JONSWAP-spectrum and the Torsethaugen-spectrum can be seen in figure 4.8:

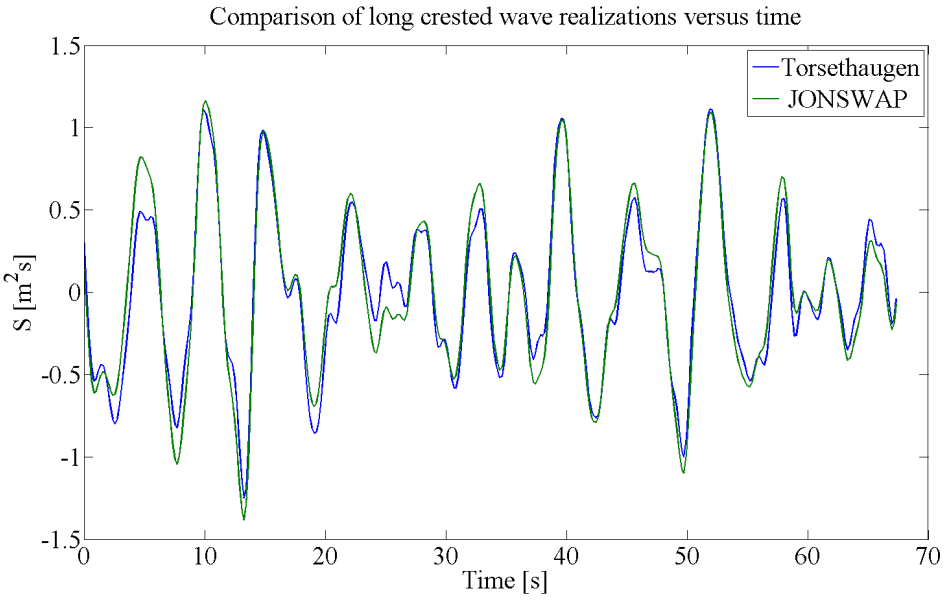

Figure 4.8: Long crested wave realizations with JONSWAP and Torsethaugen spectrum

From figure 4.8 it can be seen that the introduction of swell sea propagating in the same direction as the wind sea does not affect the wave realizations much.

To determine the heading of the incident waves during the installation the video provided by Øystein Døskeland (2014) is studied. A series of snapshots of waves propagating along the vessel during the operation can be seen in figure E.3, appendix E.3. These snapshots show that the waves can be approximated as heading waves propagating in the negative x-direction by considering the coordinate system established in figure 4.5.

The importance of having a relative direction between wind and swell sea should also be considered. This is investigated with calculation of short crested waves in appendix F.3.

4.4 Calculating dynamic air cushion pressure and buoyancy forces

To calculate the dynamic air cushion pressure inside the four suction anchors on the FPS the theoretical model described in chapter 2.2 is used. The calculation of the dynamic air cushion pressure with equation 2.6 require motion and velocity of suction anchor in addition to wave elevation and velocity calculated in chapter 4.3.3 and 4.3.4 respectively. The Runge-Kutta algorithm for calculating the dynamic air cushion pressure can be seen in the MATLAB-code odesolvernew.m shown in appendix G.6.

The dynamic air cushion pressure during the lowering of the suction anchors are shown in figure 4.9:

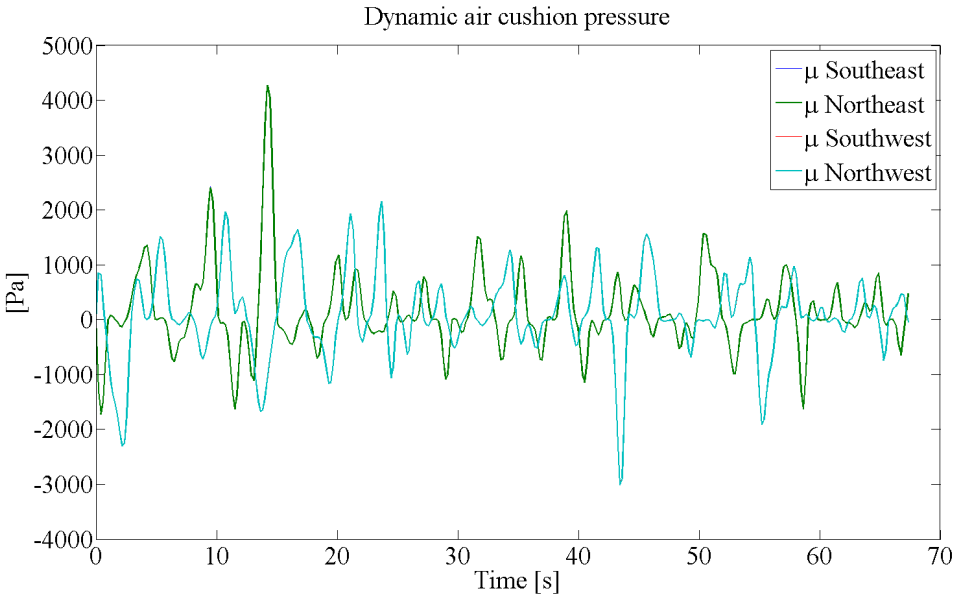

Figure 4.9: Dynamic air cushion pressure in four suction anchors

Here no time delay between the immersion of the suction anchors have been included and the dynamic air cushion pressure is similar for the eastern and western suction anchors respectively. This is due to application of long crested waves propagating in the negative x-direction in addition to the vertical motion of the suction anchors being very similar.

The effect of changing air flux conditions and different perforation ratios on the dynamic air cushion pressure and thus buoyancy forces will be investigated in chapter 4.4.1 and 4.4.2 respectively.

4.4.1 Air-flux considerations

As a modification to the code developed by Ølund Bertelsen (2013) the flux of air is now allowed to flow both in and out of the suction anchor when oscillating in large waves. According to Steen (1993) the allowance of the air to flow in and out of the ventilation hatch can be performed by modifying equation 2.5 with the signum function ($sign$). This returns zero if μ<0, 1 if μ>0 and -1 if μ<0. Now the expression for Q_{out} can be seen in equation 4.7:

$$Q_{out} = CA_l sign(\mu)\sqrt{\frac{2|\mu(t)|}{\rho_{atm}}} \tag{4.7}$$

When using equation 4.7 with C as a constant contraction coefficient for allowing air flux in and out of the suction anchor a uniform ventilation hatch must be

utilized. This is to ensure that outflow and inflow conditions are as similar as possible as shown in figure 4.10.

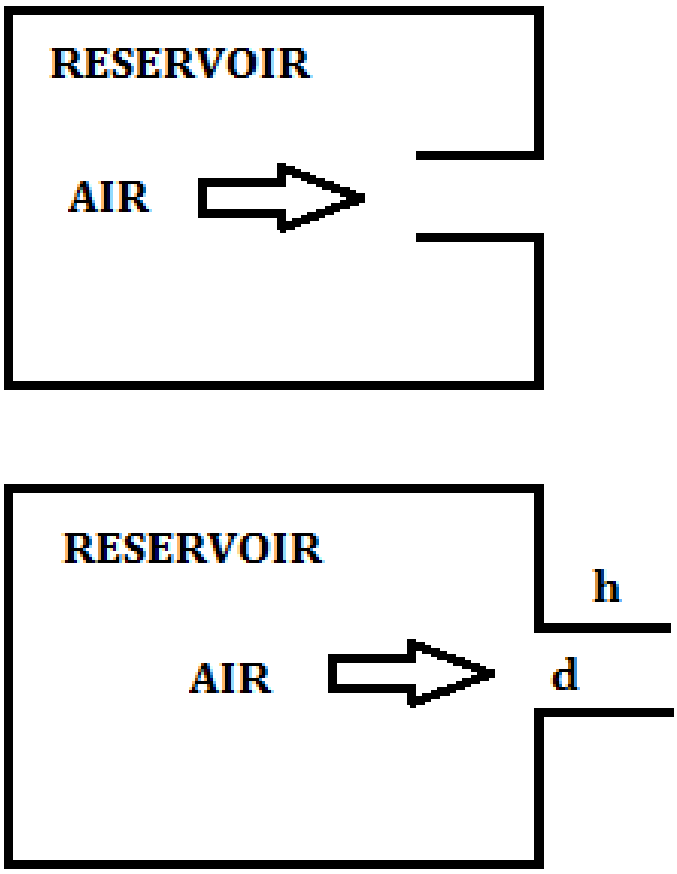

Figure 4.10: Uniform ventilation hatch for inflow and outflow of air

The contraction coefficient for this type of outlet can be found in Blevins (1984), table 7-5 and is equal to 0.61 [-] as established in Ølund Bertelsen (2013). This coefficient must satisfy the ratio between the height of ventilation hatch (h_{hatch}) and the D_{hatch2} given in equation 4.8:

$$\frac{h_{hatch}}{D_{hatch}} = [0 - 0.5] \tag{4.8}$$

This ratio is valid for the largest ventilation hatch (D_{hatch2}) used on the suction anchors on the FPS.

The effect of the air flux on the total force in the lifting wire accounting for I) air flux into and out-of the suction anchor versus II) only air flux out of the suction anchor is shown in figure 4.11:

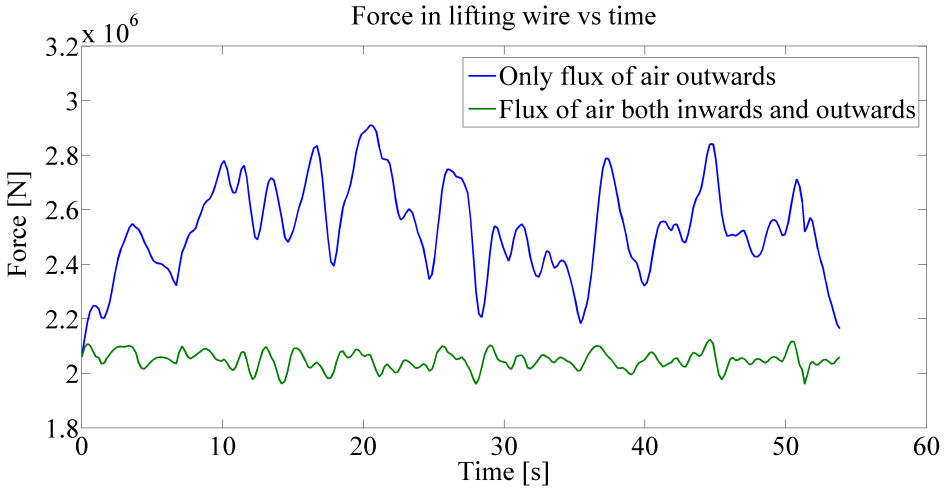

Figure 4.11: Comparison of force in lifting wire for air flux both in and out versus air flux outwards only

For comparison of the magnitude of the buoyancy forces the calculation in figure 4.11 is stopped before the largest slamming peak in the measurements occurs. From figure 4.11 it can be seen that case I) includes a negative force contribution to the buoyancy force when the suction anchor is oscillating upwards (rising up from the water). This is due to the suction pressure will pull the suction anchor downwards which leads to an increased force in the lifting wire.

For case II) the dynamic air cushion pressure is negative for nearly the whole lowering. This may be due to the calculation of μ in the numerical code with initial value $\mu = 0$ and taking the maximum between 0 and μ in the expression for outflow of air shown in equation 2.5. In this way only real values of μ are accounted for. However, μ is negative for almost all time instants which indicate that this calculation is for inflow of air only when it should be outflow only.

This is also checked by calculating μ as the maximum between μ and 0 instead. However, the results are the same compared using 0 as the lowest value. This means that there is a possible numerical limitation in representing only the outflow of air when both inflow and outflow will occur. This results in a large negative force contribution from the suction pressure to the buoyancy forces such that the total force in the lifting wire will be over predicted as shown in figure 4.11.

4.4.2 Changing perforation ratio

By decreasing or increasing the perforation ratio of the suction anchors, the buoyancy force is assumed to increase or decrease respectively. Referring to the lowering videos of a single suction anchor in chapter 2.2 a lowering with a perforation ratio of 0.2 [%] was performed to evaluate the feasibility of a very low perforation ratio. The videos showed that the suction anchor started to tilt dur-

ing the splash zone transition and further immersion was stopped due to large buoyancy forces.

Based on discussion in chapter 4.1 three different perforation ratios are introduced in the suction anchors used on the Jette-field. For comparing the effect of these ratios the same wave realizations must be simulated for each case and then the total force in the lifting wire for each ratio can be calculated. This is displayed in figure 4.12:

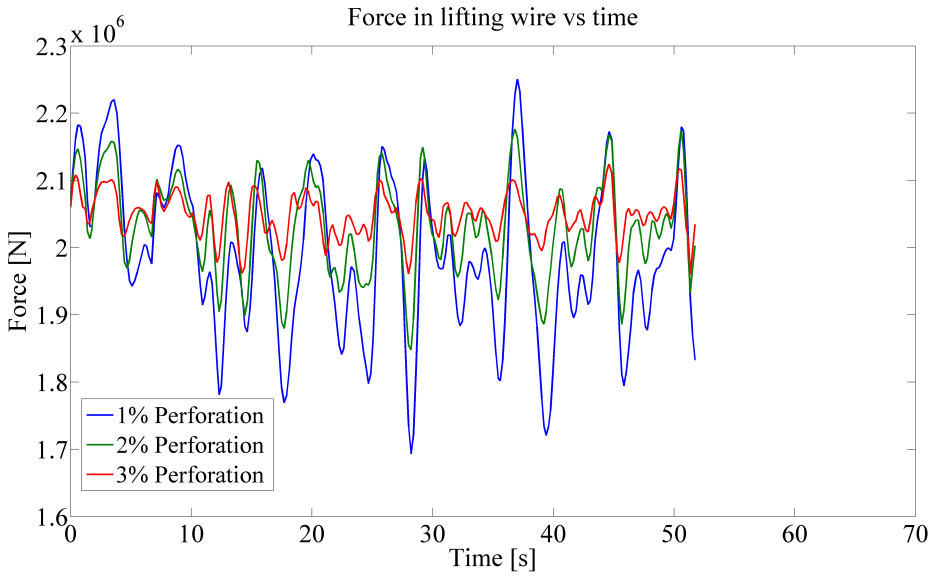

Figure 4.12: Force in lifting wire for different perforation ratios

For comparison of the magnitude of the buoyancy forces the calculation in figure 4.12 is stopped before the largest slamming peak in the measurements occurs. Figure 4.12 shows a comparison of the force in the lifting wire for perforations 1-3 [%] and the figure clearly shows that the buoyancy forces increase for decreasing perforation. This increase in buoyancy force will also decrease the vertical motion of the suction anchor.

Since the phenomena described here and in chapter 4.4.1 are well documented, a design recommendation for suction anchors with required size of ventilation hatches will be given in chapter 5.1.

4.5 Impact on top of suction anchors

In this chapter the impact force on the top of the suction anchors will be calculated. When the suction anchors are lowered through the splash zone slamming occurs when the wave elevation inside the suction anchors impacts against the top of the suction anchors. In this chapter the terms impact force and slamming force have the same meaning and are used arbitrarily.

In Ølund Bertelsen (2013) it was concluded that the slamming load was most critical with respect to slack in the lifting wire. Considering figure 4.1 the top of the suction anchors on the FPS is flat as compared to the conical shaped top for the full-scale tests studied in chapter 2.1. Therefore the slamming calculation performed in this thesis will differ from the calculation performed in Ølund Bertelsen (2013). A study of different approaches for calculating the slamming load on the flat top will be presented in this chapter.

First a description of slamming and related phenomena to flat plate impacts will be given. According to Faltinsen and Timokha (2009) slamming can be characterized as follows:

- non-linear phenomena.
- random process.
- short duration.
- damped by presence of air cushion.

O.M. Faltinsen (2005) describe results from experimental pressure measurements and theoretical studies of horizontal elastic plates subject to wave impact. These results show that the maximum pressures measured at impact are random by nature and that the slamming pressure is a non-linear phenomena. This is seen in O.M. Faltinsen (2005), figure 8.10 where the effect of small changes in physical conditions during the initial phase of the impact result in significant changes of the largest impulse pressures. Therefore the slamming forces calculated during splash zone transition of the suction anchors are assumed to vary significantly with different wave conditions.

Of relevance to the impact on the flat suction anchor top is the flat plate drop tests performed by Verhagen (1967). There it was found that an air cushion may be formed due to entrapped between the water surface and the impacting object. The cushioning effect showed a damping of the impact. Also, according to O.M. Faltinsen (2005) if the air cushion collapses air bubbles will be created that will influence the water flow. These phenomena should be taken into account if the air inside the suction anchor is not ventilated sufficiently at impact.

However, an effort in assessing the effect of these phenomena has not been performed in the present thesis. Therefore the air is assumed to be fully evacuated during impact and the water flow is assumed to be described with potential theory in the slamming calculations performed in this thesis.

4.5.1 Slamming force with wedge-approach

Ølund Bertelsen (2013) used a strip-theory approach for calculating the slamming-load on a suction anchor with a conical-shaped top. The pressure was integrated

around the conical top for each strip and the wetted length for a wedge with Wagner (1932) and von Karman (1929) were used. The wetted length from the latter gave most similar results with the measurements. This will therefore be used when integrating the pressure around the top of the suction anchor assuming that the inner wave elevation is stepping through the top like a wedge. This is shown in figure 4.13:

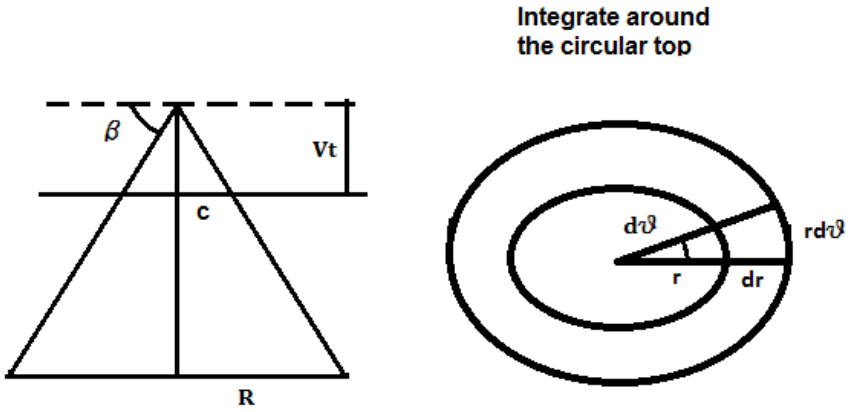

Figure 4.13: Integration model for calculating slamming force on suction anchor top

Now the wetted length will be smallest at impact and increase post-impact. During impact the slamming force is found by integrating the pressure over the horizontal area of the wedge hitting the flat top at each time instant.

As mentioned potential theory is assumed for the water such that the Laplace equation shown in equation 3.18 is satisfied. According to Faltinsen (1990) the body boundary condition for the wedge can be transferred to an equivalent flat plate as shown in figure 4.14:

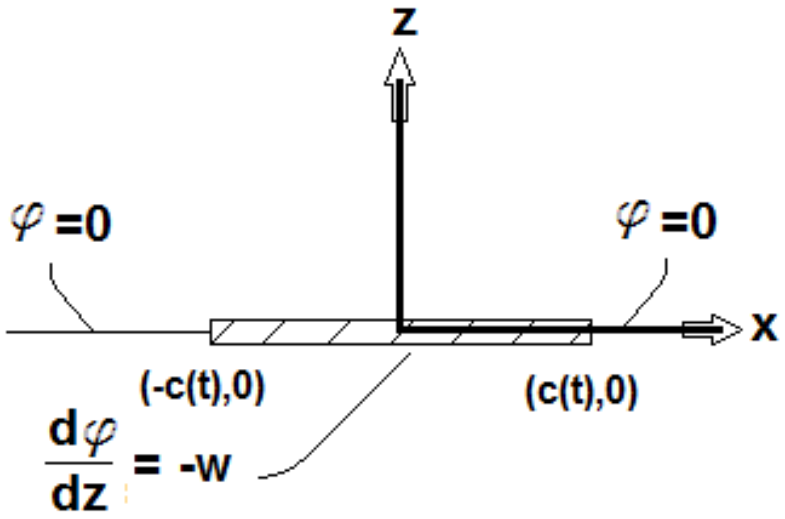

Figure 4.14: Boundary conditions for flat plate at impact

Here the free surface boundary condition ϕ_{slam}=0 and body boundary condition $\frac{d\phi_{slam}}{dz} = -V_{rel}$ are applied on z=0. According to Faltinsen (1990) the velocity potential satisfying these boundary conditions can be written as shown in equation 4.9:

$$\phi_{slam} = -V_{rel}\sqrt{c^2 - x^2} \tag{4.9}$$

Where:

- ϕ_{slam} is the velocity potential during impact
- V_{rel} is the relative velocity between body and waves and will be calculated in equation 4.14
- c is the wetted length of suction anchor top during impact

The pressure on the body is found from Bernoulli's equation shown in equation 3.20. Since the time instant during the slamming load is very small, the time rate of change of ϕ_{slam} will be much larger than the rate of change of ϕ_{slam} with respect to x and z such that $\left(-\frac{\rho}{2}\mathbf{VV}\right)$ can be neglected. Also, since the submergence of the suction anchor is small, the hydrostatic term (-ρgz) can be neglected. According to Faltinsen (1990) the hydrodynamic pressure becomes:

$$p = -\frac{d\phi_{slam}}{dt} = \rho V \frac{c}{(c^2 - x^2)^{\frac{1}{2}}}\frac{dc}{dt} \tag{4.10}$$

Setting x=r and considering figure in 4.13 the pressure can be integrated around the area of the flat top represented by $rd\theta dr$. The radius r will decrease during the impact like r=R-c where R is the total radius. The integral limits for r

becomes 0 to c when integrating around the circular area such that the force can be calculated as shown in equation 4.11:

$$\begin{aligned} F_3 &= \int_A p\mathbf{n}_3 d\mathbf{A} = \int_0^{2\pi}\int_0^c prdrd\theta \\ &= 2\pi c\rho V_{rel}\frac{dc}{dt}\left[\underbrace{\int_0^c \frac{rdr}{(c^2-r^2)^{\frac{1}{2}}}}_{=\mathrm{c}}\right] \\ &= 2\pi\rho V_{rel}\left[\frac{1}{3}\frac{d}{dt}(c^3)\right] \end{aligned} \tag{4.11}$$

The solution of the integral in equation 4.11 is found in Rottmann (2003). The wetted length of suction anchor top during impact is calculated by using von Karman (1929)'s approach as shown in equation 4.12:

$$c(t) = \frac{V_{rel}t_s}{tan(\beta)} \tag{4.12}$$

Where:

- t_s is the time step used in slamming calculation starting from zero at impact.
- β is the impact- or deadrise-angle between the impacting body and water surface.

Inserting equation 4.12 into 4.11 the impact force can be calculated with equation 4.13:

$$F = \frac{2\pi\rho {V_{rel}}^4 t_s^2}{tan^3\beta} \tag{4.13}$$

V_{rel} can be calculated with equation 4.14:

$$V_{rel} = \dot{\eta}_3 + \dot{\zeta}_{inc} \tag{4.14}$$

$\dot{\eta}_3$ is the vertical velocity of the suction anchor due to lowering velocity and crane tip velocity. Since the vertical motion of the suction anchor is already known from equation 4.6 the velocity can be calculated with forward differentiating as shown in equation 4.15:

$$\dot{\eta}_3 = \frac{\eta_3(t+h) - \eta_3(t)}{h} \tag{4.15}$$

Where h is the time step used in forward differentiation and is equal to the time step Δt from the time vector loaded from the time series described in chapter 4.3.1.

It should be noted that the Wagner-method used here will only be applicable for calculating the slamming loads for the first impact. The fluid conditions inside the suction anchor will be different after the first impact where it is assumed that potential theory is no longer applicable. Therefore a constraint for only including the first impact on each of the suction anchors are introduced in the calculations. This will be explained in chapter 4.5.4.

4.5.2 Slamming force with different slamming coefficients

According to Faltinsen (1990) the slamming force can be calculated by introducing a non-dimensional slamming coefficient (Cs) as shown in equation 4.16:

$$F_3 = \frac{Cs}{\frac{1}{2}\rho_w A_{top} V_{rel}^2} \tag{4.16}$$

The introduction of Cs is based on the hypothesis that the slamming load is proportional to the diameter of a horizontal cylinder and V_{rel}^2 at impact. For the flat top impact the slamming load will be proportional to area of suction anchor top (A_{top}). According to Faltinsen (1990) the lower and upper limit for Cs is equal to π and 2π for von Karman (1929)'s and Wagner (1932)'s equivalent flat-plate approach respectively. However, these coefficients are only valid during the initial stage of the impact and are assumed to be conservative when calculating the slamming load post impact. Det Norske Veritas (2011) recommends a simplified and conservative approach for calculating the slamming force during impact against flat structures. There it is recommended using equation 4.16 together with a constant slamming coefficient (Cs_{rp}) defined by Det Norske Veritas (2010) to Cs_{rp}=2π for impacts against flat plates. This is equal to Wagner (1932)'s initial slamming coefficient described above.

Since the initial slamming coefficient is only applicable for a short time duration after the impact, a time varying slamming coefficient (Cs_{var}) by Campbell and Weynberg (1977) is proposed. This was found by integrating the pressure distribution from the Wagner (1932) model over a flat plate. The expression for the slamming coefficient for varying submergence of a horizontal cylinder can be seen in equation 4.17:

$$Cs_{var} = \frac{2\pi}{1 + 1.5\frac{V_{rel} t_s}{R}} \tag{4.17}$$

Results using this coefficient has not been validated and therefore this should be used with care.

4.5.3 Slamming occurrence-criterion

Slamming occurs when the inner wave elevation reach the top of the suction anchor. A criterion for when this occurs can be made by considering figure 2.2

and calculate the relative vertical motion between the suction anchor and the inner wave elevation ($\eta_{3,rel}$) with equation 4.18:

$$\eta_{3,rel} = \eta_3 - \zeta_c \tag{4.18}$$

Inserting equation 2.3 into equation 4.18 the slamming criterion can be defined as shown in equation 4.19:

$$\eta_{3,rel} = \eta_3 + \frac{\mu(t)}{rho_w g} - \zeta_{inc} = H \tag{4.19}$$

This slamming criterion is shown together with $\eta_{3,rel}$ for the splash zone transition of suction anchors on the FPS in figure 4.15:

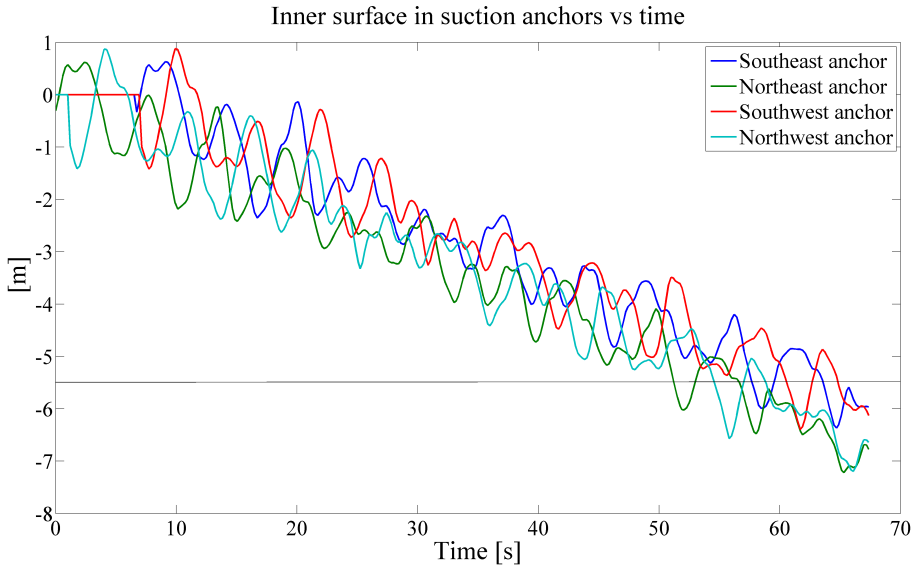

Figure 4.15: Relative motion between inner wave elevation and vertical motion

In figure 4.15 the crossing of the horizontal line defines the occurrence of slamming when the inner wave elevation touches the top of the suction anchor. However, for the slamming load to be active when the suction anchor top is wet a threshold value for the magnitude of the relative velocity between the suction anchor and waves and the slamming pressure will be given in chapter 4.5.4.

4.5.4 Duration of impact

A criterion for the duration of the slamming load will be defined in this chapter. Then a description of a threshold value for the relative velocity and slamming pressure will that determine if the slamming loads are active will be given.

Considering the relative motion of the inner water elevation shown in figure 4.15, large oscillations may lead to multiple impacts against the top of the suction anchors that are immersed first. Therefore a constraint on the duration of the

impact is applied such that the slamming is only allowed to act from the time instant the inner wave elevation touches the top of the suction anchor until the top is no longer wet.

In the slamming calculations this is done by comparing neighbouring values of $\eta_{3,rel}$ and checking when the zero down- and up crossing of the value $\eta_{3,rel} - H = 0$ occurs. The index corresponding to the values within this interval define the maximum duration of the slamming. This principle can be seen in figure 4.16:

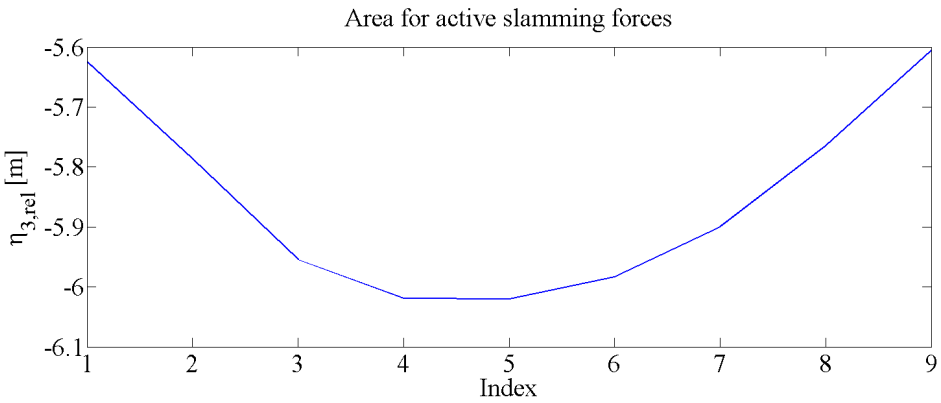

Figure 4.16: Illustration of slamming constraint

During the time interval where the slamming forces are defined as active, another constraint for the occurrence of slamming is introduced. Then the slamming pressure and relative velocity must be higher than a given threshold value for the slamming force to be acting. These threshold values are found from Greco and Lugni (2012) who performed numerical studies of bottom slamming on a ship. There they used a method to determine the occurrence of slamming by considering two contemporary satisfaction criteria of both slamming pressure and entry velocity. Two criteria for the former is defined as:

- *The instantaneous local slamming pressure should be larger than the instantaneous local hydrostatic pressure.*
- *The maximum local slamming pressure should be larger than the local mean-draft hydrostatic pressure.*

The former of these two pressure-criteria will be used in the slamming calculations in the present thesis where the instantaneous local slamming pressure is calculated with equation 4.20:

$$P_{slam} = \frac{F_{slam}}{A_c} \tag{4.20}$$

Where:

- P_{slam} is the instantaneous local slamming pressure.

- F_{slam} is the slamming force.

The criterion for the relative velocity is referred to as Ochi (1964)'s criterion and defines a threshold for the entry velocity that should be greater than $0.0928\sqrt{gD_{anchor}}$.

It should be noted that if the relative vertical motion between top and inner wave elevation does not have a zero up-crossing after the slamming has occurred, only the contemporary satisfaction criteria of the magnitude of the velocity and pressure will apply.

4.6 Results for slamming calculations

In this chapter the results for the slamming load calculated with the different approaches described in chapter 4.5.1 to 4.5.2 will be discussed.

4.6.1 Results of slamming load with different slamming coefficients

A comparison of slamming loads with different Cs acting on the suction anchors during splash zone transition is displayed in figure 4.17:

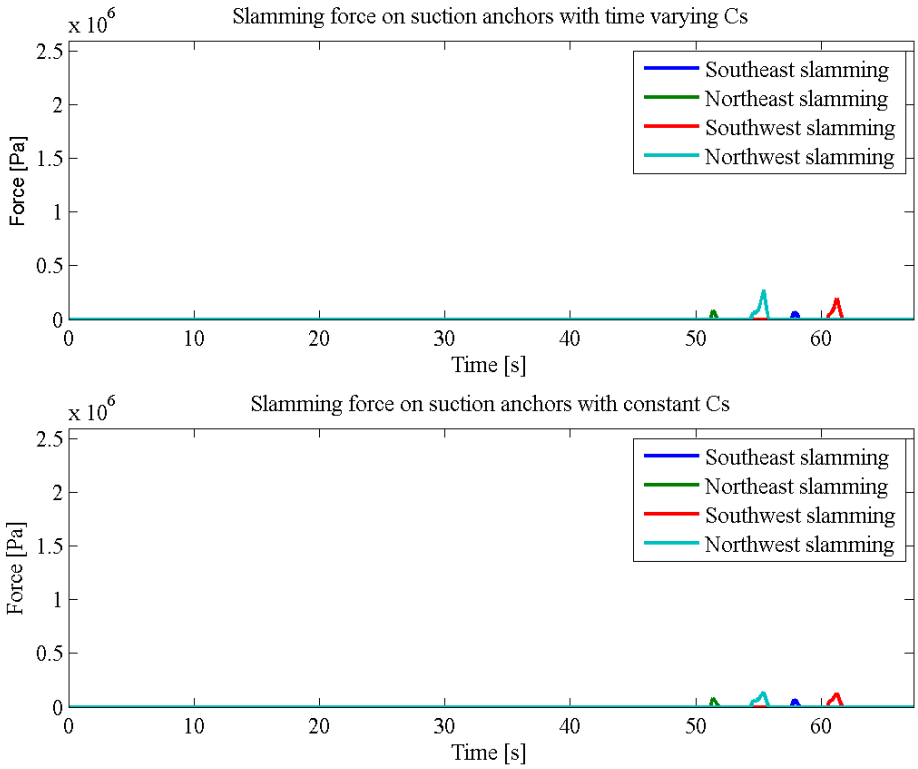

Figure 4.17: Comparison of slamming loads with varying and constant slamming coefficients

In figure 4.17 the slamming load is is defined as zero until impact occurs. It is seen that the slamming force with constant Cs is under predicted while the force with time varying Cs show more correspondence with the measured slamming.

4.6.2 Results of slamming loads with wedge approach

Considering figure 9.9 in Faltinsen (1990) the theory for the classical slamming method Wagner (1932) will break down for deadrise angles below 5 [deg]. By recommendation from Greco (2014) the method developed in chapter 4.5.1 will be applied with deadrise angles in the range of 5-20 [deg] for the wedge impact against the flat top of the suction anchor. A sensitivity study for the comparison of the slamming force acting on the suction anchors during splash zone transition with different deadrise angles has been performed. A deadrise angle of 17.5 [deg] proved most similar with the results. A comparison of slamming forces for the three different deadrise angles 5, 10 and 17.5 [deg] is shown in figure 4.18:

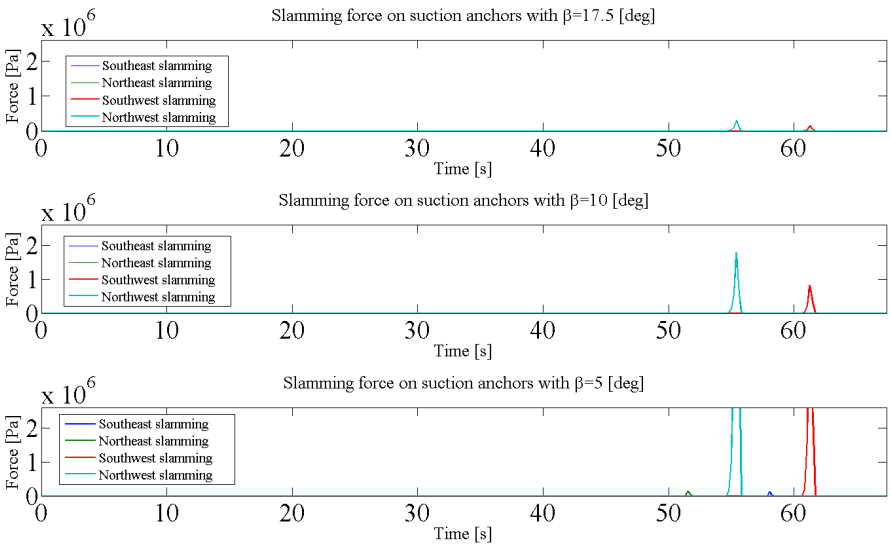

Figure 4.18: Comparison of slamming loads with different deadrise angles

Figure 4.18 show that the slamming load is over predicted for the deadrise angles equal to 5 and 10 [deg].

4.7 Calculating force in lifting wire

The present thesis only take into account the vertical force contributions from the buoyancy force due to dynamic air cushion pressure when calculating the force in the lifting wire. Then the total force in the lifting wire due to buoyancy and slamming forces can be calculated for the splash zone transition of the suction anchors with equation 4.21:

$$F_{wire} = F_{stat} - \sum_{i=1}^{4} F_{buoy,i} - \sum_{i=1}^{4} F_{slam,i} \tag{4.21}$$

Where:

- F_{wire} is the force in lifting wire
- F_{stat} is the static weight of structure in air
- F_{buoy} is the buoyancy force on suction anchor
- F_{slam} is the slamming load acting on top of suction anchor

The buoyancy forces due to the dynamic air cushion pressure are set equal to zero when the wave elevation inside each of the suction anchors reach the top. Then the slamming loads acting on each of the suction anchor tops will be calculated. A direct comparison between the calculated force in the lifting wire with the measured force during the splash zone transition of the four suction anchors on the FPS is shown in figure 4.19:

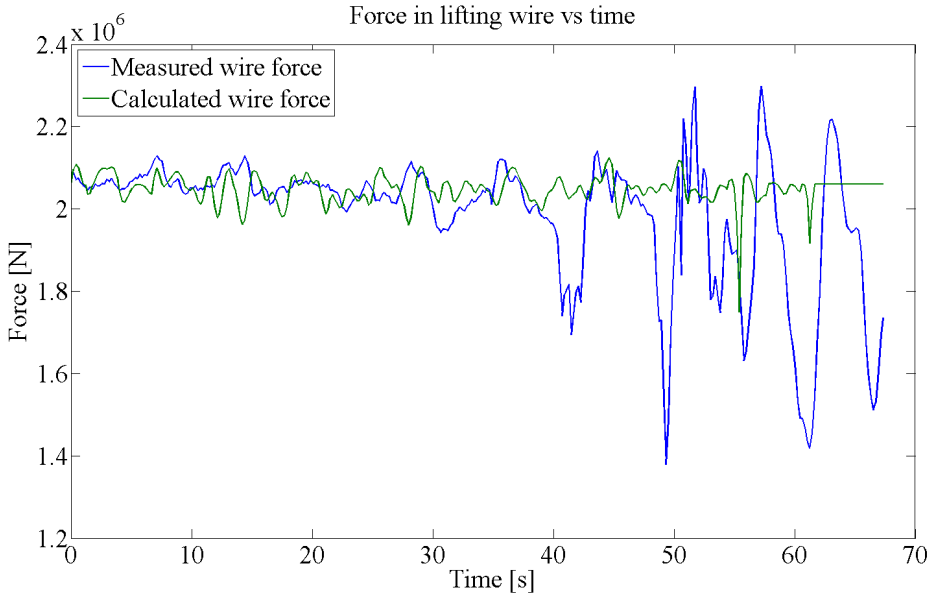

Figure 4.19: Comparison of calculated force in lifting wire versus measured force

Until the first impact of the suction anchors at 40 [s] the calculated force is of the same order of magnitude as the measured force. At 50 [s] the largest impact is recorded where it is seen from videos that two suction anchors experience slamming simultaneously. At around 55 [s] the slamming load is calculated with the wedge-approach with a deadrise angle of 17.5 [deg] in equation 4.11. From figure 4.18 is is seen that the slamming load calculated here is only for one suction anchor. The magnitude of the load seem to be reasonable compared with the magnitude of the measured slamming force acting on only one suction anchor.

A direct measurement between measurements and calculations as shown in figure 4.19 is not applicable since the wave realizations used in the calculations are not the same as those during the installation. With respect to comparing the largest buoyancy or impact force a statistical comparison between the measurements and calculated minima should be performed. A statistical comparison for the calculated minima in the wire-force using the approach described in this chapter will be performed in chapter 5.1.

4.8 Summary of Jette-analysis

Measurements from the installation of a subsea protection structure with four suction anchors have been extracted and post-processed. The post processed data are then used in the calculation of the dynamic air cushion pressure model given in chapter 2.2 with the modifications given in chapter 4.4. This model have also been modified for calculating the buoyancy and slamming forces acting on the four suction anchors with different time of water entry. The calculated buoyancy forces showed correspondence with the magnitude of the measured forces.

Since the time series of the wave elevations are not given, these have been generated. Recommendations given in Faltinsen (1990) suggest that when deploying large subsea structures typical sea states consist of both wind and swell. Det Norske Veritas (2010) recommend that when simulating operations for subsea installations performed on the NCS with Hs in the range of 1-3 [m] the two-peaked Torsethaugen wave-spectrum accounting for both wind and swell sea should be used. This is also advocated by NORSOK (2007) and this has therefore been used to calculate the wave realizations during splash zone transition of the suction anchors.

The slamming calculations on the flat top of the suction anchor performed with Wagner (1932)'s initial slamming underestimated the results. Using Campbell and Weynberg (1977)'s time-varying slamming coefficient more correspondence with the measurements were obtained. Integrating the pressure around the flat suction anchor top with Wagner (1932)'s approach for a wedge impact overestimated the slamming load for the range of deadrise angles below 17.5 [deg] while under predicted for deadrise angles above 17.5 [deg]. The slamming calculation with both Wagner's wedge model for a $\beta = 17.5$ [deg] in addition to the varying slamming coefficient is assumed applicable for further use in statistical analyzes in chapter 5.1.

Only including the vertical force component from the buoyancy forces acting on the suction anchors is assumed conservative. In reality large forces will induce a certain moment about the lifting wire which will lead to some tilting of the structure. The forces will then not be taken as only vertical forces, but a contribution to horizontal motion will also be present.

4.8.1 Uncertainties and error sources

Large uncertainties are related to the different time of water entry used for the suction anchors. This is read off from the installation videos which are not synchronized with the measurements. Also, there are large uncertainty related to the exact time of immersion of the suction anchors. However, a sensitivity study of different water entries and initiation of the calculations have been performed to get the most correspondence between measurements and calculations.

The wave realizations from the JONSWAP-spectrum have generally a larger peak and trough than the realizations from the Torsethaugen-spectrum. Since the latter is including contribution from both wind- and swell-sea propagating in the same direction more wave energy is associated with these waves. Thus these waves should have larger amplitude. Therefore the calculation of the spectral values from the Torsethaugen spectrum with WAFO can be questioned and different methods for calculating the wave realizations due to wind and swell sea should be investigated.

Regarding slamming load calculated with the Wagner-wedge approach, the load is assumed to be acting on the whole wetted area at each time instant represented by the wetted area of the water-wedge at that instant. From the videos of the lowering, a mixture of water and air spraying out the ventilation hatches is observed at impact. This indicate that the wave elevation inside the suction anchor is not hitting the top uniformly as assumed in the calculations. This is assumed to be the reason for the over estimation of the slamming load with the wedge-approach for deadrise angles below 17.5 [deg].

There are some uncertainty regarding the satisfaction criterion of the relative velocity that is based on empirical studies of slamming on conventional ships. Using Ochi (1964)'s original criterion the diameter of suction anchor is replaced by the ship length. Since the ship lengths are $>> D_{anchor}$ it us doubtful if this criterion is applicable for the relative velocity during impact on the suction anchor. Therefore the criterion is multiplied with a factor of 0.8 to introduce more strict requirements for the magnitude of the relative velocity.

5 Design recommendation for suction anchors

In this chapter a recommendation for suction anchors with respect to avoiding slack in lifting wire during splash zone transition will be given. For this purpose a statistical analysis will be performed investigating the effect of large buoyancy forces with different perforation ratios and also including slamming forces. Then a recommendation on the shape of the ventilation hatch outlet will be given. Finally, a proposal for methods to evaluate the effect of different shapes of suction anchor tops to avoid large impact forces will be given.

5.1 Recommendation on perforation ratios

In this chapter a design recommendation for suction anchors with required size of ventilation hatches for avoiding large dynamic air cushion pressure and thus large buoyancy forces that may be critical to slack in lifting wire will be given. The FPS-installation described in chapter 4 will be used as a case study for this purpose and the relevant safety criteria will be given in chapter 5.1.1.

5.1.1 Safety criteria

For ensuring a safe lowering through the splash zone of suction anchors slack in lifting wire must be avoided. Slack lifting slings should also be avoided since occurrence of snatch loads after slack may be critical for the load capacity of the lifting wire. The impulse from these snatch loads may also induce resonant motion in the lifting wire.

Since slack in lifting slings will occur before slack in lifting wire, a definition of slack-sling criterion should be made for lowering of the suction anchors through splash zone. A slack-sling criterion often used for lowering through splash is taken from Det Norske Veritas (2011) and is shown in equation 5.1:

$$F_{hyd} \leq 0.9 F_{stat} \tag{5.1}$$

Where F_{hyd} is the total hydrodynamic forces that acts on the suction anchor and should never be larger than 90 [%] of the static weight of the FPS in air. According to Det Norske Veritas (2011) this criterion ensure that snap loads in lifting wire and slings are avoided. By turning this around in terms of the force in the lifting wire, slack in the lifting wire are assumed to be avoided if the criterion in equation 5.2 is met:

$$\frac{F_{wire}}{0.1 F_{stat}} \geq 1 \tag{5.2}$$

With respect to the slack wire criterion given in 5.2 it is interesting to see the effect of changing the perforation ratio versus the diameter of the suction anchor.

A description of the perforation ratios that will be studied is given in chapter 5.1.2.

5.1.2 Relvant perforation ratios

For evaluating the criterion given in equation 5.2 for the FPS-installation, the force in the lifting wire calculated with equation 4.21 will be compared with 10 [%] of the static weight of the FPS in air.

Based on discussion with Larsen (2013) perforation ratios ranging from 1-3 [%] versus suction anchor diameter ranging from 3-6 [m] will be studied in this chapter. 9 combinations of perforation ratios and diameters of suction anchors are shown in table 5.1:

	Suction anchor diameters [m]		
	3	4.5	6
Perforation ratios [%]	1	1	1
	2	2	2
	3	3	3

Table 5.1: Combinations of diameters and perforation ratios

When changing the diameter of the suction anchors the static weight will also be reduced. The relevant static weight in air corresponding to the different diameters of the suction anchors are shown in table 5.2:

	Suction anchor diameters [m]		
	3	4.5	6
F_{stat} [tonnes]	164g	186g	210g

Table 5.2: Static weight in air of FPS corresponding to different diameters of suction anchors

The magnitude of the wire force for the different perforation ratios in study can be seen in figure 4.12 for a suction anchor with D=6 [m]. A statistical analysis for evaluating the slack-wire criterion with the combinations given in table 5.1 will be performed in chapter 5.1.3.

5.1.3 Statistical analysis of slack-wire criterion

This chapter will make a recommendation for the optimal design of suction anchor diameter versus perforation ratio for avoiding slack in lifting wire based on a statistical analysis of different perforation ratios. Considering table 5.1 9 different combinations will be evaluated versus the slack-wire criterion. For obtaining a statistical confidence interval quantifying the effect of the different combinations several runs should be performed for each of the combinations. Considering

Jacobsen et al. (2012) who performed statistical comparison of time-domain simulations with full-scale force measurements, 15 runs with different random seeds were assumed sufficient when comparing maxima or minima. However, due to limited time available in this thesis only 10 runs for calculating the lifting wire force for each of the combinations in table 5.1 will be performed. This results in a total of 90 runs and will be performed with the super-computer Vilje at NTNU.

In Ølund Bertelsen (2013) it was concluded that the slamming load is most critical with respect to slack in the lifting wire or slings. Comparing with the force in the lifting wire in figure 4.12 for the perforation ratios given in table 5.1 the range of perforation ratios should be much smaller than those shown in table 5.1 if slack in lifting wire should occur due to buoyancy forces from dynamic air cushion pressure alone. Therefore, to capture the largest minima of the wire loads slamming loads have been included when the wave elevation impacts against each of the suction anchor top.

However, as described in chapter 4.5 slamming is a random phenomena and due to the contemporary satisfaction criteria for the relative velocity and slamming pressure defined in chapter 4.5.4 it is not certain if slamming will occur. Therefore if these slamming criteria are not met, the minimum wire force calculated will be due the buoyancy forces from the dynamic air cushion pressure.

The slamming calculation with both the wedge-approach and time varying slamming coefficient will be used due to the discussion in chapter 4.8.

5.1.4 Results from statistical analysis

The minima for the 10 runs performed for each of the perforation ratio combinations has been extracted. Then the smallest minimum of each of the 10 runs were then taken as representative for each of the 9 combinations and inserted into equation 5.2. The results from this analysis are shown in table 5.3:

		$F_{wire}/0.1F_{stat}$ [-]		
Perforation ratio %		3	2	1
Suction anchor diameter [m]	6.0	8.52	8.25	4.87
	4.5	8.53	6.83	7.89
	3.0	7.84	4.93	8.92

Table 5.3: Wire force versus slack-wire criteria for different perforation ratios and diameters

The results in table 5.3 show that for the combinations used here no risk of slack wire during lowering occurs. Further, the results for the largest suction anchor with 1 [%] perforation ratio increase the risk of slack in lifting wire with

50 [%] compared to a perforation ratio of 3 [%]. However for the rest of the results there is no clear trend in the decrease of perforation versus diameter of the suction anchor. The results for the smallest suction anchor with a 2 [%] perforation ratio shows 50 [%] increased risk of slack in the lifting wire versus the combination with 1 [%]. This is opposite to what is expected.

Another approach considering the slack in individual lifting slings could also be used. Then slack in the lifting slings can be defined as when the forces in each sling are overcome by the hydrodynamic force in each suction anchor. This can easily be done by considering the buoyancy and slamming force in each of the suction anchors. However, this was found out in a late stage of the thesis work and has not been performed.

5.1.5 Uncertainties and error sources

Since some combinations show deviations from what was assumed to be the worst case on beforehand, time series of the wire force for some of the runs performed in the statistical analysis is investigated. Then it is seen that the minima depend greatly if slamming occur. As mentioned in chapter 4.5 slamming is a highly random phenomena where the extent of the slamming pressure depend highly on the wave conditions during impact. Additionally the contemporary satisfaction criteria used for determining the duration of the slamming may be too strict as mentioned in chapter 4.5.4.

Also, the author found out in a late stage during this thesis that were only sufficient amount of time to perform the statistical analyzes with the time-varying slamming coefficient. Since this is method show less magnitude of the slamming force compared with the wedge-approach, the results may be non-conservative. Also, the slamming calculation with the varying slamming coefficient is not validated. However, due to limiting amount of time the author has not been able to perform additional statistical analyzes with the slamming calculation from the wedge-approach.

Another error in the slamming calculation performed during the statistical analysis is the occurrence of slamming. During further modification of the slamming calculations the slamming criterion was proven too strict such that the occurrence of slamming became too low.

Considering the minimum load at impact measured at around 50 [s] in figure 4.4, this corresponds to a value for slack-wire criterion equal to 6.56 [-]. This yields 30 [%] larger risk of slack in the lifting wire than the calculated minimum for this combination shown in table 5.3. Thus, more runs should be performed with additional combinations than those given in table 5.1 and with different slamming methods for flat plate impacts. Then a sufficient confidence interval for a conservative model for the slack-wire criterion can be obtained. Due to a

limited time available for studying this, only 9 combinations of perforation ratios and diameters have been studied.

Another error source is the and random seed generation in MATLAB that use a clock based Random Number Generator (RNG). When running the ten different runs for each perforation ratio with the supercomputer right after one another this proved to be too fast for the MATLAB-RNG such that repeated results were obtained. To overcome this, the author had to wait some time before running each script. Therefore the script should be modified with an improved RNG in order to avoid inherent errors like this.

5.2 Design of ventilation hatch

Based on the validity of the air cushion model developed in this thesis, a recommendation on the characteristics of the ventilation hatch can be given. As seen in figure 4.15 the top of the suction anchor will oscillate in and out of water prior to total submergence. This is due to the small lowering velocity compared with velocity of incident waves.

If the water starts flowing into the ventilation hatch during water exit and entry the flow of air will be affected. Then a mixture of air and water will create different conditions than assumed in the simplified theoretical model for the dynamic air cushion pressure discussed in chapter 2.2.

Due to this the optimal height of the ventilation hatch should be so large that when water starts flowing into the hatch, the wave elevation inside the suction anchor has already reached the ventilation hatch inlet. However, for the validity of the equation used for modelling air flux into and out of the ventilation hatch the height of the hatch has a certain limit. This limit is taken from Blevins (1984) and is given in equation 4.8. Therefore, if the calculation model developed in this thesis shall be used when calculating the dynamic air cushion pressure for a suction anchor with a given ventilation hatch, the ratio given in equation 4.8 must be satisfied.

If a non-uniform ventilation hatch is installed on a suction anchor the conditions for the inflow and outflow of air will be different and can not be represented by a constant contraction coefficient as established in chapter 4.4. The continuity equation, 2.4 representing the air mass, will then have to be modified for including both an inflow term and and outflow term.

5.3 Design of suction anchor top

When the suction anchor top oscillates out of water, the lifting wire will experience added weight due the extra effort needed when the top pushes the water

above it. The suction anchor top shaped like a cone will then have less resistance than the shape of a flat suction anchor such that the wire-force will be largest for the latter. However, considering the top of the suction anchors in figure 4.1 stiffener plates and equipment required for pumping out water during landing on seabed will be located here in addition to the ventilation hatch. A conical top will limit the amount of space available for mounting this equipment.

Therefore, a different methods to assess the criticality of impact between water and flat suction anchor top should be studied further than performed in this thesis. This will be performed in chapter 8.4 where an improved theoretical method for calculating slamming load for flat plate impacts is discussed.

Also, a proposal for a small-scale model test with proper scaling of impact pressure is discussed in chapter 8.3.1.

6 Notes on MATLAB-scripts

All MATLAB-scripts used during the present thesis will be described briefly in this chapter.

6.1 Parameter-study

Here the script used for performing a parameter-study of important parameters affecting the dynamic air cushion pressure will be described. This is performed with the script `CalcRK.m` shown in appendix G.1. This script is able to use a time-varying lowering velocity and also includes regular and irregular waves in the calculation of the dynamic air cushion pressure and buoyancy forces. In addition slamming forces are calculated with Von Karman and Wagner's method when calculating the total force in the lifting wire.

6.2 Resonance analysis

The resonance-analysis of the different systems that were assumed to be the source for the oscillations shown in figure 3.2 is also analyzed with `CalcRK.m`. This calculates the natural period of the piston mode of air cushion, coupled air cushion and water column and water column alone. This can also be seen in appendix G.1.

6.3 Jette-study

To calculate the force in the lifting wire during the splash zone transition of the four suction anchors, the code developed in Ølund Bertelsen (2013) has been further developed. Now this script is able to load arrays of time series from any operation. This is done with the script `Main.m` shown in appendix G.3. This script loads the time series from the suction anchors splash zone transition stored in the file `crane_020620.mat` in addition to defining global parameters for the suction anchor and ventilation hatch to be studied. This script calls other functions that performs the actual calculations. When all calculations required for the force in the lifting wire have been made, the wire force can be calculated with `Main.m` and plotted versus the measured force. The flowchart of the calculation process can be seen in figure 6.1:

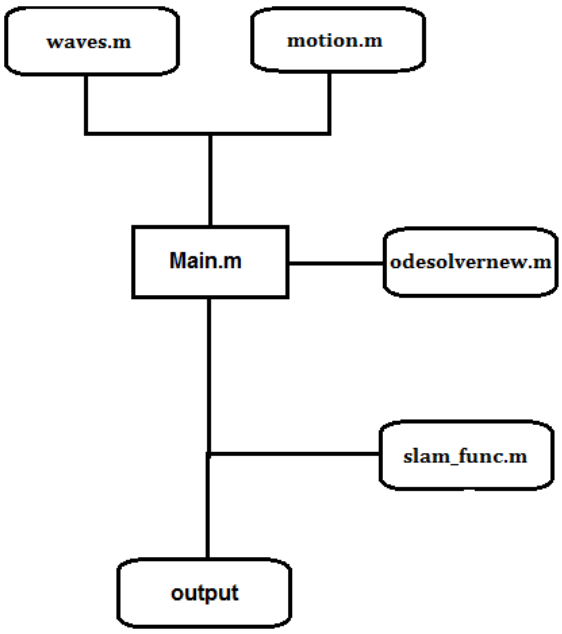

Figure 6.1: Flowchart of calculation of force in lifting wire during splash zone transition of suction anchors

Here it is seen that `Main.m` first makes call to to the `motion.m` and `waves.m` scripts. In motion.m the vertical motion and velocity of each of the suction anchors are calculated from input of time series of vessel motions and lowering velocity. This is shown in the script `motion.m` in appendix G.4. For waves propagating in one direction, different wave elevations are calculated for the eastern and northern suction anchors with the script `waves.m` shown in appendix G.5. This script loads the spectral values for the Torsethaugen spectrum stored in the file `S_torset.mat` which is created on beforehand with WAFO.

For comparing the wave realizations from both the JONSWAP spectrum and Torsethaugen spectrum the same random phase angles are used. These random phase angles are generated on beforehand and are stored in the file `epsilon10000.mat`. This is also loaded by the script `waves.m`.

When the motions and wave elevations at the suction anchor are known the dynamic air cushion pressure inside four suction anchors can be calculated with the script `rkown1.m` shown in appendix G.2. However, the runtime of this script becomes long for the small time-steps needed for obtaining convergence. There-

fore, to save time a built-in numerical solver in MATLAB called ODE45 will be used instead of the Runge-Kutta algorithm used in `rkown1.m`.

ODE45 utilize an optimized and explicit Runge-Kutta method for solving non-stiff differential equations. For calculating the dynamic air cushion pressure ODE45 require input of the initial value for μ and a time-array for the operation in which it performs interpolation between the given time-steps in its own manner. The script using this solver is called `odesolvernew.m` and is shown in appendix G.6. To check that the results from `odesolvernew.m` are physically correct a comparison is made with the results from `rkown1.m` for one single suction anchor. A detailed description of this built-in solver in MATLAB can be found in Mathworks (2014b).

When the dynamic air cushion pressure is calculated then the buoyancy force acting on each of the suction anchors can be calculated. This is calculated with the script `slam_func.m` shown in appendix G.7. A time delay between the immersion of the different suction anchors is implemented in this script. This script also calculates the slamming forces and outputs the total force contribution which are used in Main.m for calculating and plotting the total force in the lifting wire.

7 Conclusion

The non-linear model for the dynamic air cushion pressure developed in Ølund Bertelsen (2013) has been compared with full-scale force measurements in lifting wire with a single suction anchor. Buoyancy forces acting on the suction anchor due to the dynamic air cushion pressure has been well represented.

Introducing regular and irregular waves in the calculation of the dynamic air cushion pressure show that the results are very sensitive to large oscillations and amplitudes. Introducing a varying lowering velocity and contraction coefficient on the dynamic show that the maximum deviation between the wire force due to buoyancy from dynamic air cushion pressure alone and the mean force in the lifting wire of three similar experiments is 2.5 [%]. Therefore it can be concluded that the theoretical model for the dynamic air cushion pressure developed in Ølund Bertelsen (2013) give satisfying results when comparing with experiments in small waves and small variation in lowering velocity.

A slamming calculation for a conical-shaped suction anchor top with Wagner (1932)'s wedge approach and von Karman (1929)'s wetted length have also proved to be satisfying compared with these experiments. This approach will therefore be recommended for calculating impact forces on conical shaped tops.

Initial pressure measurements obtained from full-scale experiments showed a possible resonant motion with large oscillation amplitudes measured after impact. Observations from lowering videos also showed oscillation of the suction anchor with the same period. Possible resonant phenomena connected with these oscillations are investigated.

The investigation of a resonant motion of the air cushion induced by the impulse from the impact show no correspondence between the natural period of the air cushion and measured oscillations. A coupled piston mode motion of air cushion and water column also gave much smaller natural period than the measured oscillation periods. Therefore it can be concluded that a resonant motion connected with the air cushion is not excited. However, the natural period of piston mode of the water column were similar to the measured oscillations.

This was ruled out as the possible source for the oscillations since more recent pressure measurements of the inner pressure showed no large oscillations. The source of the oscillations in the measurements is due to the oscillation of the hydrostatic pressure from the suction anchor. Calculating the wave period of generated waves after impact showed no correspondence with the measurements. Also the natural period of the hoisting system showed much less period than the suction anchor. Also, snapping of wire due to sudden stop of lowering after slack wire were observed in the full-scale test after impact. Therefore it is likely that an impulse from this is exciting a resonant motion of the hoisting system which again will be the source of the suction anchor oscillations.

The heave added mass for the piston mode of the inner fluid calculated with WAMIT seemed too large for the air cushion. The added mass from WAMIT proved more relevant for the coupled piston mode between the air cushion and water column. However, the convergence study did not show correspondence with assumption of infinite fluid. Therefore, improved methods for calculating added mass of the piston mode of the air cushion should be performed.

Wave realizations calculated with the JONSWAP-spectrum show correspondence with realizations calculated with the two peaked Torsethaugen-spectrum. Wave realizations for wind- and swell-sea propagating in the same direction is used for the calculation of dynamic air cushion pressure inside suction anchors during splash zone transition with Hs=1.9 [m] an Tp=5.9[s].

Large oscillations of the wave elevation inside the suction anchor required proper modelling of both outflow and inflow of air to the suction anchor. This accounted for both positive (compressive) and negative (suction) pressure which lead to positive and negative buoyancy forces respectively. By comparison with force measured during FPS-installation it can be concluded that the magnitude of the calculated varying buoyancy forces acting on the suction anchors correspond to the measured forces. However, a statistical comparison by fitting a probabilistic model to the measurements should be performed to establish a sufficient confidence interval for the validity of the calculations.

Slamming calculations on a flat suction anchor top with the Wagner-wedge model overestimate the impact force for deadrise angles up to 17.5 [deg]. However, well correspondence is obtained for the impact on one suction with Wagner's method with deadrise angle of 17.5 [deg] and measured impact force.

Using Wagner's initial slamming coefficient for the whole impact-duration underestimates the impact force. A time varying slamming coefficient developed by integrating the Wagner model on a flat plate gave more correspondence similar impact force compared with the measured force.

The effect of decreasing the perforation ratio show that the magnitude of the dynamic air cushion pressure and thus the buoyancy forces increase. Based on comparison between calculations and measurements from the FPS-installation a method for evaluating a commonly used slack-wire criterion has been proposed for different perforation ratios.

A statistical investigation of calculated force in lifting wire for 10 runs with 9 different combinations of perforation ratios and suction anchor diameters has been conducted. It can be concluded that perforation ratios in the range 1-3 [%] used on suction anchors with diameter in the range 3-6 [m], for the structure and sea state studied here, are considered safe with respect to the slack-wire criterion. However, it is advised to perform more runs in order to obtain a certain

confidence interval for ensuring that slack wire is avoided.

8 Further work

8.1 Expanding theoretical model

The theoretical model developed in this thesis have the following features:

- load time series from measurements to be used directly in calculations
- calculate suction anchor motion due to vessel motion and lowering velocity
- calculate wave realizations from both wind- and swell-sea
- initiate water entry at different time instants between the suction anchors
- calculate varying dynamic air cushion pressure inside suction anchors during splash zone transition
- calculate varying buoyancy forces acting on suction anchors during splash zone transition
- calculate impact forces against conical and flat suction anchor top
- calculate total force in lifting wire due to these buoyancy and impact forces only
- calculate natural period of oscillating air cushion after impact
- calculate natural period of piston mode of coupled air cushion and water column and water column alone
- calculate natural period of hoisting system
- evaluate slack-wire criterion for different perforation ratios and suction anchor diameters

The theoretical model developed in this thesis should be expanded to evaluate transition through splash zone of suction anchors in different sea states. In order to do this the RAO of the installation vessels must be known, such that the vertical motion of the suction anchors can be calculated. Further, to account for diffracted and radiated waves the installation vessel could be modelled in WAMIT such that the calculation of suction anchor motion could take into account the waves generated by the vessel.

If the length of paid out wire length of the tugger winches are known in addition to the vessel-heeling, the time of water entry of each of the suction anchors can be determined by geometrical considerations of figure E.2 in addition to knowing the vertical motion of each anchor.

Regarding force in lifting wire, the horizontal force components from the vertical

forces acting on the different suction anchors could also be included when tilting of the FPS occur.

Considering the force during lowering of FPS in figure 4.3 the most critical load with respect to slack wire or slings in is the water entry of the densely compounded roof of the FPS. In order to evaluate this the model could be expanded to include the splash zone transition of the whole FPS. Then to calculate the buoyancy forces acting on the structure the water filling rate for tubular members must be determined in addition to calculation of added mass and drag for the structural members. A recommendation on if the roof should be removed prior to the splash zone transition could therefore be performed.

8.1.1 Vibrant motion

According to Faltinsen (1990) the duration of the slamming pressure may be in the order of milliseconds. High peak pressures with short duration can create a strong impulse. This can in some cases excite resonant vibrations of structures and may be the case for the high frequency oscillations shown in figure 4.4. These high frequency oscillations may be due to resonant motion of piston mode of air cushion or coupled air cushion and water excited at impact.

If these oscillations induce large vibrations in the structure, these may propagate from structure to the lifting slings or wire. This may be critical for the wire-capacity. To see if the sampling rate is sufficient for obtaining these oscillations the sampling rate should be compared with the natural period of either the air cushion alone, the coupled piston mode of the air cushion and water column and water column alone.

This vibrant motion may also cause the force measured in a lifting wire from a load cell to be erroneous. This may occur if the frequency of vibrant oscillations are in the proximity of the natural frequency of the load cell. The load cells should be calibrated to avoid this.

To account for this vibration in the calculation model the vertical motion of the suction anchor induced by impact can be found by considering the piston mode of air cushion as a linear mass-spring system. The vertical motion is then found by solving the equation of motion for this system. The added mass of the coupled piston mode motion can possibly be calculated with WAMIT.

8.2 Discussion of different effects regarding air cushion piston model

In the theoretical models used for calculating the natural frequencies of the oscillating air cushions in chapter 3.2 to 3.6 no damping effects are accounted for.

Some damping mechanisms that will be present for the piston motions of air and liquid inside the suction anchor which might influence the natural frequencies will therefore be discussed in this chapter.

First the main processes influencing energy dissipation of a 3-D spherical gas cavity discussed by Devin (1959) will be given. These are A) thermal conductivity, B) shear viscosity and C) acoustic wave radiation. A) and B) will be considered here and are discussed in chapter 8.2.1. Another mechanism affecting oscillation of air pockets is air leakage from the air pocket as discussed by Abrahamsen and Faltinsen (2011). This will be discussed in chapter 8.2.2. Finally the geometry of the air pocket will be discussed in chapter 8.2.3.

8.2.1 Heat exchange and viscous effects

Abrahamsen and Faltinsen (2011) has performed experiments of impacting waves with formation of air pockets along a vertical wall. It was shown that heat exchange from the air with water provided a damping ratio of 0.66 - 1.2 % for all test cases. The adiabatic constant γ_a used in equation 3.13 will therefore be affected by this and will deviate some from the value for air which is 1.4 [-]. Abrahamsen (2011) has also shown that viscous boundary layers provide damping of the same order of magnitude as the heat exchange. A study of the viscous boundary layers inside the suction anchor could therefore be studied to improve the results.

8.2.2 Air leakage

Abrahamsen and Faltinsen (2011) also investigated the effect of air leakage from the pockets and heat exchange with the water on the oscillation of the air pockets. For air pockets with leakage a trend of decay in the oscillations was observed in some cases. However, the period was not affected much by the air leakage.

8.2.3 Geometry of air cushion

Abrahamsen and Faltinsen (2012) developed formulas based on the Boundary Element Method (BEM) and investigated a semi-circular air pocket formed on a vertical wall during breaking wave impact. The results from these formulas were compared with sloshing experiments performed by Lugni et al. (2010). The natural frequencies calculated by Abrahamsen and Faltinsen (2012) were smaller than those obtained by Lugni et al. (2010). However, this work show that the natural frequency of the air pocket is sensitive to the assumed shape of the air pocket and also the shape of the free surface outside the air pocket.

8.2.4 Summary of damping mechanisms for oscillating air cushion

Both the simplified, enclosed and polytropic Bagnold-model described in chapter 3.2 and the model describing fluid motion in a well in chapter 3.6 with no damping sources are a simplification of the air cushion inside the suction anchor. Due to the ventilation hatch there will be air leaking from the air cushion. Due to the discussions in chapter 8.2.1 to 8.2.3 the results for the natural frequency based on the simplified models in chapter 3.2 and 3.6 should be compared with experiments or other formulas that accounts for these phenomena.

Since the conditions for the entrapped air cushion described by these experiments are not totally the same as for the air cushion inside the suction anchor, it would be interesting to perform and experiment with a suction anchor-model. This could then investigate if the motion of the inner wave elevation is moving like a piston mode as assumed in the Bagnold- and well-model. A model test of a suction anchor with transparent walls that shows the wave elevation of the water inside the model during splash zone transition could then be performed. This could also be combined with an impact test between the inner wave elevation and the suction anchor top as will be described in chapter 8.3.

8.3 Small-scale impact model test

In Ølund Bertelsen (2013) a proposal for further study of model test with a suction anchor lowered through the water was performed. The goal of this test was to measure force in lifting wire when lowering the suction anchor with a constant velocity. To avoid large buoyancy forces affecting the constant lowering velocity, an actuator should be utilized on top of the suction anchor in order to force a constant downwards motion.

However, after discussion with Sverre Steen (2013) the scaling of the pressure during this test would not be captured in the model-scale studied. Therefore alternative approaches should be considered. In the present thesis a model-test based on assessing the impact pressure will be discussed. Considering sloshing tests performed by Bogart et al. (2010) the impact pressure may be hard to scale from model scale to full-scale. Therefore a discussion of different physical effects and a proposal for a method to perform a proper scaling will be performed in chapter 8.3.1.

8.3.1 Small scale model test with pressure measurement

This chapter will present a method for performing impact tests with a small-scale suction anchor lowered through the splash zone. This test must be set up in such a way that the impact pressure can be scaled properly from model- to full-scale.

When scaling the impact pressure, complex phenomena related to the impact as described in table 3.2 must be accounted for. In order to take these phenomena into account a theoretical approach according to Braeunig et al. (2010) or a model test with proper scaling of the impact pressure can be performed. The latter will be discussed in this chapter.

To obtain Complete Froude Scaling (CFS) when scaling the impact pressure a one dimensional (1D) Bagnold-model as shown in figure 3.3 where no evacuation of air is present will be considered. According to Bogart et al. (2010) (CFS) can be achieved for the Bagnold-model if the excitations at impact conditions are Froude-scaled in addition to proper scaling of the phenomena described in table 3.2. Then, to achieve a CFS a good starting point is to have similar global flow conditions in both model and full scale according to Braeunig et al. (2009). This is performed by keeping the hydrodynamic pressure $\rho_L U^2$ and the hydrostatic pressure $\rho_L g L$ constant at both scales.

For global flow conditions in a time instant prior to impact the water is incompressible compared to impact where the water is compressed and local interactions between the water and the air will occur. According to Maillard and Brosset (2009) the global flow is deterministic, and it is the local flow that will determine if model tests at small scale is relevant for scaling the impact pressure with Froude-scaling. Since the local flow accounts for interaction between the water and air, the simplified Bagnold-model where no evacuation of air is present cannot be utilized.

To account for the air escape through the ventilation hatch during splash zone transition a similar approach as performed by Maillard and Brosset (2009) could be performed. Maillard and Brosset (2009) performed small scale sloshing experiments where the air was allowed to escape with different density ratios between the liquid and the gas. It was discovered that in order to Froude-scale the impact pressure in a model test performed with both water and air, the density ratio between water and air should be exactly 0.004 [-].

However, in Maillard and Brosset (2009)'s experiments the density ratio between water and air was found to be 0.0012 [-] which were not sufficient. Therefore a mixture of a heavier gas with Sulphur hexafluoride (Sf_6) and Nitrogen dioxide (N_2) were introduced in the experiments to get the desired density ratio. This trend of adding a heavier gas to improve scaling ratios in experiments was also performed by Braeunig et al. (2009) who investigated scaling of speed of sound in liquid and gas. There it was discovered that to properly account for the gas compressibility the fluid and the gas should be in Froude-scaling accordance. To satisfy the requirement of similar speed of sound in fluid and gas Braeunig et al. (2009) found that water will require a gas with a speed of sound equal to 45 $\frac{m}{s}$. This is extremely high, and a gas with higher density and thus lower speed of sound was therefore advised.

This can also be argued theoretically as performed by Braeunig et al. (2010). There the conservation equations for mass, momentum and energy were applied to have the right balance both in model and full scale for the phenomena described in table 3.2. To account for the escape of the air and the compressibility effects of both the air and the water Braeunig et al. (2010) states that: "*impose at both scales the same density ratio between the air and the water and to have also the Equations of State in Froude-agreement in both the air and the water*".

If this is satisfied a conservative approach to scale the pressure properly could then be performed by assuming that no other phenomena than those given in 3.2 are present according to Maillard and Brosset (2009). Then the conservation equations will be satisfied by scaling the impact pressures as shown in equation 8.1:

$$p^{fs} = \left(\frac{\rho L^{fs}}{\rho L^{ms}}\right) \lambda_{scale} p^{ms} \tag{8.1}$$

Where:

- pressure at full-scale is the p^{fs}
- pressure at model-scale is the p^{ms}
- length at full-scale is the L_{fs}
- length at model-scale is the L_{ms}
- scaling factor between model- and full-scale λ_{scale}

For determining the scale of the suction anchor during this type of impact test, scales used during sloshing experiments by Bogart et al. (2010) can be used as guidance. There a test scale of $\frac{1}{40}$ was been adopted with water as fluid and a heavy gas tuned to match the density ratio. However, the size of the ventilation hatches to be used at this scale cannot be scaled according to the requirement of geometrical similarity. The air evacuation corresponding to the size of the ventilation hatch must be sufficient for obtaining CFS of the impact pressure. However, this requires tuning of the gas mixture. Results from Bogart et al. (2010) show that it is not possible to avoid a compressibility bias for the gas compressibility modulus when tuning the gas to get satisfying CFS conditions.

If these conditions are satisfied in the experiment the impact pressure can be Froude-scaled according to Bogart et al. (2010). Their results also showed that the pressure could be scaled by a factor of λ_{scale} while a parallel study by Kimmoun et al. (2010) obtained a scaling factor of $\sqrt{\lambda_{scale}}$ for the pressure. Therefore there are no general method to scale the impacting pressures present today. However, the requirements for a sloshing model-test and an impact test of a suction anchor with proper modelling of air flow through ventilation hatch during lowering through splash zone at constant velocity are similar for obtaining CFS.

Based on the discussions given above a method for performing small-scale impact test on suction anchors with proper modelling of air flux through ventilation hatch is proposed. If proper scaling of density ratio between fluid and gas are satisfied a Complete Froude Scaling of the impact pressure can be obtained with a scale factor of $\frac{1}{40}$. The test should be performed in a controlled environment with a gas mixture satisfying the desired density ratio between fluid and gas.

A possible controlled environment could be a cylinder containing a certain level of the correct fluid and gas. Then to perform the impact, a piston inside the cylinder will be forced downwards with a constant velocity into the fluid. The piston should then incorporate the desired ventilation area on the top. In order to maintain the density ratio between fluid and gas, the combustion process in a diesel engine can be utilized. In that way when the piston is impacting against the fluid, the gas flowing out of the ventilation hatch will be evacuated to a container. During this evacuation of gas, new gas from a surrounding reservoir should be introduced in order to keep the density ratio between the fluid and gas correct for scaling the pressure. This principle is shown in figure 8.3.1:

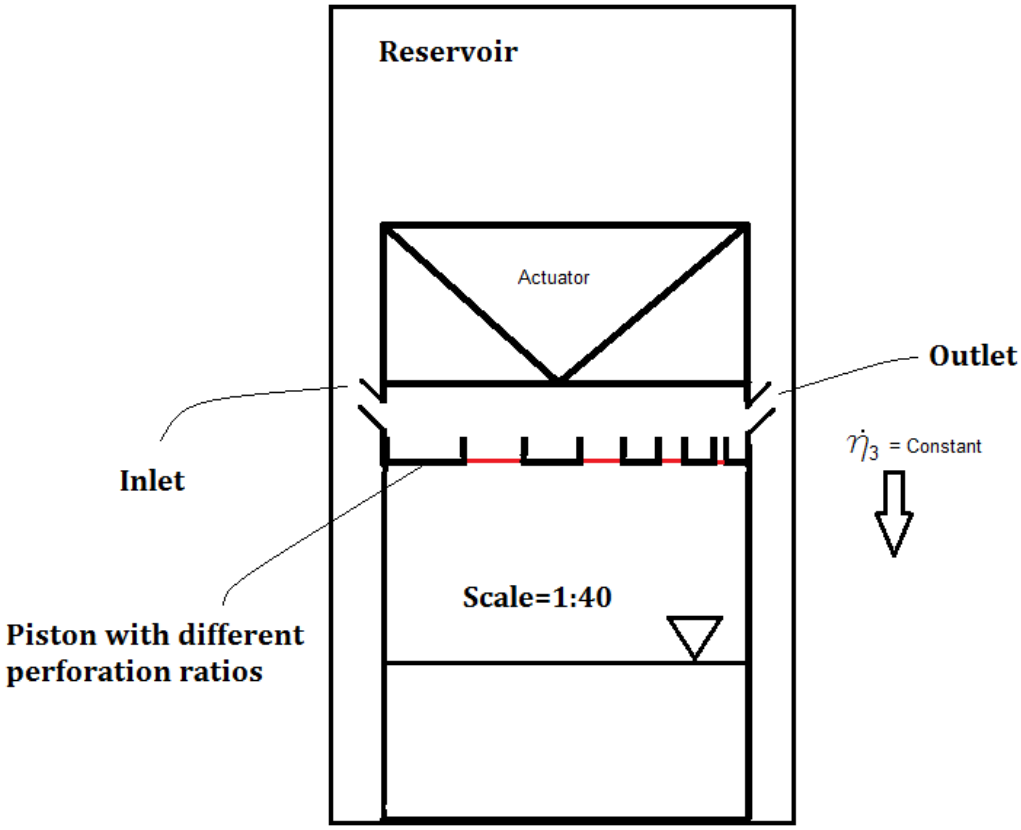

Figure 8.1: Model of suction anchor to be used in piston-mode impact test at different perforation ratios

The pressure inside the suction anchor can be measured using absolute pressure sensors applicable for measuring pressures in air pockets entrapped by water as used in Abrahamsen and Faltinsen (2011). The pressure can then be used to estimate the slamming load, which can be used to verify the theoretical slamming calculations established in chapter 4.5.

Also, the effect of impact on oscillating air cushion could be investigated. A study of different damping contributions as discussed in chapter 8.2 could then be studied if the test is performed with transparent suction anchor walls.

Limitations

In reality the water elevation impacting against the suction anchor top will be varying greatly with different wave conditions. Therefore it is not easy to predict how much of the suction anchor top that will be wetted during the impact. Therefore a model test with transparent suction anchor walls should be carried out in order to describe the behaviour of the wave elevation while measuring the

slamming pressure. In the piston-mode impact test described here only impact against a flat surface will be possible, and therefore the influence of waves will not be accounted for.

The gas mixture satisfying the correct density ratio for obtaining must be satisfied for each size of the ventilation hatch that will be used. This will be time consuming and will therefore limit the number of possible hatch openings to be used in the test.

8.4 Slamming calculation with Pressure-impulse method

Ølund Bertelsen (2013) has already shown that the slamming model with a wedge approach give good results for conical shaped tops. Now a more improved slamming calculation that has given good results for flat plate impacts will be proposed. This is known as the pressure-impulse method and has been used by Peng and Peregrine (2000) previously. Peng and Peregrine (2000) states that prior to the impact it is assumed that the peak pressure increase linearly until impact. Post-impact it is assumed that the relative velocity decreased linearly to zero. With these assumptions Peng and Peregrine (2000) were able to calculate the post impact velocity by the linear relation shown in equation 8.2:

$$V_a = \frac{m_{top} V_{rel}}{m_{top} + A_{33,disk}} \tag{8.2}$$

Where:

- m_{top} is the mass of flat suction anchor top
- Va is the velocity of plate after impact

The impulse is found by integrating the pressure over a small time step δt. Then Peng and Peregrine (2000) found that the total impulse for a flat plate was equal to $I = V_a \pi L^2$. The peak pressure can then be calculated with equation 8.3:

$$P_{peak} = \frac{2I}{\Delta t} \tag{8.3}$$

Where:

- P_{peak} is the peak pressure at impact
- I is the pressure impulse at impact
- Δt is the duration of impulse at impact

This approach could be adopted to the flat suction anchor top, where the impulse is integrated around the circular.

Bibliography

Abrahamsen, B. C. (2011). *Sloshing induced tank-roof impact with entrapped air pocket*, PhD thesis, Norwegian University of Science and Technology, Centre for Ships and Ocean Structures.

Abrahamsen, B. C. and Faltinsen, O. (2011). The effect of air leakage and heat exchange on the decay of entrapped air pocket slamming oscillations, *Physics of fluids 23* .

Abrahamsen, B. C. and Faltinsen, O. (2012). The natural frequency of the pressure oscillations inside a water-wave entrapped air pocket on a rigid wall, *Fluids and structures* (35): 200–212.

Aerohydro (2014). Multisurf for wamit 8.5.
URL: *http://aerohydro.com/?wpsc-product=multisurf-for-wamit-8-5*

Araujo, R., Vaz, M. and Couto, P. (2012). Methodology for overboarding operations, *Marine operations Specialty Symposium*, Subsea 7.

Arunjyoti, S. and Gudmestad, O. T. (2010). Splash zonel ifting analysis of subsea structures, *International Conference on Ocean, Offshore and Arctic Engineering*.

Aspelund,Leiv (2014). Mail correspondance during project and master thesis work.

Bagnold, R. (1939). Interim wave report on wave-pressure research, *ICE* **12**(201).

Bitner-Gregersen, E. M. and Hagen, O. (2003). Effects of two-peak spectra on wave crest statistics, *ASME 2003 22nd International Conference on Offshore Mechanics and Arctic Engineering*, American Society of Mechanical Engineers, pp. 305–312.

Blevins, R. D. (1984). *Applied fluid dynamics handbook*, Krieger publishing company, Malabar, Florida.

Bogart, H., Leonard, S., Brosset, L. and Kaminski, M. (2010). Sloshing and scaling: Results from the sloshel project, *International Offshore and Polar Engineering Conference*, number 20.

Braeunig, J.-P., Brosset, L., Dias, F. and Ghidaglia, J., M. (2009). Phenomenological study of liquid impacts through 2d compressible two-fluid numerical simulations, *International Offshore and Polar Engineering Conference*, number 19.

Braeunig, J.-P., Brosset, L., Dias, F., Ghidaglia, J.-M. and Maillard, S. (2010). On the effect of phase transition on impact pressures due to sloshing, *International Society of Offshore and Polar Engineering Conference*.

Campbell, T., W. J. and Weynberg, P. (1977). An investigation into wave slamming loads on cylinders, *OSFLAG 2A*.

Det Norske Veritas (2010). Recommended practice Det Norske Veritas DNV-RP-C205, Environmental conditions and environmental loads.

Det Norske Veritas (2011). Recommended practice Det Norske Veritas DNV-RP-H103, Modelling and analysis of marine operations.

Devin, C. J. (1959). Survey of thermal, radiation, and viscous damping of pulsating air bubbles in water, *Acoustical Society of America* **31**(12).

Faltinsen, O. (1990). *Sea Loads on ships and offshore structures*, Cambridge University press, New York.

Faltinsen, O. and Timokha, A. N. (2009). *Sloshing*, Cambridge University press, New York.

Greco, M. (2014). Conversations and mail correspondance during thesis work. Professor in Marine hydrodynamics at the Norwegian University of Science and Technology.

Greco, M., Colicchio, G. and Faltinsen, O. (2009a). Bottom slamming for a very large floating structure: Coupled global and slamming analyses, *Journal of fluids and structures* **25**: 420–430.

Greco, M., Colicchio, G. and Faltinsen, O. (2009b). Bottom slamming for a very large floating structure: Uncoupled global and slamming analyses, *Journal of fluids and structures* **25**: 406–419.

Greco, M. and Lugni, C. (2012). 3-d seakeeping analysis with water on deck and slamming. part 1: Numerical solver, *Fluids and structures* **33**.

Haavard Haaskjold (2013). Conversations and mail correspondance during summer internship in det norske.

Holm, H. (2013). Lecture notes in computer methods applied for marine technology.
URL: *http://www.ivt.ntnu.no/imt/courses/tmr4160/exercises/simship/ex3/*

Jacobsen, T., Næss, T.-B. I. and Karunakaran, D. (2012). Comparison with full scale measurements for lifting operations, *Marine operations specialty symposium*.

Kimmoun, O., Ratouis, A. and Brosset, L. (2010). Sloshing and scaling: Experimental study in a wave canal at two different scales, *International Society Offshore and Polar Engineering Conference*, number 20.

Kreyzig, E. (2006). *Advanced engineering mathematics*, 9th edn, John Wiles and Sons Inc.

Lankhorst Ropes (2014).
URL: *http://www.lankhorstropes.com/Offshore/Offshore-Steel-Wire-Ropes*

Larsen, C. M. (2014). Personal communcation.

Larsen, H. (2013). Personal communication, Meetings during summer internship.

Lewis, A. (2008). Load handling presentation.

Li, P. (2014). Personal communcation during thesis work.

Lugni, C., Brocchini, M. and Faltinsen, O. M. (2010). Evolution of the air cavity during a depressurized wave impact. ii. the dynamic field, *Physics of Fluids (1994-present)* **22**(5): –.
URL: *http://scitation.aip.org/content/aip/journal/pof2/22/5/10.1063/1.3409491*

Ølund Bertelsen, T. (2013). Project work 2013: Hydrodynamic challenges with installation of subsea structures through splash zone. •.

Maillard, S. and Brosset, L. (2009). Influence of density ratio between liquid and gas on sloshing model test results, *International Offshore and Polar Engineering Conference*, number 19.

Mathworks (2014a). *MATLAB documentation-center*, Mathworks.
URL: *http://www.mathworks.se/help/signal/ref/butter.html*

Mathworks (2014b). *ODE45 a numerical solver for non-stiff differential equations*, matlab 2013a edn, Mathworks.
URL: *http://www.mathworks.se/help/matlab/ref/ode45.html*

Miles, J. (2002). On slow oscillations in coupled wells, *Fluid Mechanics* **455**: 283–287.

Myrhaug, D. (2007). Marine dynamics - irregular sea compendium.

Newman, J. N. (1977). *Marine hydrodynamics*, MIT press.

NORSOK (2007). *NORSOK N-003, Action and action effects*, 2 edn, Standards Norway.
URL: *https://www.standard.no/en/sectors/energi-og-klima/petroleum/norsok-standard-categories/n-structural/n-0031/*

Ochi, M. (1964). Prediction of occurrence and severity of ship slamming at sea, *5th Symposium on Naval Hydrodynamics*.

O.M. Faltinsen (2005). *Hydrodynamics of high speed vehicles*, Cambridge University press, New York.

Peng, W. and Peregrine, D. (2000). Pressure-impulse theory for plate impact on water surface, *International Workshop on Water Waves and Floating bodies*.

Rottmann, D. K. (2003). Matematische formelsammlung.

Sandvik, P. C. (2014). Mail correspondance and conversations during thesis work, Personal communication.

Seatex, K. (n.d.). *Seatex MRU 6 and 4, Installation Manual*, 9 edn, Kongsberg Seatex.
URL: *ftp://poseidon.hcmr.gr/pub/mru4.2/Man˙inst˙mru˙6˙r9.pdf*

Sparrevik, P. M. (2014). Penetration test dudgeon venting test, *Technical report*, Norwegian Geotechnical Institute.

Steen, S. (1993). *Cobblestone effect on SES*, PhD thesis, Norges tekniske høgskole.

Storvik, T. (2012). Jette-structures installation report, *Technical report*, Det norske oljeselskap ASA.

Storvik, T. (2013). Personal communication, Mail correspondance and meetings during summer internship.

Sub (2014). *Data sheet for Normand Oceanic*.
URL: *http://www.subsea7.com/en/what-we-do/our-vessels.html*

Sverre Steen, Professor in marine hydrodynamics, N. (2013). Conversations and mail correspondance during project work.

Tormod Bøe (2013). Conversations and mail correspondance during project work.

Torsethaugen, K. and Haver, S. (2004). Simplified double peak spectral model for ocean waves, *International Society of Offshore and Polar Engineers*, number JSC-193.

Verhagen, J. (1967). The impact of a flat plate on a water surface, *J. Ship Res* **11**(4): 211–223.

von Karman, T. (1929). The impact of seaplane floats during landing, *Technical report*, NACA, Washington. Technical note 321.

WAFO-group (2000). *WAFO - A Matlab Toolbox for Analysis of Random Waves and Loads - A Tutorial*, Math. Stat., Center for Math. Sci., Lund Univ., Lund, Sweden.

Wagner, H. (1932). Über stoss- und gleitvorgänge an der oberfläche von flüssigkeiten, *Zeitschr. f. Angewandte Mathematik und Mechanik* **12**(4): 192–235.

WAMIT user manual (2006). 6.4 edn.
URL: *www.wamit.com*

www.subseaworldnews.com (2013).
URL: *http://subseaworldnews.com/2013/05/02/det-norske-to-use-subsea-facilities-on-jette-field-norway/*

Øystein Døskeland (2012). *Operations manual for installation of FPS at Jette field*, Subsea 7.

Øystein Døskeland (2014). Mail correspondance during internship in det norske oljeselskap and during master thesis.

A Rules and regulations

Rules and regulations influence the installation of subsea structures all the way from the design phase to the actual installation. Different factors influencing the construction of a subsea structure can be seen in figure A.1:

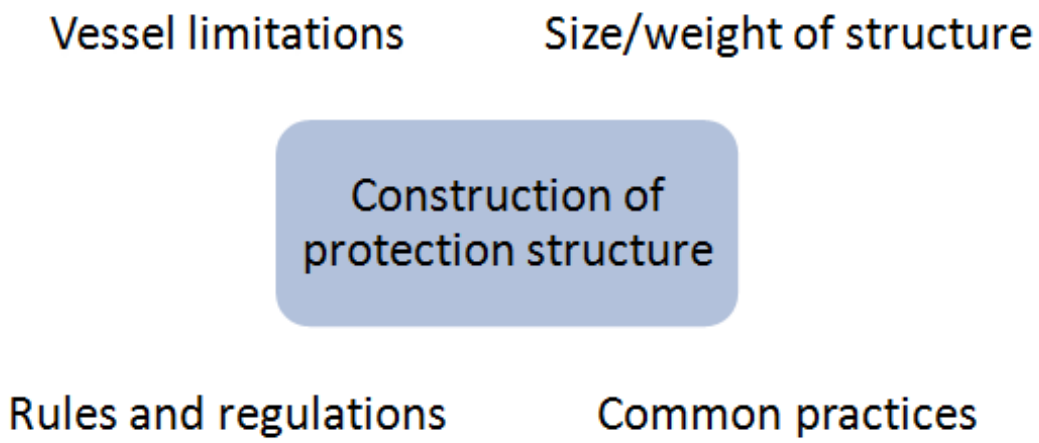

Figure A.1: Factors influencing construction of subsea structure

Before the relevant rules and regulations on NCS are given, the responsibilities between oil companies, structural manufacturer ,contractors and class societies during installation of subsea structures will be discussed. The hierarchical relationship between these actors are illustrated in figure A.2:

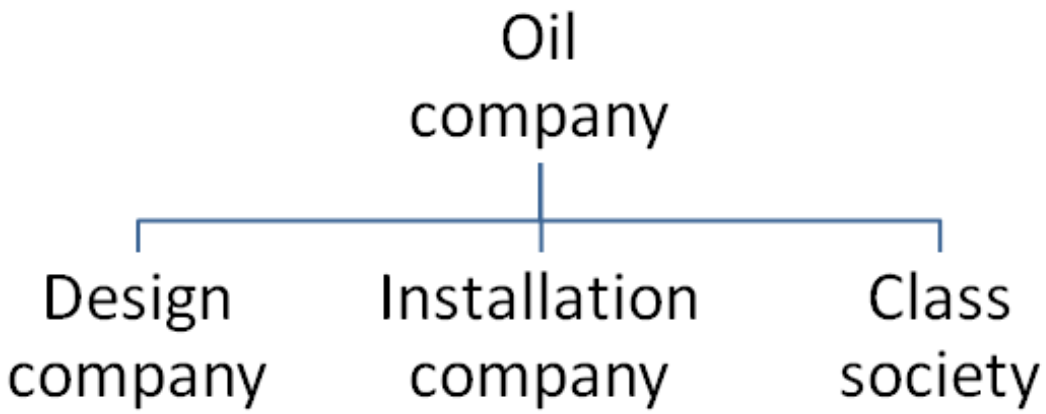

Figure A.2: Relationship between different actors during a subsea installation

In Ølund Bertelsen (2013) a literature study of the relevant rules and recommended practises used for installations of subsea structures have been carried out. An illustration of the governing rules, standards and common practices used on the NCS are given in figure A.3:

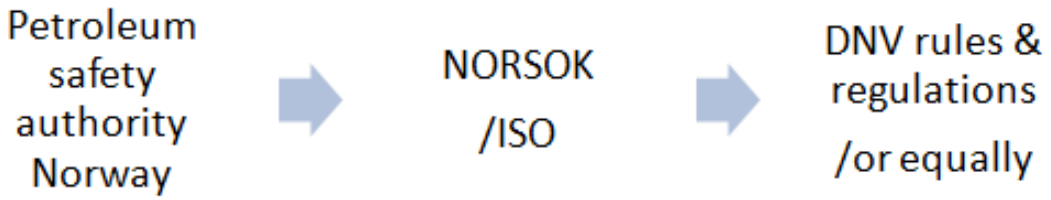

Figure A.3: Relevant rules, standards and practices on the NCS

B Full-scale tests

B.1 Suction anchor studied in full-scale tests

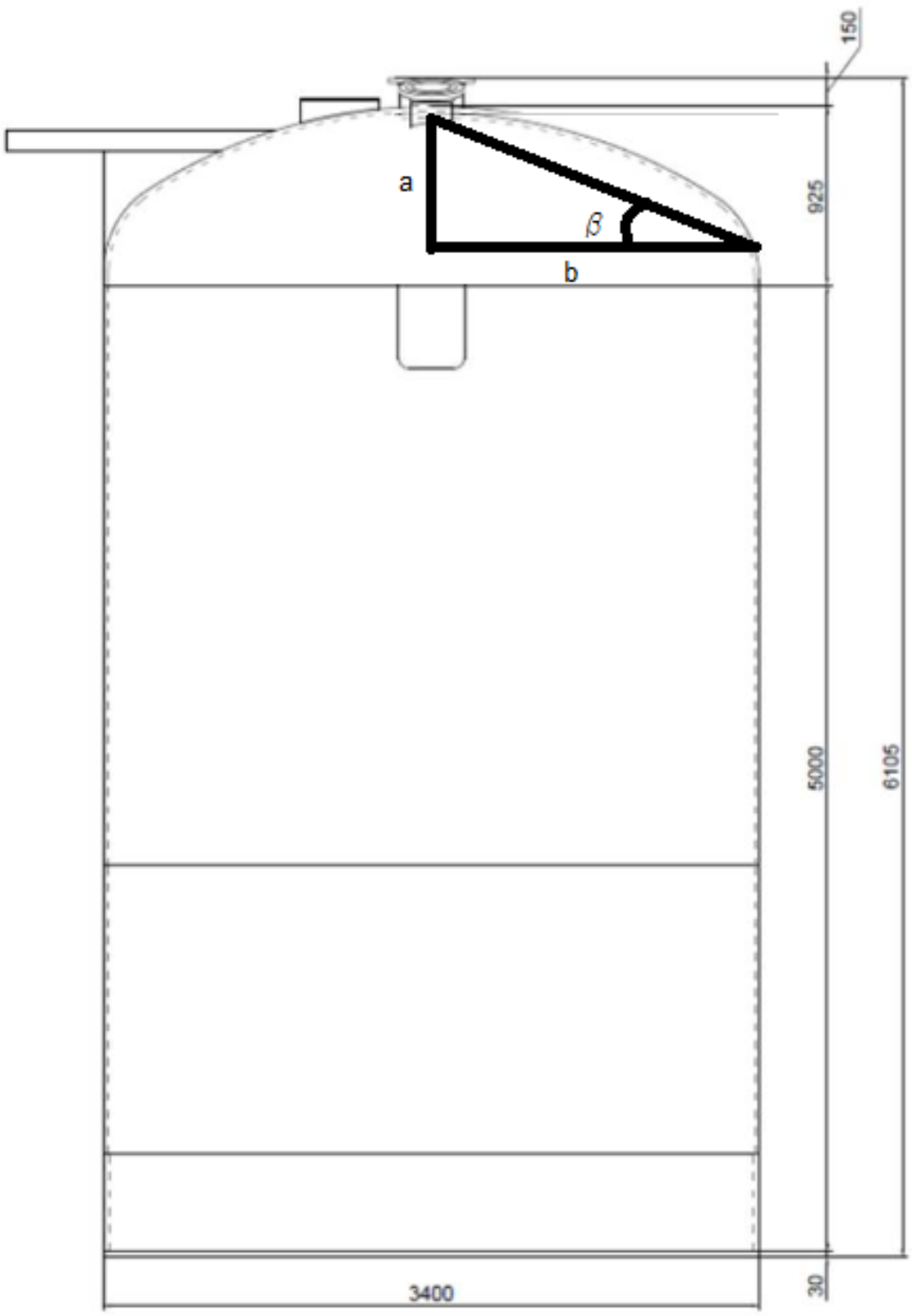

Figure B.1: Drawing of suction anchor used in full scale measurements, courtesy of (Aspelund,Leiv; 2014), Subsea 7

C Parameter study

C.1 Decreasing contraction coefficient

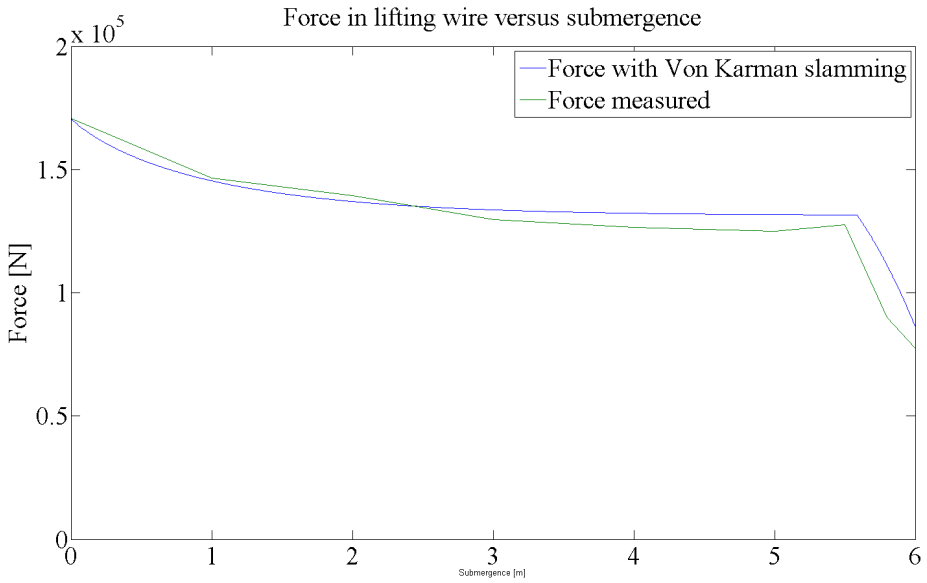

Figure C.1: Parameter study with different contraction coefficient

C.2 Introducing varying lowering velocity

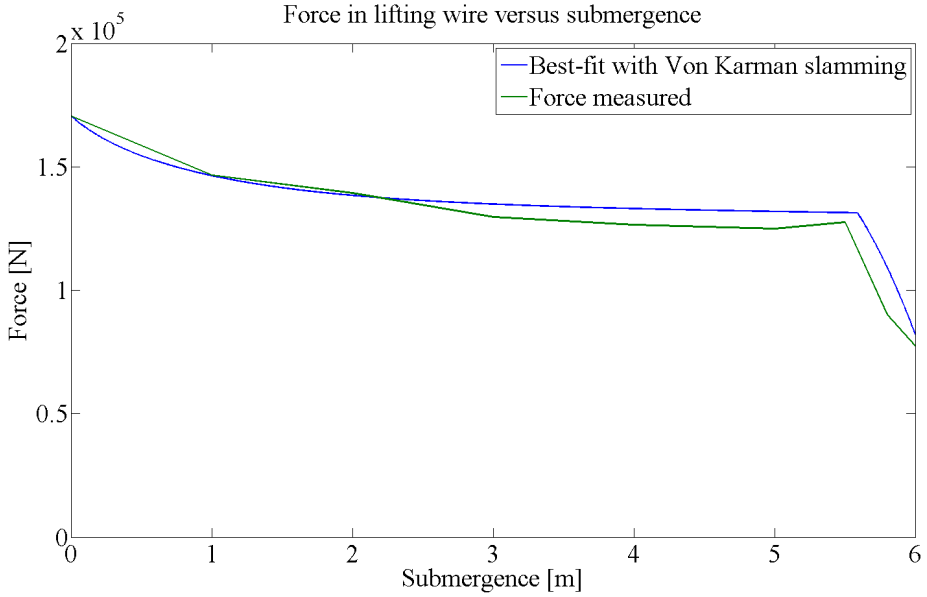

Figure C.2: Parameter study with varying lowering velocity

C.3 Varying impact area

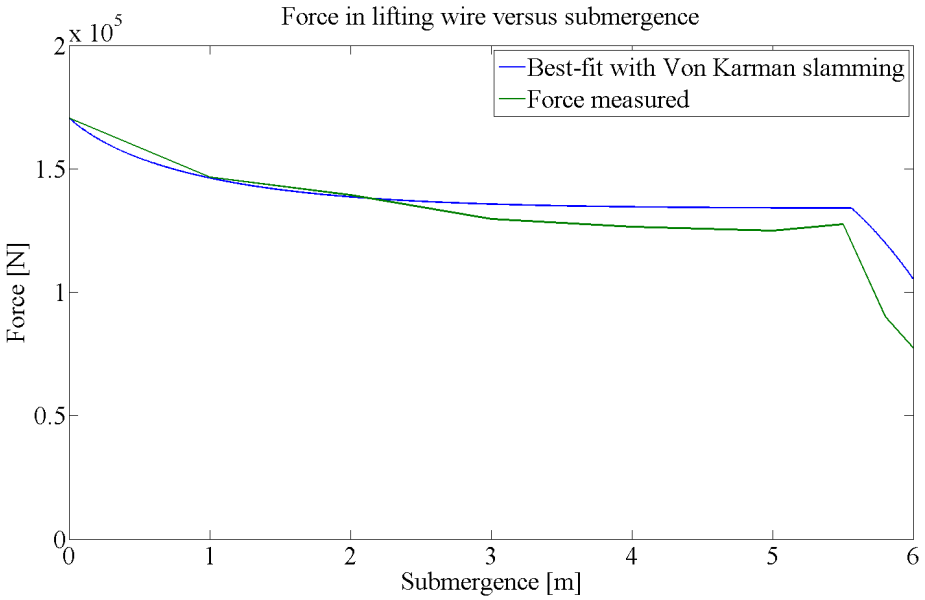

Figure C.3: Parameter study with decreasing cylindrical height and increasing deadrise angle

C.4 Including regular waves

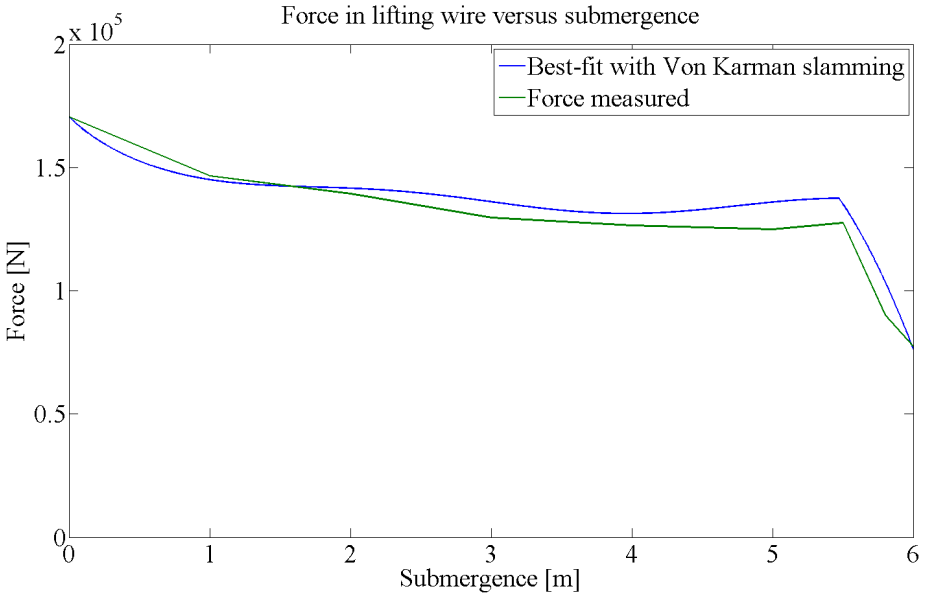

Figure C.4: Parameter study with incoming regular waves with Hs equal to 0.1 [m]

C.5 Parameter study with irregular waves created from JONSWAP spectrum

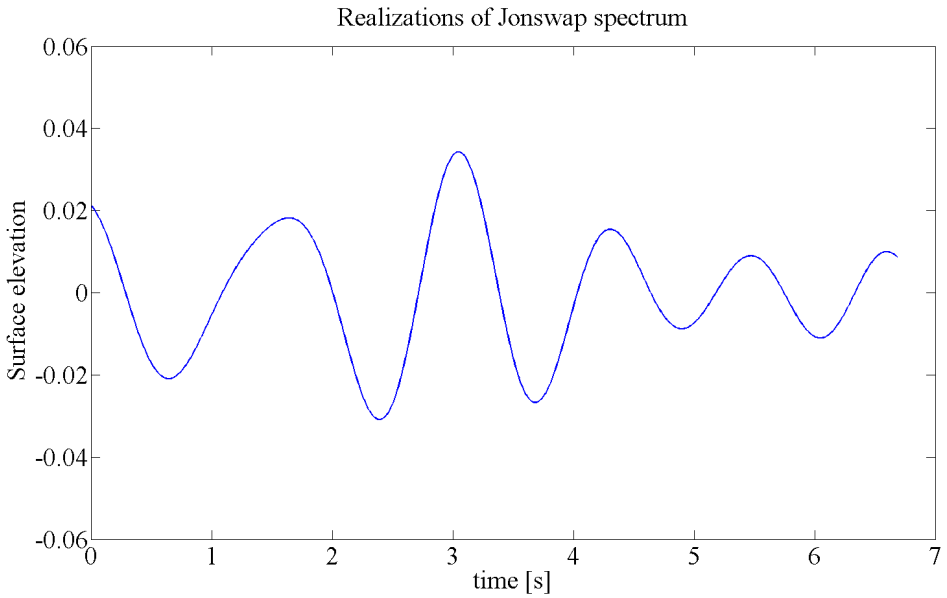

Figure C.5: Realization irregular waves by the JONSWAP spectrum with Hs equal to 0.1 [m]

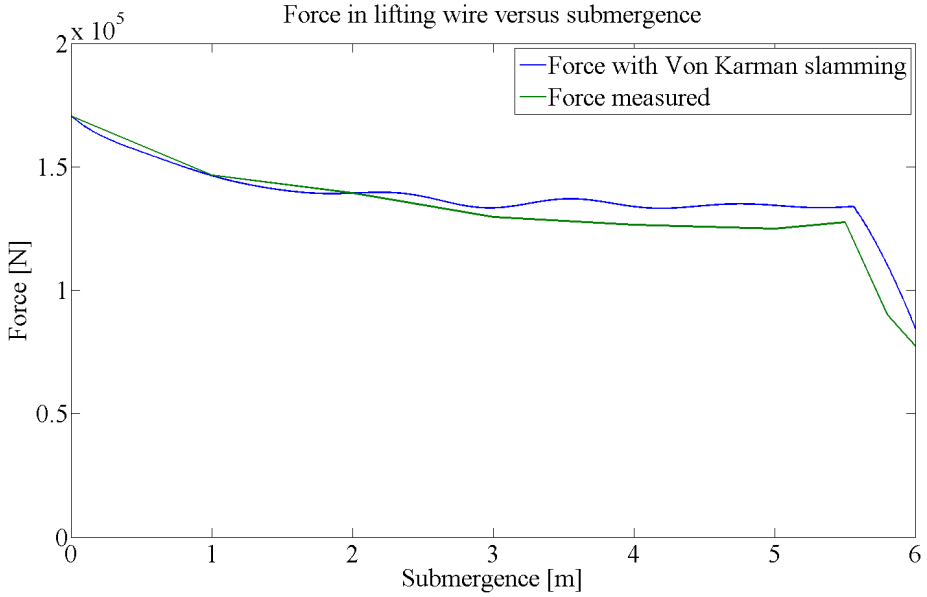

Figure C.6: Parameter study with incoming irregular waves with Hs equal to 0.1 [m]

D Pressure measurement investigations

D.1 Slamming on suction anchor

Figure D.1: Snapshot of slamming on single suction anchor

D.2 Natural period of hoisting system

Calculation of eigenperiod of hoisting system according to DNV-RP-H103

Anchor		**Dimension**	**Notes**
Mass	15900	kg	Calculated
H	5.9	m	
D	3.4	m	
rho	1025	kg/m^3	
g	9.81	m/s^2	
Area of 3D cylinder project on a plane	9.08	m^2	
Vertical added mass coeff(2D)	0.318309886	[-]	Half of circular disk
Added mass parameter λ for the suction anchor	0.34	[-]	sec 4.6.3.3
Added mass for flat circular plate	21.09	[tonnes]	sec 4.6.3.3
Simplified added mass in heave for a 3D cylinder	34.39	[tonnes]	sec 4.6.3.3
Crane tip			
Crane tip deflection	0.3	m	assumed
Stiffness due to crane tip deflection	519930	N/m	
Cable			
Wire length	15	m	assumed
E modulus	8.54E+10	N/m^2	assumed
Weight pr m	6.54	kg/m	assumed
Total weight of cable	98.1	kg	
Diameter	0.0408	m	assumed
Area	0.001307405	m^2	
Elastic stiffness cable	7.44E+06	N/m	
Theta	1	-	
Slings	-		
D	68	mm.	assumed
Resonance period hoisting system	5.00E-01	s	

D.3 WAMIT-input files

These are attached in the DAIM.zip file, folder D3.

E Jette-installation

E.1 Installation vessel

Figure E.1: Installation vessel at Jette-field, Normand Oceanic, courtesy of Sub (2014)

E.2 FPS-installation and related challenges

During the FPS-installation the maximum lifting radius of 20.5 [m] for the heavy lift crane on board Normand Oceanic was used with the corresponding maximum lifting capacity of 299 [tonnes] according to Sub (2014). When the FPS is lifted from the deck and during the over boarding phase of the installation Subsea 7 utilize tugger winches for controlling the pendulum motion of the FPS until it is lowered through the splash zone. When the FPS is submerged sufficiently below the free surface a Remote Operated Vehicle (ROV) release the wires from the tugger winches connected to the FPS. The installation method is illustrated in figure E.2 where the vessel is seen from behind:

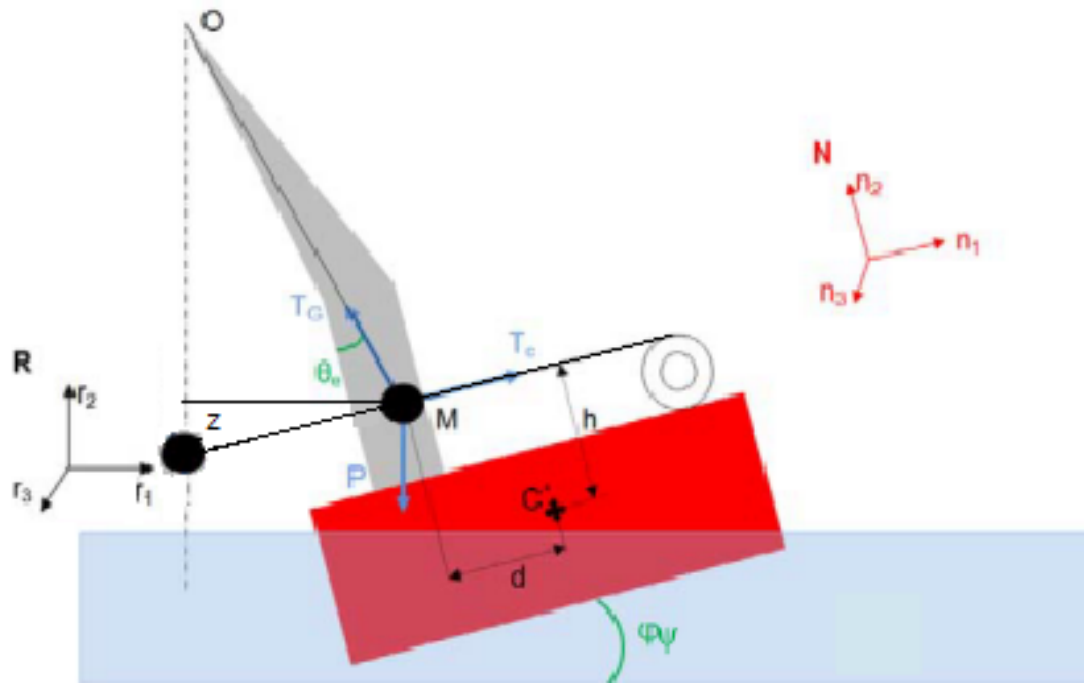

Figure E.2: Tilting of FPS during lowering

Here the vessel is heeled in order to increase the distance between the structure and vessel-side. With this installation-method the maximum load capacity in the tugger winches will be the limiting criteria for the installation during lift in air. If the vessel has large roll-motions the crane tip accelerations can become so large that the maximum load in the tugger winches is exceeded. However the pitch motions may also be large if the incoming waves have periods close to the vessel's natural period in pitch. Therefore it is important to monitor both the roll motions with the MRU during the installation.

If the sea state, when the installation is to be performed, is lower than the maximum sea state it is not certain if the installation can be performed. This is due to the vessel response may be too large if the relative direction between the wind and swell sea is badly conditioned Jacobsen et al. (2012). Therefore important operational decisions as the heading of the vessel are made by the captain which also confers with the operation manager and the engineer who has performed the installation-analyses.

Good seamanship will be important for performing a safe installation, especially when deciding to "go for the operation" is important and may be depending on the crew experience. When the wind direction change, the sea flattens out and one may get a short window of flat sea before building up from another direction. When the wind strength drops, a slow decrease in the swell may be experienced. Often with small directional change, the swell will be reduced. This is the likely period for commencement of operations according to Lewis (2008).

E.3 Wave propagation

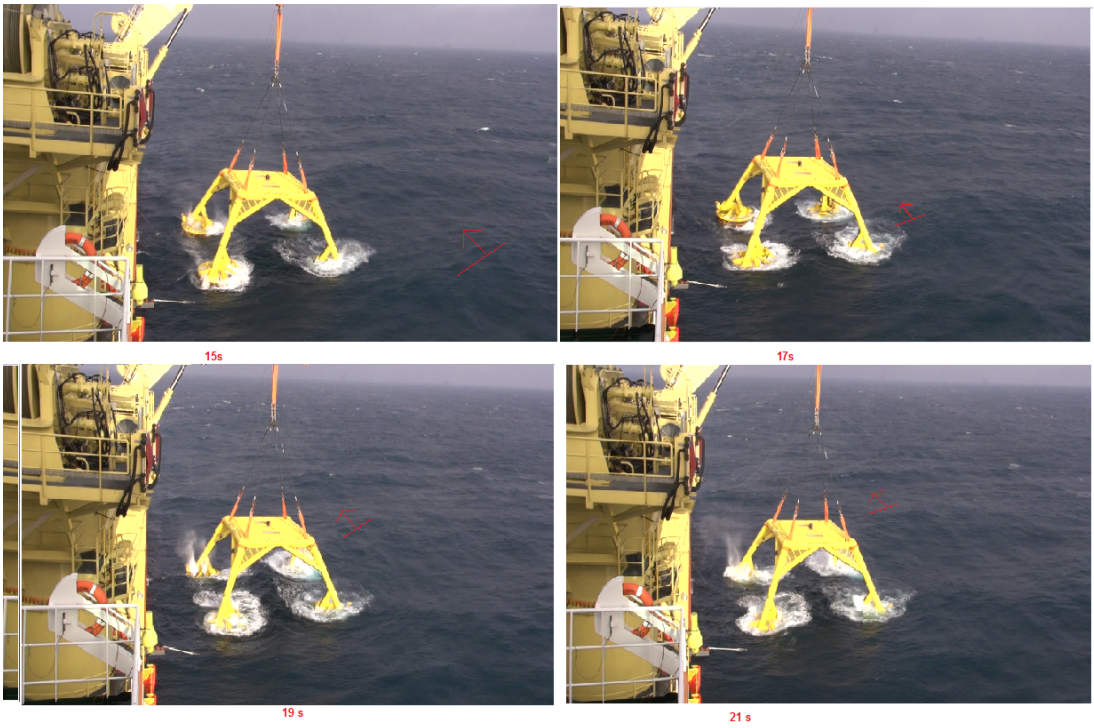

Figure E.3: Waves from video of FPS-installation

E.4 3D-waves

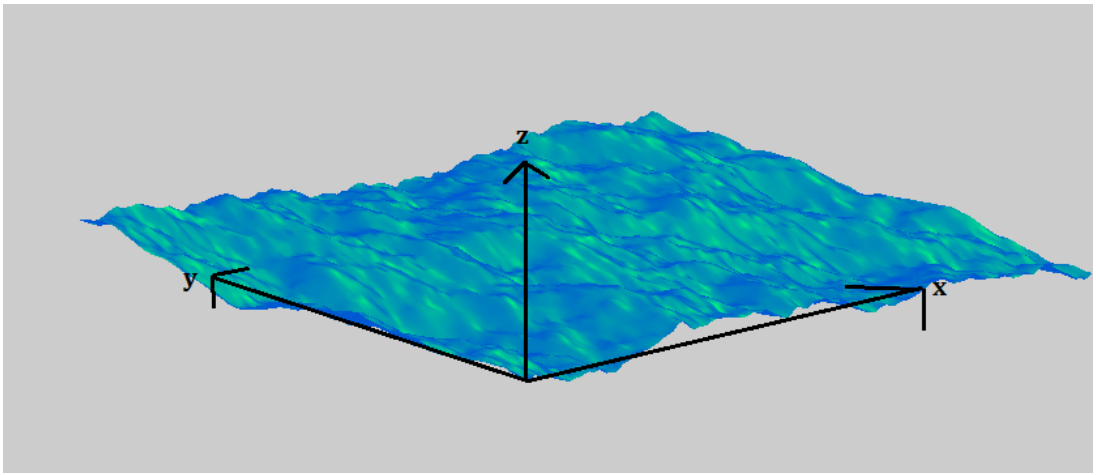

Figure E.4: 3D-waves created with directional spectrum

F Jette-analysis

F.1 Principle of air flux in and out of ventilation hatch

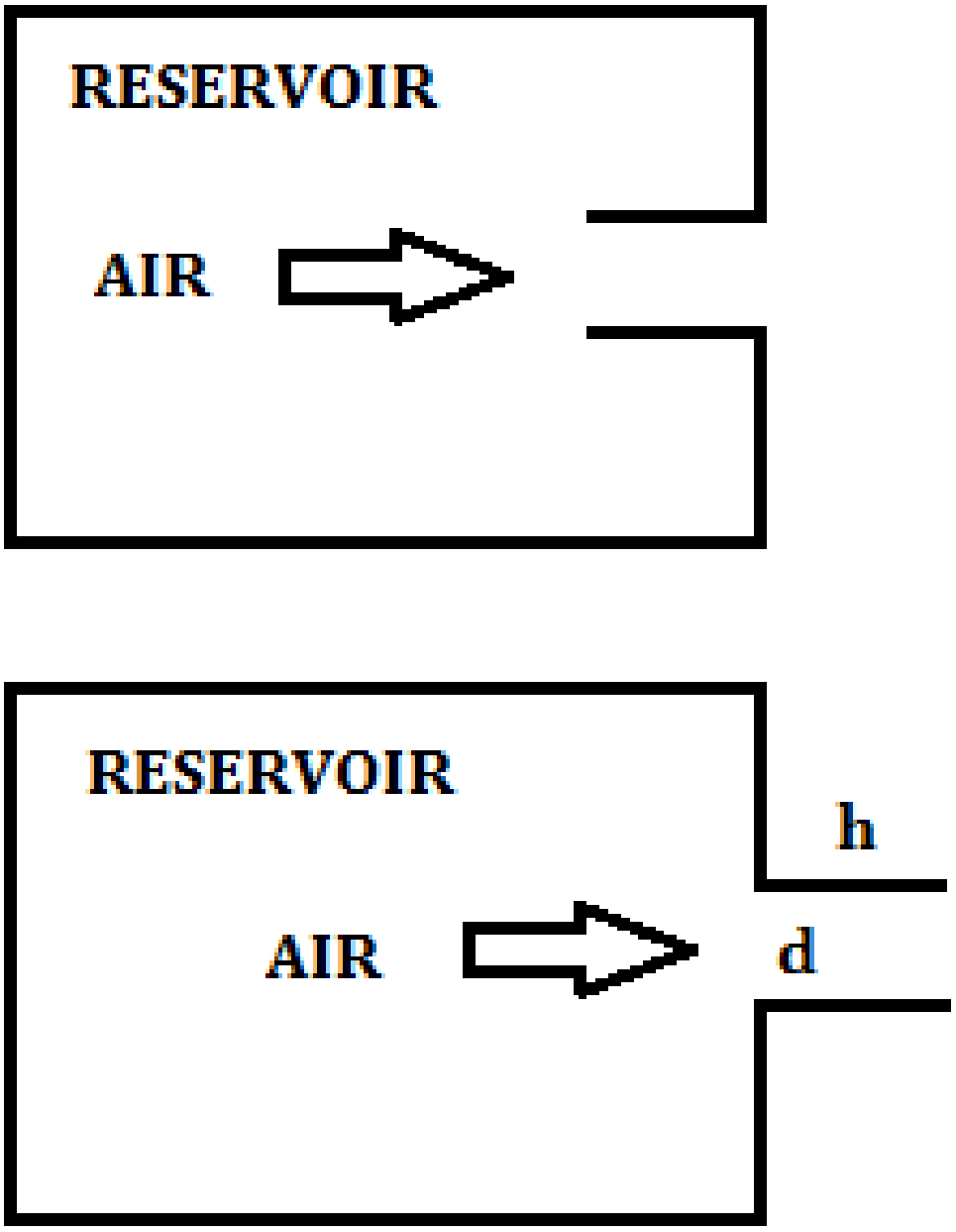

Figure F.1: Model used for inflow and outflow of air flux

F.2 Weather-data during FPS-installation

According to Storvik (2013) when planning the FPS-installation weather statistics from previous years measured at the Heimdal-field which is close to Jette-field were used. These weather statistics are important for preliminary installation analyses.

Prior to the FPS-installation weather forecasts were used together with a weather buoy to determine the appropriate date of the installation of the FPS. The weather buoy measures the sea state at a 30 [s] interval at a location close to the Jette-field. According to Haavard Haaskjold (2013) when determining the appropriate time of installation the wave heights are often used as the limiting criteria, however it is also important to consider the wave periods and compare these against the critical natural periods of the ship and the lifting system. The limiting sea states for the different phases during the FPS-installation are found from hydrodynamic-analyses of the splash zone transition by Øystein Døskeland (2014) and are shown in table F.1:

Hs [m]	Tp [s]
2	5 to 15
1.5	15 to 18

Table F.1: Limiting sea states for FPS through splash zone, courtesy of Øystein Døskeland (2014)

These sea states are limited by the limiting criterion defined as maximum load capacity in the tugger winches as described in chapter E.2.

Measurements of Hs and Tp from the wave buoy before and during operation is shown in figure F.2:

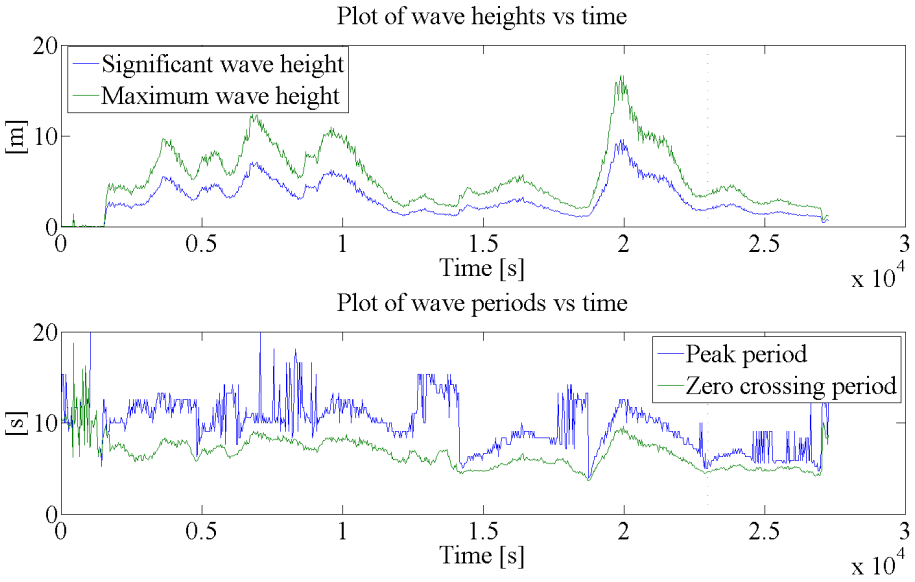

Figure F.2: Significant wave height and Peak period from wave buoy, courtesy of Øystein Døskeland (2014)

Considering the ranges indicated by the red lines in figure F.2 it can be seen that the deployment of the FPS could be performed earlier than indicated if only considering the limiting Hs. However, this is not possible due to large the peak periods possibly due to swell sea with wave periods in the proximity of the natural period in heave of the installation vessel according to Øystein Døskeland (2014). Also a weather window with sufficient time to perform the installation was not present in between the acceptable Hs-range prior to the operation.

F.3 Short crested waves

Forecasted weather data from the operation at the Jette-field show that the wind and swell-sea has a relative direction to each other. The weather-forecast at the time of installation provided by Øystein Døskeland (2014) is shown in figure F.3:

Forecast Data Table

Date time UTC	Wind 10m			Wind 50m			Comb sea			Swell			Weather			Water level
Parameter:	dir	speed 10 min	gust	dir	speed 10 min	gust	sign wave	max wave	mean period	swell dir	swell ht	mean period	air temp	sea temp	visibility	water level
Unit:	deg	knots	knots	deg	knots	knots	m	m	s	deg	m	s	°C	°C	km	m
16/02 at 06	190	14	19	190	18	23	1.5	2.5	5	290	1.4	7	6	6	4-10	-0.81
16/02 at 09	180	17	23	180	21	27	1.6	2.6	5	290	1.1	7	6	6	4-10	-0.93
16/02 at 12	180	19	26	180	24	31	1.7	2.9	4	290	0.9	8	6	6	4-10	-0.50
16/02 at 15	180	20	27	180	25	32	1.8	3.0	4	290	0.9	8	6	6	4-10	-0.21
16/02 at 18	180	22	30	180	27	35	1.9	3.1	4	290	0.8	8	6	6	4-10	-0.66
16/02 at 21	190	21	28	190	26	33	2.0	3.3	4	160	0.9	8	6	6	4-10	-0.81

Figure F.3: Weather-forecast during operation, courtesy of Øystein Døskeland (2014)

By comparing the forecasted Hs in figure F.3 with the measured wave height in 4.7 the forecasted Hs is underpredicted by 0.3 [m]. This illustrates the importance of having a wave buoy present during the installation of subsea structures.

According to Jacobsen et al. (2012) who compared results from simulation of a FPS-installation with full-scale measurements the relative direction between wind and swell sea can be important for the vessel motions. Jacobsen et al. (2012) concluded that a vessel direction of $\pm$ 15 degrees relative to the incoming waves was found to be the optimal direction to create a sheltered region when lowering subsea structures through the splash zone. Then the structure is lowered at the leeward side of the vessel avoiding large roll and pitch motions of the vessel.

Jacobsen et al. (2012) used two JONSWAP-spectra to represent the wind and swell sea as input in the software Simulation of Marine Operations (SIMO) developed by MARINTEK and obtained very similar results when comparing with the measured dynamic response.

In this thesis a short crested-spectrum will be created for taking into account the relative direction of the wind- and swell-sea shown in figure F.3. This is performed by applying a spreading function to the unidirectional Torsethaugen-spectrum described in chapter 4.3.4. The directional spectrum is defined by equation F.1:

$$S(\omega, \theta) = S(\omega) D(\theta, \omega) \tag{F.1}$$

Where:

- $S(\omega, \theta)$ is the directional spectrum
- θ_s is the relative direction between wind and swell sea
- $S(\omega)$ is the uni-directional Torsethaugen spectrum

- $D(\theta, \omega)$ is the directional spreading function taking into account the relative direction between wind and swell-sea.

As a simplification it is assumed that the spreading function is not dependent on frequency. According to Myrhaug (2007) the most common form of the spreading function is defined as a $cos^{n_s}\theta$ function. The most common form of this function is setting the spreading parameter $n_s = 2$. Taking into account the wind- and swell-sea directions shown in figure F.3 the spreading function can be expressed with equation F.2:

$$D(\theta) = cos^2\theta \tag{F.2}$$

Where θ is found from figure F.3 to be varying between $-55 < \theta < 55$ [deg]. Since the vessel heading during operation is unknown the application of the data given in F.3 directly in the spreading function will not be correct. A rough estimate for θ when calculating the short crested spectrum is to assume θ as uniformly distributed around the propagation direction in the interval $-\pi[rad] < \theta < \pi[rad]$. By applying the spreading function in equation F.1 on the long crested Torsethaugen-spectrum developed in chapter 4.3.4 the resulting spreading of the directional spectrum can be seen in figure F.4:

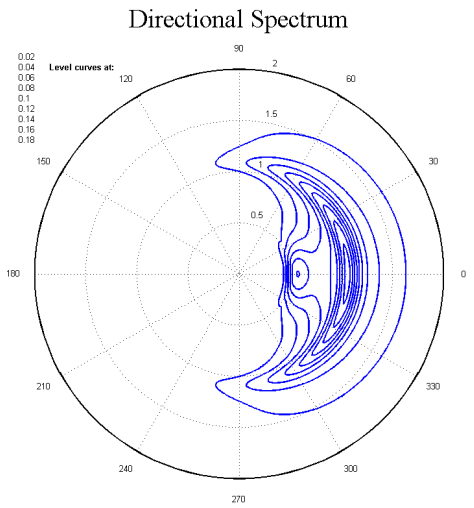

Figure F.4: Spreading from short crested spectrum

From figure F.4 the maximum spectral density is concentrated around the x-direction where $\theta = 0$.

According to Myrhaug (2007) the wave realizations for short crested waves can be calculated with equation F.3:

$$\zeta_{inc}(x,y,t) = \sum_{i=1}^{I}\sum_{j=1}^{J}\sqrt{2S(\omega_i,\theta_j)\Delta\omega\Delta\theta}sin(\omega_i t - k_i x cos\theta_j - k_i y sin\theta_j + \epsilon_{ij}) \tag{F.3}$$

Where random and uniformly distributed phase angles between 0 and 2π in longitudinal and transverse direction is the ϵ_{ij}. For a sinusoidal wave the random phase angles are assumed equal both x- and y-direction. Assuming that the wave number in deep water and short crested waves (k_i) is only depending on the propagation direction, the x- and y- component of the wave number will also be equal.

Calculation of wave realizations with equation F.3 will be performed with WAFO. To save calculation time the 3D wave-carpet will only cover the length of the vessel in the longitudinal direction and from the center of the vessel to the northern anchors in transverse direction. The 3D-wave carpet is shown in appendix E.4,figure E.4.

A comparison between the long crested Torsethaugen and JONSWAP spectrum and the short crested Torsethaugen spectrum can be seen in figure F.5:

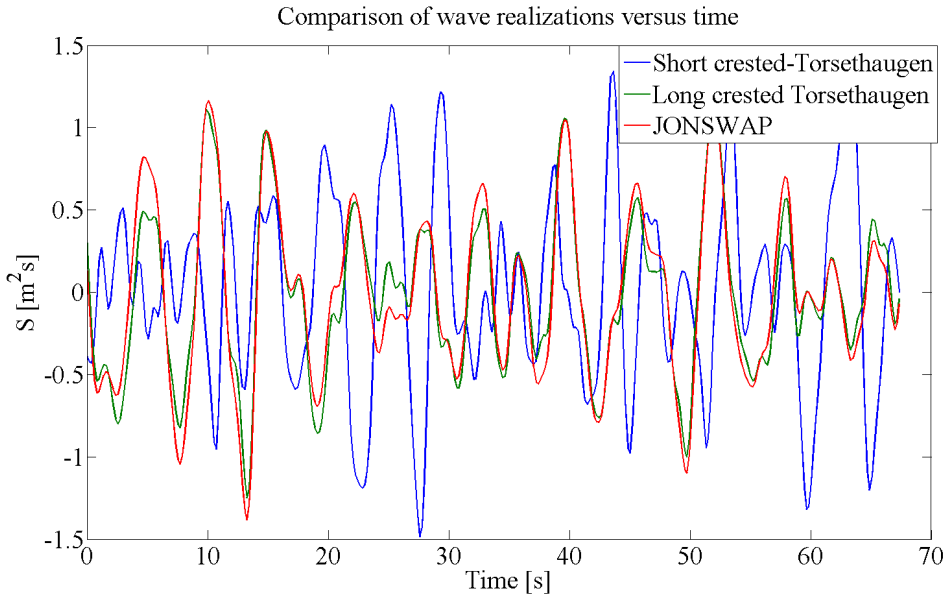

Figure F.5: Spreading from short crested spectrum

It should be noted that the comparison performed in figure F.5 is not made with the same random phase angles between the short crested waves and the long crested waves. However, the difference in magnitude between the realizations can be seen.

Figure F.5 shows that the short crested waves have larger peak and trough than

the long crested waves. This contradicts findings by Bitner-Gregersen and Hagen (2003) who performed numerical simulations of short crested versus long crested waves in deep waves showing that the highest crests were obtained for long crested waves. Therefore the wave realizations obtained from the directional spectrum created with WAFO will not be used further in this thesis.

G Matlab scripts

G.1 Parameter-study and calculation of natural periods

```
clc
clear all
close all
```

Simplified calculation of dynamic air cushion pressure

Also calculates force in lifting wire for parameter-study and natural periods of air cushion/water column
Author: Torleif Ø. Bertelsen Last updated 10.03.2014

```
%%%%%%%%%%%%%%%%%%%%%%%%%%%%%%%%%%%%%%%%%%%%%%%%%%%%%%%%%%%%%%%%%%%%%%%%%%%%%%%
%Defining characteristic dimensions and physical properties
D=3.4;                                  %Diameter of suction anchor
H=5.955;                                %Height of suction anchor
t=0.02;                                 %Wall thickness suction anchor
Ac=pi/4*(D)^2;                          %Area of air cushion
% dv=[0.61 1.02];                       %Diameter of small & large vent hatch
perf=0.019765;                          %Perforation ratio
dve=(D)*sqrt(perf);                     %Diameter of vent hatch
Al=(pi/4)*dve^2;                        %Leakage area
Patm=101300;                            %Atmospheric pressure
gamma_a=1.4;                            %Specific heat ratio of air
C_con=0.61;                             %Contraction coefficient
rho_a=1.225;                            %Density of air at 15 degC
rho_w=1025;                             %Density seawater
rho_s=7850;                             %Density steel
g=9.81;                                 %Gravitational acceleration
%Wave data
Hs=0.000001;                            %Characteristic significant wave height
Tzmin=3.4;% Or (8.9)*sqrt(Hs/g);    %Min zero crossing T from DNV-RP-H103
                                        %Should be larger or equal to 3.4 [s]
Tzmax=13;                               %Upper zero crossing T from DNV-RP-H103
omega_max=(2*pi)/Tzmin;                 %Maximum wave frequency from DNV-RP-H103
lambda=(g*Tzmin^2)/(2*pi);              %Wave length for the most critical Tz
k=2*pi/lambda;                          %Wave number for lowest wavelengths
count=1;                                %Plot counter
%Denoting time and u as symbols so they will not be calculated until
%it is needed. (Here u is the dynamic pressure \mu)
syms t_t u
%Operational data
w_const=-0.98;                          %Constant lowering velocity
w_var=-0.01;                                %Varying lowering velocity
w_tot=w_const+w_var*t_t;                %Total lowering velocity
N_t=1000;                               %Number of steps
step=H/N_t;                             %Step size
h_sub=0:step:1.1*H;                     %Depth until total submergence + 10%
% time_test=h_subabs(w_tot);
%%%%%%%%%%%%%%%%%%%%%%%%%%%%%%%%%%%%%%%%%%%%%%%%%%%%%%%%%%%%%%%%%%%%%%%%%%%%%%%
%%%%%%%%%%%%%%%%%%%% Constant lowering velocity %%%%%%%%%%%%%%%%%%%%%%%%%%%%%%
%Set w_var=0
```

```
%%%%%%%%%%%%%%%%%%%%%%%%%%%%%%%%%%%%%%%%%%%%%%%%%%%%%%%%%%%%%%%%%%%%%%%%%%%%
%%%%%%%%%%%%%%%%%%%%%%%% Varying lowering velocity %%%%%%%%%%%%%%%%%%%%%%%%
%Calculate the time during submergence with 2nd degree formula if the
%velocity is not constant
time_tot=zeros(1,length(h_sub));    %Define time during submergence
for i=1:length(h_sub)
    if w_var ~= 0
    time_tot(i)=(w_const+sqrt((w_const)^2+4*abs(w_var)*h_sub(i)))...
        /(2*abs(w_var));
    end
end
%Since the velocity is defined with a symbolic variable, the velocity must
%be evaluated with matlabFunction such that the numerical values can be
%stored in w_saved for later use.
F_wtot=matlabFunction(w_tot);
w_saved=F_wtot(time_tot);
d_sub=w_const*t_t+0.5*w_var*t_t^2;  %Integrated vel=Submergence level
Fsub=matlabFunction(d_sub);         %Saving the submergence level
dsub_saved=Fsub(time_tot);
%Wave elevation of considered incident waves evaluated at center of anchor
x_0=0;
%%%%%%%%%%%%%%%%%%%%%%%%%%%%%%%%%%%%%%%%%%%%%%%%%%%%%%%%%%%%%%%%%%%%%%%%%%%%
%%%%%%%%%%%%%%%%%%%%%% Regular or constant waves %%%%%%%%%%%%%%%%%%%%%%%%%%
% Define incident wave elevation for regular waves
zeta_inc=Hs/2;%*sin(k*x_0-omega_max*t_t);                %Max for sin()=1
% %Time derivative of the incident wave elevation
zeta_inc_dot=omega_max*Hs/2;%*cos(k*x_0-omega_max*t_t);  %Max for cos()=1

%%%%%%%%%%%%%%%%%%%%%%%%%%%%%%%%%%%%%%%%%%%%%%%%%%%%%%%%%%%%%%%%%%%%%%%%%%%%
%%%%%%%%%%%%%%%%%%%%%%% Irregular waves %%%%%%%%%%%%%%%%%%%%%%%%%%%%%%%%%%%
%Call function which calculates surface elevation from JONSWAP spectrum
% [omega_js1,zeta_js]=jonswap(time_tot);
%Use a random phase angle such that no dominating wave component is present
% epsilon=rand(1,length(time_tot))*2*pi;
% epsilon=load('epsilonnew.mat');             %Random number vector [0,2pi]
% epsilon=new.epsilon;
% k_wave=omega_js1.^2/g;                      %Wave number deep water
%Calculating surface elevation by superimposing the elevations from the
%spectrum
% zeta_inc=sum(zeta_js.*cos(k_wave.*x_0-omega_js1.*t_t+epsilon));
% zeta_inc_dot=sum(zeta_js.*omega_js1.*sin(k_wave.*x_0...
% -omega_js1.*t_t+epsilon));

%%%%%%%%%%%%%%%%%%%%%%%%%%%%%%%%%%%%%%%%%%%%%%%%%%%%%%%%%%%%%%%%%%%%%%%%%%%%
%%%% Calculate ODE using Runge-Kutta 4th order method %%%%
%%%%%%%%%%%%%%%%%%%%%%%%%%%%%%%%%%%%%%%%%%%%%%%%%%%%%%%%%%%%%%%%%%%%%%%%%%%%

%Non-linear function of \mu and t
F_tu=matlabFunction((zeta_inc_dot-w_tot-C_con*(Al/Ac)*...
    sqrt((2*u)/(rho_a)))/(1/(gamma_a*Patm)*(1+u/Patm)^(-1)*...
    (H+d_sub+u/(rho_w*g)-zeta_inc)+(1/(rho_w*g))));

uu = zeros(1,length(time_tot));                          %Initial condition
```

```
%Runge Kutta-4 Time integration loop
% tic;
for i=1:(length(time_tot)-1)                              %Calculation loop
    a_1 = F_tu(time_tot(i),uu(i));
    a_2 = F_tu(time_tot(i)+0.5*step,uu(i)+0.5*step*a_1);
    a_3 = F_tu(time_tot(i)+0.5*step,uu(i)+0.5*step*a_2);
    a_4 = F_tu(time_tot(i)+step,uu(i)+a_3*step);

    uu(i+1) = uu(i) + (1/6)*(a_1+2*a_2+2*a_3+a_4)*step;  %main eq

%     error(i)=abs(uu(i+1)-uu(i));
%     Convergence criterion
%     if abs(uu(i+1)-uu(i))<1*10^-3
%         disp('conv');
%     else
%         break;
%     end
end
% toc                                                 %End of time measurement
% figure(1)
% plot((0:step:t_sub-step),error);
% title('Residual \mu(i+1)-\mu(i)');
% % Plotting the dynamic pressure variation:
% figure(count)
% plot(time_tot,(uu),'LineWidth',3); set(gca,'FontSize',15);
% title(['Time integration of dynamic air cushion pressure \mu with RK4 '...
%     'at no. of steps=', num2str(N_t)]);
% xlabel('time [s]');
% ylabel('\mu(t) [Pa]');

%Calculating total load in lifting wire including slamming force
%Define quantities to be used for the conical top
H_cyl=5.158472222;                      %Height of cylinder volume
H_cone=H-H_cyl;                         %Height of cone volume
t_cone=H_cone/abs(w_tot);               %Time until submergence of cyl-area
beta=atan(5/11.1);%beta=atan(6.4/11.2); %Deadrise angle in radians
F_hook=4500*g;                          %Hook load
F_anchor=12900*g+F_hook;                %Load of anchor in air
F_wire_vc=zeros(1,length(time_tot));    %Total load in lifting wire Von C.
F_wire_wag=zeros(1,length(time_tot));   %Total load in lifting wire Wagner
zeta_i=zeros(1,length(time_tot));       %Distance from SWL to inner
                                        %water surface
wsurf_i=zeros(1,length(time_tot));      %Water surface level inside suction
                                        %anchor
wave_inc=zeros(1,length(time_tot));     %Saved wave elevation
wave_inc_dot=zeros(1,length(time_tot)); %Saved time-der. of wave elevation
sub_depth=zeros(1,length(time_tot));    %Saved submergence level

for i=1:length(time_tot)
    %Saving the wave elevation and its time derivative for later use
%     Constant or regular wave height
    wave_inc(i)=Hs/2;%*sin(k*x_0-omega_max*time_tot(i));
    wave_inc_dot(i)=omega_max*Hs/2;%*cos(k*x_0-omega_max*time_tot(i));
%     Irregular wave height
```

```
%     wave_inc(i)=sum(zeta_js.*cos(k_wave.*x_0...
%         -omega_js1.*time_tot(i)+epsilon));
%     wave_inc_dot(i)=sum(zeta_js.*omega_js1.*sin(k_wave.*x_0...
%         -omega_js1.*time_tot(i)+epsilon));
    zeta_i(i)=(wave_inc(i)-uu(i)/(rho_w*g));
    sub_depth(i)=w_saved(i)*time_tot(i);
    wsurf_i(i)=sub_depth(i)-(zeta_i(i));  %Defined as negative

    F_buoy_wag=uu(i)*Ac;          %Load for the cylinder area
    F_buoy_vc=uu(i)*Ac;           %Load for the cylinder area
    last=F_buoy_vc;               %Initial value for the load on cone area

    if wsurf_i(i) <= -H_cyl  && wsurf_i(i) >= -1.0075*H  %Slamming criteria

        %Start-time(=0) for calculating load on cone area
        tstep_cone(i)=wsurf_i(i)/w_saved(i)+H_cyl/w_saved(i);

        %Load for the cone area with Von Karman's wetted length
        F_vc=last+rho_w*(pi*2)*(w_saved(i)^3/(tan(beta))^2)*...
    (-(tstep_cone(i)*(pi*D/4))+(w_saved(i)*(tstep_cone(i))^2)/(tan(beta)));
        %Include initial load from \mu at transition cylinder to cone area
            F_buoy_vc=F_vc;
        %Load for the cone area with Wagner's wetted length
        F_wag=last+(rho_w*pi^4/4)*(w_saved(i)^3/(tan(beta))^2)*...
     (-(tstep_cone(i)*(D/2))+(w_saved(i)*(tstep_cone(i))^2)/(4*tan(beta)));
            F_buoy_wag=F_wag;
    end
    F_wire_wag(i)=F_anchor-abs(F_buoy_wag);
    F_wire_vc(i)=F_anchor-abs(F_buoy_vc);
end
%Plotting realization of the incident waves generated from the JONSWAP
%spectrum
% figure(2)
% plot(time_tot,wave_inc,'LineWidth',3); set(gca,'FontSize',15);
% title('Realizations of regular waves');
% xlabel('time [s]');
% ylabel('Surface elevation');

%%%%%%%%%%%%%%%%%%%%%%%%%%%%%%%%%%%%%%%%%%%%%%%%%%%%%%%%%%%%%%%%%%%%%%%%%%%%
% Comparison-data from Subsea7's full scale measurement
d_fs=[0 1 2 3 4 5 5.5 5.8 6];
d_ss7=[0 1 2 3 4 5 6];
F_fs=[F_anchor 149112 142245 130473 127333.8...
    123017.4 119878.2 86524.2 62195.4; F_anchor 147542.4 136947.6...
    128903.4 125175.6 119878.2 119289.6 77499 75733.2;...
    F_anchor 143030 138713.4 129688 126745 131650 143422 106144 94176];
F_mean=mean(F_fs,1);
% F_fit=fit(time_tot,F_mean','smoothingspline');
F_ss7=[F_anchor 147000 146000 132000 130000 131000 98000];

% count=count+1;
% figure(count)
% plot(abs(dsub_saved),F_wire_vc,d_fs,F_mean,'LineWidth',3);
% set(gca,'FontSize',15);
```

```
% % plot(abs(dsub_saved),F_wire_vc, abs(dsub_saved),...
% % F_wire_wag,d_fs,F_fs(1,:), d_fs, F_fs(2,:),d_fs,F_fs(3,:),'LineWidth',3);
%
% legend('Decreased contraction coefficient',...
%      'Average of full-scale measurements');
% % Plotting the total force in the wire vs depth
% title(['Total force in crane wire during submergence']);% with'...
% %     ,num2str(eta3_dot),' [m/s] lowering speed',...
% %     ' and contraction coefficient =',num2str(C_con)]);
% axis([0 6 0 2*10^5])
% xlabel('Depth [m]');
% ylabel('Force in lifting wire [N]');
% grid on;
%%%%%%%%%%%%%%%%%%%%%%%%%%%%%%%%%%%%%%%%%%%%%%%%%%%%%%%%%%%%%%%%%%%%%%%%%%%%%%%
% Calculate natural frequency for oscillating air cushion / water(piston)
%%%%%%%%%%%%%%%%%%%%%%%%%%%%%%%%%%%%%%%%%%%%%%%%%%%%%%%%%%%%%%%%%%%%%%%%%%%%%%%
Vol_c=zeros(1,length(time_tot));       %Instantaneous air cushion volume
A33_disk=9790;                         %3D-Added mass of disk
A33_water=51800;                       %3D-Added mass of fluid from WAMIT
uu_dot=zeros(1,length(time_tot));
omega_wn1=zeros(1,length(time_tot));
omega_wn2=zeros(1,length(time_tot));
T_wn1=zeros(1,length(time_tot));
T_wn2=zeros(1,length(time_tot));
%
for i=1:length(time_tot)


    Vol_c(i)=Ac*(H-zeta_i(i)+w_saved(i)*time_tot(i));
    omega_wn1(i)=sqrt((g+(Ac*gamma_a*(Patm+uu(i)))/(rho_w*Vol_c(i)))/...
        ((4*D)/(3*pi)-wsurf_i(i)));
    T_wn1(i)=2*pi/omega_wn1(i);  %Natural period of water and air coupled

%Calculating Natural freq. for oscillating water and air: Miles' approach
    %Defining the natural frequency of the oscillating water with the
    %dynamic air cushion pressure as the upper boundary (coupled)

    omega_wn2(i)=sqrt(g/((4*D)/(3*pi)-wsurf_i(i)));
    %Defining the natural frequency of the oscillating water with the
    %atmospheric pressure as the upper boundary (uncoupled)
    T_wn2(i)=2*pi/omega_wn2(i);   %Natural period of water uncoupled
        if wsurf_i(i) <= -H_cyl*0.999 && wsurf_i(i) >= -H_cyl*1.0001
%             disp(['Air cushion volume is',num2str(Vol_c(i))]);

%Calculating Natural frequency for oscillating air cushion: Sloshing appr
            omega_cn=Ac*sqrt(gamma_a*(Patm+uu(i))/(A33_water*Vol_c(i)));
             %Natural period air cushion
            T_cn1=2*pi/omega_cn;

    %Defining the natural frequency with use of added mass instead of the
    %dynamic air cushion pressure
    omega_wn3=sqrt(g/((4*D)/(3*pi)-wsurf_i(i)-A33_water/(rho_w*Ac)));

%         T_wn1=2*pi/omega_wn1   %Natural period of water and air coupled
```

```
%         T_wn2=2*pi/omega_wn2   %Natural period of water uncoupled
        T_wn3=2*pi/omega_wn3;   %Natural period of water with added mass

        end
        %Calculating frequency according to measured volume and pressure
%         if H+wsurf_i(i)>=0.99*0.174 && H+wsurf_i(i)<=1.01*0.174
%             wsurf_i(i)
%         vol_meas=pi/3*0.174*0.914^2;
%         P_meas=4.8939e+03;
%         omega0=sqrt((g+(Ac*gamma_a*(Patm+uu(i)))/(rho_w*vol_meas))/...
%         ((4*D)/(3*pi)-wsurf_i(i)));
%         T_0=2*pi/omega0        %Natural period corresp. to measured P,V
%         end
end
% count=count+1;
% figure(count)
% plot(abs(sub_depth),T_wn1,abs(sub_depth),T_wn2);
% legend('Air cushion and water coupled','Water column');
% title(['Natural period comparison vs depth']);
% xlabel('Depth [s]');
% ylabel('Natural period T [s]');
```

Published with MATLAB® R2013a

G.2 Script verifying calculation of dynamic of dynamic air cushion pressure

rkown1.m Calculation of dynamic air cushion pressure by own algorithm

Author: Torleif Ø. Bertelsen Last updated 10.03.2014

```
%%%%%%%%%%%%%%%%%%%%%%%%%%%%%%%%%%%%%%%%%%%%%%%%%%%%%%%%%%%%%%%%%%%%%%%%%%%%%%%
clc
clear all
close all
global cranedata nn time_tot count g s3_SEi vel_fitted s3_fitSE...
zeta_inc_fit_E zeta_inc_dot_fit_E zeta_inc_fit_W...
    zeta_inc_dot_fit_W zeta_inc_main_E zeta_inc_main_W omega_js1 k_wave...
    v_water_E v_water_W
%Defining characteristic dimensions and physical properties
D=6;                                %Diameter of suction anchor
H=5.5;                              %Height of suction anchor
t=0.02;                               %Wall thickness suction anchor
Ac=pi/4*(D-2*t)^2;                        %Area of air cushion
dv=[0.61 1.02];                     %Diameter of small & large vent hatch
perf=0.019765;                        %Perforation ratio
% dve=(D)*sqrt(perf);                   %Diameter of vent hatch
Al=(pi/4)*dv(1,2)^2;                      %Leakage area
Patm=101300;                          %Atmospheric pressure
gamma_a=1.4;                          %Specific heat ratio of air
C_con=0.61;                           %Contraction coefficient
rho_a=1.225;                          %Density of air at 15 degC
rho_w=1025;                           %Density seawater
rho_s=7850;                           %Density steel
g=9.81;                               %Gravitational acceleration
%Wave data
Hs=1.895;                             %Characteristic significant wave height
Tz_buoy=5.89;% Or (8.9)*sqrt(Hs/g);   %Min zero crossing T from DNV-RP-H103
                                    %Should be larger or equal to 3.4 [s]
Tzmax=13;                           %Upper zero crossing T from DNV-RP-H103
omega_buoy=(2*pi)/Tz_buoy;          %Maximum wave frequency from DNV-RP-H103
lambda=(g*Tz_buoy^2)/(2*pi);          %Wave length for the most critical Tz
k=2*pi/lambda;                      %Wave number for lowest wavelengths

%Denoting time and u as symbols so they will not be calculated until
%it is needed. (Here u is the dynamic pressure \mu)

count=1;                                %Starting counter for figure plots
%Loading the crane and vessel measurements from the cdata.mat matrix
% cranedata=load('cdata.mat');
cranedata=load('crane_020620.mat');
cload=cranedata.num(:,2)*10^4;    %Crane load measured
syms t_t u
assume(u >= 0)
%%%%%%%%%%%%%%%%%%%%%%%%%%%%%%%%%%%%%%%%%%%%%%%%%%%%%%%%%%%%%%%%%%%%%%%%%%%%%%%
%%%%%%%%%% Calculating lowering velocity and submergence level %%%%%%%%%%%%
%Creating a new starting time for the wire-load measurements
```

```
%such that it starts on t=0 at the measuring time 11:00:21
nn=1;
time_jette=cranedata.num(:,1)-17722.484;
% time_jette=cranedata.num(:,1)-17707.922;
time_load=interp(time_jette,nn);          %Interpolated time vector
% steps=1/length(time_tot);
motion(time_jette);
syms d_tot w_tot

% %%%%%%%%%%%%%%%%%%%%%%%%%%%%%%%%%%%%%%%%%%%%%%%%%%%%%%%%%%%%%%%%%%%%%%%%%%%%%%%
% %%%%%%%%%%%%%%%%%%%%%% Regular or constant waves %%%%%%%%%%%%%%%%%%%%%%%%%%%%%

waves(time_jette);
x_E=round(91.42);                                %Eastern anchors' x-location
x_W=round(112.75);                               %Western anchors' x-location
y_S=round(18.8);
y_N=round(3);
% torset=load('dirsave.mat');
% zeta_inc_SE(:,1)=torset.dirsaved(y_S,x_E,:);

% zeta_inc_fitSE=fit(time_load,zeta_inc_SE,'smoothingspline');
% for i=1:length(time_load)-1
%     zeta_inc_dot_SE(i)=(zeta_inc_SE(i+1)-zeta_inc_SE(i))/...
%         (time_load(i+1)-time_load(i));
%     zeta_inc_dot_NE(i)=(zeta_inc_NE(i+1)-zeta_inc_NE(i))/...
% (time_load(i+1)-time_load(i));
%     zeta_inc_dot_SW(i)=(zeta_inc_SW(i+1)-zeta_inc_SW(i))/...
% (time_load(i+1)-time_load(i));
%     zeta_inc_dot_NW(i)=(zeta_inc_NW(i+1)-zeta_inc_NW(i))/...
% (time_load(i+1)-time_load(i));
% end
%Extrapolating to find the last value of the time derivative of wave elev.
% extrapSE=interp1(time_load(1:length(time_load)-1),...
%     zeta_inc_dot_SE,'spline','pp');
% zeta_inc_dot_SE(length(time_load))=ppval(extrapSE,max(time_load));
% zeta_inc_dot_fitSE=fit(time_load,zeta_inc_dot_SE','smoothingspline');

syms zeta_inc zeta_inc_dot


% %%%%%%%%%%%%%%%%%%%%%%%%%%%%%%%%%%%%%%%%%%%%%%%%%%%%%%%%%%%%%%%%%%%%%%%%%%%%%%%
% %%%% Calculate ODE using Runge-Kutta 4th order method %%%%
% %%%%%%%%%%%%%%%%%%%%%%%%%%%%%%%%%%%%%%%%%%%%%%%%%%%%%%%%%%%%%%%%%%%%%%%%%%%%%%%
N_t=10;

% time_int=0:time_step:max(time_load);
%Non-linear function of \mu and t on east side suction anchor
F_tu=((zeta_inc_dot-w_tot-C_con*(Al/Ac)*sign(u)*...
    sqrt((2*feval(symengine,'abs',u))/(rho_a)))/(1/(gamma_a*Patm)*...
    (1+u/Patm)^(-1)*(H+d_tot+u/(rho_w*g)-zeta_inc)+(1/(rho_w*g))));

for j=1:length(time_load)-1
    time_step(j)=(time_load(j+1)-time_load(j));
end
```

```
% uu = zeros(1,length(time_int));                        %Initial condition
% F_new=zeros(1,length(time_int));
% % %
%Runge Kutta-4 Time integration loop
u_new=zeros(1,length(time_load));
tic;
for i=1:(length(time_load)-1)                             %Calculation loop
%     assume(u_new>=0)
    d_new=feval(s3_fitSE,time_load(i));
    w_new=feval(vel_fitted,time_load(i));
    zeta_new=feval(zeta_inc_fit_E,time_load(i));
    zeta_inc_dot_new=feval(zeta_inc_dot_fit_E,time_load(i));
    F_new=subs(F_tu,[d_tot,w_tot,zeta_inc,zeta_inc_dot,u],...
        [d_new,w_new,zeta_new,zeta_inc_dot_new,u_new(i)]);

    a_1 = time_step(i)*F_new;

    d_new=feval(s3_fitSE,time_load(i)+0.5*time_step(i));
    w_new=feval(vel_fitted,time_load(i)+0.5*time_step(i));
    zeta_new=feval(zeta_inc_fit_E,time_load(i)+0.5*time_step(i));
    zeta_inc_dot_new=feval(zeta_inc_dot_fit_E,time_load(i)+...
        0.5*time_step(i));
    F_new=subs(F_tu,[d_tot,w_tot,zeta_inc,zeta_inc_dot,u],...
        [d_new,w_new,zeta_new,zeta_inc_dot_new,u_new(i)+0.5*a_1]);

    a_2 = time_step(i)*F_new;

    F_new=subs(F_tu,[d_tot,w_tot,zeta_inc,zeta_inc_dot,u],...
        [d_new,w_new,zeta_new,zeta_inc_dot_new,u_new(i)+0.5*a_2]);

    a_3 = time_step(i)*F_new;

    d_new=feval(s3_fitSE,time_load(i)+time_step(i));
    w_new=feval(vel_fitted,time_load(i)+time_step(i));
    zeta_new=feval(zeta_inc_fit_E,time_load(i)+time_step(i));
    zeta_inc_dot_new=feval(zeta_inc_dot_fit_E,time_load(i)+time_step(i));
    F_new=subs(F_tu,[d_tot,w_tot,zeta_inc,zeta_inc_dot,u],...
        [d_new,w_new,zeta_new,zeta_inc_dot_new,u_new(i)+a_3]);

    a_4 = time_step(i)*F_new;

    u_new(i+1) = u_new(i) + (1/6)*(a_1+2*a_2+2*a_3+a_4);  %main eq
%     error(i)=abs(uu(i+1)-uu(i));
%     Convergence criterion
%     if abs(uu(i+1)-uu(i))<1*10^-3
%         disp('conv');
%     else
%         break;

end
toc    %End of time measurement
save('mu_new.mat','u_new');
count=count+1;
```

```
figure(count)
plot(time_load,(u_new),'LineWidth',3); set(gca,'FontSize',15);
title(['Time integration of dynamic air cushion pressure \mu with RK4 '...
    'at no. of steps=', num2str(nn)]);
xlabel('time [s]');
ylabel('\mu(t) [Pa]');
```

Published with MATLAB® R2013a

G.3 Main script for Jette-analysis

```
clear all
close all
clc
```

Main script for calculating force in lifting wire in jette operation

Makes calls to the other functions Last updated at 08.06.2014, 13:56.

```
%Calculate the force in the lifting wire and compare with the measurements
%Defining global parameters which will also be used in subroutines
%Plots the force in the lifting wire and statistical comparison
%Made at 14.06.2014, 04:08.
%Call global parameters defined in the Main script
global  g cranedata count D dv rho_s thick nn time_tot H Ac Al Patm...
    gamma_a rho_a rho_w C

count=1;                        %Starting counter for figure plots
H=5.5;                          %Height of suction anchor
D=6;                            %Diameter of suction anchor
thick=0.02;                     %Wall thickness suction anchor
Ac=pi/4*(D-2*thick)^2;          %Area of air cushion
dv=[0.61 1.016];                %Diameter of small & large vent hatch
Al=(pi/4)*(dv(1,2)^2+dv(1,1)^2);
C=0.59;                         %Contraction coefficient
Patm=101300;                    %Atmospheric pressure
gamma_a=1.4;                    %Specific heat ratio of air
g=9.81;                         %Gravitational acceleration
rho_a=1.225;                    %Density of air at 15 degC
rho_w=1025;                     %Density seawater
rho_s=7850;                     %Density steel

%%%%%%%%%%%%%%%%%%%%%%%%%%%%%%%%%%%%%%%%%%%%%%%%%%%%%%%%%%%%%%%%%%%%%%%%%%%%%%%
% Importing data from full scale measurements
% From movies: Immersion of first anchor at: 02:06:11
% [num,txt,raw]=xlsread('cranedata.xlsx','FPSPLEM', 'C42177:J42589');
%Loading the cranedata.mat file containing the numerical data into the
%vector data where the indices 1:8 represent the following 1:time [s],
%2:wire force, 3: Crane tip velocity, 4: Crane tip acceleration, 5:
%Roll motion of the vessel, 6: Pitch motion of the vessel, 7: Length of
%payed out wire, 8: Wire speed
%save('crane_020620','num')     %Save this to directory to be loaded later
%Loading the crane and vessel measurements from the either the
%crane_020606.mat or crane_020620.mat matrix where 17707.922 or 17722.484
%must be subtracted from time_load to start time at 0 and respectively
%%%%%%%%%%%%%%%%%%%%%%%%%%%%%%%%%%%%%%%%%%%%%%%%%%%%%%%%%%%%%%%%%%%%%%%%%%%%%%%
%Loading matrix for Jette-measurements
cranedata=load('crane_020620.mat');
c_load=cranedata.num(:,2)*10^4;      %Wire load measured
%time_load defines the immersion of the first suction anchor (NE)
time_load=cranedata.num(:,1)-17722.484; %Time vector from operation
```

```
%Interpolate to get new time vector
nn=1;                                       %Interpolation factor
time_tot=interp(time_load,nn);              %Interpolated time vector
c_interp=interp(c_load,nn);                 %Interpolated wire load
%%%%%%%%%%%%%%%%%%%%%%%%%%%%%%%%%%%%%%%%%%%%%%%%%%%%%%%%%%%%%%%%%%%%%%%%%%%%%%%
%Calling the function jonsjette which calculates the wave elevation and its
%time derivative from the JONSWAP spectrum
waves(time_load);
%%%%%%%%%%%%%%%%%%%%%%%%%%%%%%%%%%%%%%%%%%%%%%%%%%%%%%%%%%%%%%%%%%%%%%%%%%%%%%%
%Calling the heave-function which calculates the total interpolated
%lowering velocity and interpolated vertical motion of the suction anchors
%and saves these to files which will be evaluated for each time step
%inside the solveSE,NE,SW,NW functions
motion(time_load);
%%%%%%%%%%%%%%%%%%%%%%%%%%%%%%%%%%%%%%%%%%%%%%%%%%%%%%%%%%%%%%%%%%%%%%%%%%%%%%%
%Calling the function which calculates the dynamic pressure with ODE45 a
%numerical solver for stiff problems
[mu_SE,mu_NE,mu_SW,mu_NW]=odesolvernew();

%%%%%%%%%%%%%%%%%%%%%%%%%%%%%%%%%%%%%%%%%%%%%%%%%%%%%%%%%%%%%%%%%%%%%%%%%%%%%%%
% For calculating the slamming load on the suction anchor top Wagner's
% approach will be used.
%%%%%%%%%%%%%%%%%%%%%%%%%%%%%%%%%%%%%%%%%%%%%%%%%%%%%%%%%%%%%%%%%%%%%%%%%%%%%%%
[F_buoy_SE,F_buoy_NE,F_buoy_SW,F_buoy_NW]=...
    slam_func(mu_SE,mu_NE,mu_SW,mu_NW);
%%%%%%%%%%%%%%%%%%%%%%%%%%%%%%%%%%%%%%%%%%%%%%%%%%%%%%%%%%%%%%%%%%%%%%%%%%%%%%%
% Calculate the force in the lifting wire
%%%%%%%%%%%%%%%%%%%%%%%%%%%%%%%%%%%%%%%%%%%%%%%%%%%%%%%%%%%%%%%%%%%%%%%%%%%%%%%
% Defining the static weight in air of the PLEM protection structure
F_stat=210*10^3*g;
F_wire=zeros(1,length(time_tot));   %Wire load
for i=1:length(time_tot)
    F_wire(i)=F_stat-F_buoy_SE(i)-F_buoy_NE(i)-F_buoy_SW(i)-F_buoy_NW(i);
end
%%%%%%%%%%%%%%%%%%%%%%%%%%%%%%%%%%%%%%%%%%%%%%%%%%%%%%%%%%%%%%%%%%%%%%%%%%%%%%%
%Plot force in lifting wire
count=count+1;
figure(count)
plot(time_tot,c_interp,time_tot,F_wire);...
    title('Force in lifting wire vs time');
% axes([])
legend('Measured wire force','Calculated wire force');
xlabel('Time [s]');
ylabel('Force [N]');
```

Published with MATLAB® R2013a

G.4 Calculation of vertical motion of suction anchors

motion.m This function calculate vertical motion and velocity of

four suction anchors due to vessel motions and lowering velocity during splash zone transition

```
function motion(time_load)

global cranedata vel_fitted nn time_tot count s3_fitSE s3_fitNE s3_fitSW...
    s3_fitNW dsub_fit s3_SASE s3_SANE s3_SASW s3_SANW tip_vel vel_f vel...
    eta3_SE eta3_NE eta3_SW eta3_NW

%Coordinates for the four anchors relative to the MRU:
% x_c=[5.53 5.53 -10.27 -10.27];
% y_c=[18.86 31.5 18.86 31.5];

vel=cranedata.num(:,8);          %Lowering velocity from raw data
[B_f,A_f]=butter(4,0.1);         %Creating a low-pass filter
vel_f=filtfilt(B_f,A_f,vel);     %Filtered velocity
tip_vel=cranedata.num(:,3);      %Crane tip velocity from raw data
roll=cranedata.num(:,5);         %Roll motion from MRU
pitch=cranedata.num(:,6);        %Pitch motion from MRU

%Integrating the lowering velocity with the trapezoidal method to find the
%resulting vertical motion
dsub=zeros(1,length(time_load));
for i=2:length(time_load)
    dsub(i-1)=trapz(time_load(1:i),vel_f(1:i));
end
dsub(length(time_load))=trapz(time_load(1:length(time_load)),...
    vel_f(1:length(time_load)));
for i=2:length(time_load)
    test(i)=(dsub(i)-dsub(i-1))/(time_load(i)-time_load(i-1));
end

dsub_fit=fit(time_load,dsub','smoothingspline');
%Have to integrate the cranetip velocity to find the motion, also with the
%trapezoidal method to find the resulting vertical motion:

s3_tip=zeros(1,length(time_load));
for i=2:length(time_load)
    s3_tip(i-1)=trapz(time_load(1:i),tip_vel(1:i));
end
s3_tip(length(time_load))=trapz(time_load(1:length(time_load)),...
    tip_vel(1:length(time_load)));

%Since the vessel is rolling about a mean value of 4.232 deg, this must be
%subtracted from the data values in addition to correct for degrees
roll_cor=(roll-mean(roll))*pi/180;
%Since the vessel is pitching about a mean value of -0.1908 deg this must
%be added to the data values in addition to correct for degrees
pitch_cor=(pitch-mean(pitch))*pi/180;
```

```
%Total vertical motion of MRU becomes:
yc=23.6;
xc=-2.37;
eta3_mru=zeros(1,length(time_load)); %Vertical motion of MRU
for i=1:length(time_load)
    eta3_mru(i)=s3_tip(i)-roll_cor(i)*yc+-pitch_cor(i)*xc;
end

% Plotting the total vertical velocity of the protection structure
% count=count+1;
% figure(count)
%subplot(311);plot(time_tot,vel_tot); title('Tot lowering velocity [m/s]');
%subplot(312);plot(time_tot,vel_f); title('Lowering vel from wire payout');
% subplot(313);plot(time_tot,tip_vel); title('Crane tip velocity');
% Plotting the roll,pitch and heave crane tip motion
% count=count+1;
% figure(count)
% subplot(211); plot(time_load,roll,time_load,pitch);
% title('Crane tip motion due to roll & pitch [deg]');
% legend('Roll motion','Pitch motion');
% subplot(212); plot(time_load,roll_cor,time_load,pitch_cor);
% title('Corrected roll and pitch [rad]');
%Plot crane tip motion due to vessel motion
% count=count+1;
% figure(count)
% plot(time_test,s3_tip); title('Vertical crane tip motion [m]');

%Assuming a rigid connection between the ship and the hinged point
%of the suction anchors (due to large weight and tugger wires) then the
%vertical motion of the suction anchors due to vessel motion and lowering
%speed becomes:
y_1=23.6-7.9;
y_2=23.6+7.9;
x_1=5.53;
x_2=-10.27;

s3_SASE=zeros(1,length(time_load));  %Vert. mot. Southeast suction anchor
s3_SANE=zeros(1,length(time_load));  %Vert. mot. Northeast suction anchor
s3_SASW=zeros(1,length(time_load));  %Vert. mot. Southwest suction anchor
s3_SANW=zeros(1,length(time_load));  %Vert. mot. Northwest suction anchor

for i=1:length(time_load)
    s3_SASE(i)=dsub(i)+eta3_mru(i)+roll_cor(i)*y_1-pitch_cor(i)*x_1;
    s3_SANE(i)=dsub(i)+eta3_mru(i)+roll_cor(i)*y_2-pitch_cor(i)*x_1;
    s3_SASW(i)=dsub(i)+eta3_mru(i)+roll_cor(i)*y_1-pitch_cor(i)*x_2;
    s3_SANW(i)=dsub(i)+eta3_mru(i)+roll_cor(i)*y_2-pitch_cor(i)*x_2;
end

%Fitting a curve to these data by interpolation and saving the fitted data
%to variables which can be loaded when running the odesolver script
s3_fitSE=fit(time_load,s3_SASE','smoothingspline');
s3_fitNE=fit(time_load,s3_SANE','smoothingspline');
s3_fitSW=fit(time_load,s3_SASW','smoothingspline');
s3_fitNW=fit(time_load,s3_SANW','smoothingspline');
```

```
% save('s3SEsaved.mat','s3_fitSE');
% save('s3tSANE.mat','s3_fitNE');
% save('s3SASWe.mat','s3_fitSW');
% save('s3SANW.mat','s3_fitNW');
%Calculate velocity of each suction anchor
eta3_SE=zeros(1,length(time_load));
eta3_NE=zeros(1,length(time_load));
eta3_SW=zeros(1,length(time_load));
eta3_NW=zeros(1,length(time_load));

for i=2:length(time_load)
    eta3_SE(i-1)=(s3_SASE(i)-s3_SASE(i-1))/(time_load(i)-time_load(i-1));
    eta3_NE(i-1)=(s3_SANE(i)-s3_SANE(i-1))/(time_load(i)-time_load(i-1));
    eta3_SW(i-1)=(s3_SASW(i)-s3_SASW(i-1))/(time_load(i)-time_load(i-1));
    eta3_NW(i-1)=(s3_SANW(i)-s3_SANW(i-1))/(time_load(i)-time_load(i-1));
end

%No large error in having the last no. equal to zero.
%Use the linear extrapolation for the last entry in the anchor-velocities
% extrapSE=interp1(time_load(1:length(time_load)-1),..
% zeta_inc_dot_SE,'spline','pp');
% zeta_inc_dot_SE(length(time_load))=ppval(extrapSE,max(time_load));

%Saving the total lowering velocity to be used for solving the ODE for the
%dynamic air cushion pressure
vel_sum=vel_f+tip_vel;          %Total velocity of the suction anchor
%Interpolate to get a new velocity vector
% vel_tot=vel_sum;
%Plotting lowering speed of suction anchors
% count=count+1;
% figure(count)
% plot(time_tot,vel_tot); title('Total lowering velocity');
vel_fitted=fit(time_load,vel_sum,'smoothingspline');
% plot(time_tot,vel_tot,time_tot,feval(vel_fitted,time_tot));
% save('velsaved.mat','vel_fitted');
%%%%%%%%%%%%%%%%%%%%%%%%%%%%%%%%%%%%%%%%%%%%%%%%%%%%%%%%%%%%%%%%%%%%%%%%%%%%
% Plotting the pitch and roll motion of the MRU
% count=1;
% count=count+1;
% figure(count)
% subplot(211);
% plot(time_load,roll); title('roll')
% subplot(212);
% plot(time_load,pitch); title('')
%%%%%%%%%%%%%%%%%%%%%%%%%%%%%%%%%%%%%%%%%%%%%%%%%%%%%%%%%%%%%%%%%%%%%%%%%%%%
%Plot total vertical motion of suction anchors
% count=count+1;
% figure(count)
% plot(time_load,s3_SASE,time_load,s3_SANE,...
% time_load,s3_SASW,time_load,s3_SANW);
% title('Vertical motion of Suction Anchors');
% legend('SE-SA','NE-SA','SW-SA','NW-SA');
% xlabel('time [s]'); ylabel('[m]')
%%%%%%%%%%%%%%%%%%%%%%%%%%%%%%%%%%%%%%%%%%%%%%%%%%%%%%%%%%%%%%%%%%%%%%%%%%%%
```

```
%Plot velocity of suction anchors
% count=count+1;
% figure(count)
% plot(time_load,eta3_SE,time_load,eta3_NE,...
% time_load,eta3_SW,time_load,eta3_NW);
% title('Vertical motion of Suction Anchors');
% legend('SE-SA','NE-SA','SW-SA','NW-SA');
% xlabel('time [s]'); ylabel('[m]')
%%%%%%%%%%%%%%%%%%%%%%%%%%%%%%%%%%%%%%%%%%%%%%%%%%%%%%%%%%%%%%%%%%%%%%%%%%%%
% Plit vertical motion due to different contributions
% count=count+1;
% figure(count)
% plot(time_load,s3_tip); title('Vertical motion of crane tip');
% xlabel('time [s]'); ylabel('[m]')
% subplot(411); plot(time_load,dsub);
% title('Vertical motion due to lowering vel');
% subplot(412); plot(time_load,s3_tip);
% title('Vertical motion of crane tip');
% subplot(413); plot(time_load,vel_tot); title('Vertical vel of sa');
% subplot(414); plot(time_load,s3_SEi); title('Vertical motion of sa');
%%%%%%%%%%%%%%%%%%%%%%%%%%%%%%%%%%%%%%%%%%%%%%%%%%%%%%%%%%%%%%%%%%%%%%%%%%%%
% count=count+1;
% % subplot(211); plot(time_tot,vel_f); title('Filtered lowering vel');
% subplot(212); plot(time_tot,tip_vel);
% title('Crane tip velocity raw data');
end
```

Published with MATLAB® R2013a

G.5 Calculation of JONSWAP-wave spectrum and realisations

waves.m This subroutine calculate wave realisations and velocities

for both Jonswap spectrum and Torsethaugen spectrum

```
%Water particle velocities are also created
function waves(time_js)

global count g zeta_inc_fit_E zeta_inc_dot_fit_E zeta_inc_fit_W...
    zeta_inc_dot_fit_W zeta_inc_main_E zeta_inc_main_W omega_js1 k_wave...
    v_water_E v_water_W
Hs=1.935; %Significant wave height from measurements
Hmax=3.55;  %Maximum wave height measured
Tp=5.89;    %Peak period from measurements
Tz=4.634;   %Zero crossing wave period
wp=2*pi/Tp; %Peak frequency
%%%%%%%%%%%%%%%%%%%%%%%%%%%%%%%%%%%%%%%%%%%%%%%%%%%%%%%%%%%%%%%%%%%%%%%%%%%
%Calculation of Jonswap spectrum
%%%%%%%%%%%%%%%%%%%%%%%%%%%%%%%%%%%%%%%%%%%%%%%%%%%%%%%%%%%%%%%%%%%%%%%%%%%
%Calculate Steplength
b_js=33/Tp;                          %Max frequency taken from Torsethaugen
a_js=0;                              %Min frequency
N=10000;                            %Number of steps in the spectrum-calc
deltaw=(b_js-a_js)/N;                %Steplength
gamma_js=exp(3.484*(1-0.1975*(0.036-0.0056*Tp/sqrt(Hs))*Tp^4/Hs^2));%3.3;
S_js=zeros(1,N);
% omega_js1=linspace(a_js,b_js,length(time_js));
% deltaw=omega_js1(2)-omega_js1(1);
omega_js1=zeros(1,N);
omega_js2=zeros(1,N);

for i=1:length(omega_js1)
 %Calculates the frequency with midpoint formula
    omega_js1(i)=a_js+(deltaw*(i-0.5));
 omega_js2(i)=wp/omega_js1(i);

 %Determines the shape function/std.deviation of the spectrum
    if (omega_js1(i) <= wp)
     sig = 0.07;
    else
     sig = 0.09;
    end

 %The JONSWAP Spectrum is divided into parts for easier manipulation,
    %then multiplied together.
   S1 = (5/(32*pi));
    S2 = Hs^2*Tp*(1-(0.287*log(gamma_js)));
  S3 = omega_js2(i)^5;
   S4 = exp(-1.25*omega_js2(i)^4);
   S5 = ((omega_js1(i)/wp)-1)^2;
   S6 = exp(-S5/(2*sig^2));
```

```
   S7 = gamma_js^S6;
 S_js(i)=S1*S2*S3*S4*S7;

end

zeta_js=sqrt(2*S_js*deltaw);                %Wave height from spectrum
k_wave=omega_js1.^2/g;                      %Wave number deep water
%%%%%%%%%%%%%%%%%%%%%%%%%%%%%%%%%%%%%%%%%%%%%%%%%%%%%%%%%%%%%%%%%%%%%%%%%%%%%%%
%Loading the spectral values for the two peaked Torsethaugen spectrum
%accounting both for wind and swell sea obtained from Wafo-script
S_load=load('S_th.mat');
S_th=S_load.Sth;
zeta_th=sqrt(2*S_th*deltaw);

%Specifying anchor positions relative to global reference system
x_E=5.53;                                   %Eastern anchors' x-location
x_W=-10.27;                                 %Western anchors' x-location
% % Use a random phase angle such that no dominating wave component present
%Saving a random number generator between 0 and 2pi which will be used
%later when calculating the surface elevation such that no dominating wave
%component is present
% epsilon=rand(1,length(omega_js1))*2*pi;    %random number vector [0,2pi]
% save('epsilon.mat','epsilon');
eps_load=load('epsilon10000.mat');
%Wave elevation and velocity calculated from the Jonswap-spectrum
zeta_inc_jsE=zeros(1,length(time_js));
zeta_inc_dot_jsE=zeros(1,length(time_js));
zeta_inc_jsW=zeros(1,length(time_js));
zeta_inc_dot_jsW=zeros(1,length(time_js));
%%Wave elevation and velocity calculated from the Torsethaugen-spectrum
zeta_inc_thE=zeros(1,length(time_js));          %East realisations
zeta_inc_dot_thE=zeros(1,length(time_js));      %East wave velocities
zeta_inc_thW=zeros(1,length(time_js));          %West realisations
zeta_inc_dot_thW=zeros(1,length(time_js));      %West wave velocities
%Water particle velocity
v_water_E=zeros(1,length(time_js));
v_water_W=zeros(1,length(time_js));
%regular wave components
% zeta_inc_rE=zeros(1,length(time_js));
% zeta_inc_dot_rE=zeros(1,length(time_js));
% zeta_inc_rW=zeros(1,length(time_js));
% zeta_inc_dot_rW=zeros(1,length(time_js));
% omega_reg=2*pi/Tp;
% k_reg=omega_reg^2/g;

for i=1:length(time_js)

    for j=1:length(omega_js1)
        %%%%%%%%%%%%%%%%%%%%%%%%%%%%%%%%%%%%%%%%%%%%%%%%%%%%%%%%%%%%%%%%%%%%%%%
        % JONSWAP Wave realisations
    zeta_inc_jsE(i)=zeta_inc_jsE(i)+zeta_js(j)'.*...
    sin(omega_js1(j)*time_js(i)+k_wave(j)*x_E+eps_load.eps(j));
%     zeta_inc_dot_jsE(i)=zeta_inc_dot_jsE(i)+zeta_js(j)'.*...
% omega_js1(j).*cos(omega_js1(j)*time_js(i)...
```

```
%     +k_wave(j)*x_E+eps_load.eps(j));
%     zeta_inc_jsW(i)=zeta_inc_jsW(i)+zeta_js(j)'.*...
% sin(omega_js1(j)*time_js(i)+k_wave(j)*x_W+eps_load.eps(j));
%     zeta_inc_dot_jsW(i)=zeta_inc_dot_jsW(i)+zeta_js(j)'.*...
% omega_js1(j).*cos(omega_js1(j)*time_js(i)...
%     +k_wave(j)*x_W+eps_load.eps(j));

    %%%%%%%%%%%%%%%%%%%%%%%%%%%%%%%%%%%%%%%%%%%%%%%%%%%%%%%%%%%%%%%%%%%%%%%
    %Torsethaugen Wave realisations
    zeta_inc_thE(i)=zeta_inc_thE(i)+zeta_th(j)'.*...
        sin(omega_js1(j)*time_js(i)+k_wave(j)*x_E+eps_load.eps(j));
    zeta_inc_dot_thE(i)=zeta_inc_dot_thE(i)+zeta_th(j)'.*omega_js1(j).*...
        cos(omega_js1(j)*time_js(i)...
    +k_wave(j)*x_E+eps_load.eps(j));
    zeta_inc_thW(i)=zeta_inc_thW(i)+zeta_th(j)'.*...
        sin(omega_js1(j)*time_js(i)+k_wave(j)*x_W+eps_load.eps(j));
    zeta_inc_dot_thW(i)=zeta_inc_dot_thW(i)+zeta_th(j)'.*omega_js1(j).*...
        cos(omega_js1(j)*time_js(i)...
    +k_wave(j)*x_W+eps_load.eps(j));
%%%%%%%%%%%%%%%%%%%%%%%%%%%%%%%%%%%%%%%%%%%%%%%%%%%%%%%%%%%%%%%%%%%%%%%
    %Water particle velocity
    v_water_E(i)=v_water_E(i)+omega_js1(j)*zeta_th(j)'*...
        cos(omega_js1(j)*time_js(i)+k_wave(j)*x_E+eps_load.eps(j));
    v_water_W(i)=v_water_W(i)+omega_js1(j)*zeta_th(j)'*...
        cos(omega_js1(j)*time_js(i)+k_wave(j)*x_W+eps_load.eps(j));

    end
    %What about regular waves?
%    zeta_inc_rE(i)=Hs/2*sin(omega_reg*time_js(i)+k_reg*x_E);
%    zeta_inc_dot_rE(i)=omega_reg*Hs/2*cos(omega_reg*time_js(i)+k_reg*x_E);
%     zeta_inc_rW(i)=Hs/2*sin(omega_reg*time_js(i)+k_reg*x_W);
%    zeta_inc_dot_rW(i)=omega_reg*Hs/2*cos(omega_reg*time_js(i)+k_reg*x_W);
%     v_water_E(i)=omega_reg*Hs/2*cos(omega_reg*time_js(i)...
%       +k_reg*x_E);%+epsilon(j));
%     v_water_W(i)=omega_reg*Hs/2*cos(omega_reg*time_js(i)+...
%       k_reg*x_W);%+epsilon(j));
end
%Directional waves:
x_E=round(91.42);                   %Eastern anchors' x-location
x_W=round(112.75);                  %Western anchors' x-location
y_S=round(18.8);
y_N=round(3);
%%%%%%%%%%%%%%%%%%%%%%%%%%%%%%%%%%%%%%%%%%%%%%%%%%%%%%%%%%%%%%%%%%%%%%%
%Wave realizations created with directional spectrum with WAFO:
zeta_spread=load('direct_new.mat');
zeta_inc_SE(:,1)=zeta_spread.spread(y_S,x_E,:);
zeta_inc_NE(:,1)=zeta_spread.spread(y_N,x_E,:);
% zeta_inc_SW(:,1)=zeta_spread.spread(y_S,x_W,:);
% zeta_inc_NW(:,1)=zeta_spread.spread(y_N,x_W,:);
%Forward differentiation to find wave velocity
% for i=1:length(time_load)-1
%     zeta_inc_dot_SE(i)=(zeta_inc_dE(i+1)-zeta_inc_dE(i))/...
% (time_js(i+1)-time_js(i));
%     zeta_inc_dot_NE(i)=(zeta_inc_NE(i+1)-zeta_inc_NE(i))/...
```

```
% (time_js(i+1)-time_js(i));
%     zeta_inc_dot_SW(i)=(zeta_inc_SW(i+1)-zeta_inc_SW(i))/...
% (time_js(i+1)-time_js(i));
%     zeta_inc_dot_NW(i)=(zeta_inc_NW(i+1)-zeta_inc_NW(i))/...
% (time_js(i+1)-time_js(i));
% end
% % %Extrapolating to find the last value of the time derivative of wave elev.
% extrapSE=interp1(time_js(1:length(time_js)-1),...
% zeta_inc_dot_SE,'spline','pp');
% zeta_inc_dot_SE(length(time_js))=ppval(extrapSE,max(time_js));
% extrapNE=interp1(time_js(1:length(time_js)-1),...
% zeta_inc_dot_NE,'spline','pp');
% zeta_inc_dot_NE(length(time_js))=ppval(extrapNE,max(time_js));
% extrapSW=interp1(time_js(1:length(time_js)-1),...
% zeta_inc_dot_SW,'spline','pp');
% zeta_inc_dot_SW(length(time_js))=ppval(extrapSW,max(time_js));
% extrapNW=interp1(time_js(1:length(time_js)-1),...
% zeta_inc_dot_NW,'spline','pp');
% zeta_inc_dot_NW(length(time_js))=ppval(extrapNW,max(time_js));
% zeta_inc_dot_fit_E=fit(time_load,zeta_inc_dot_SE','smoothingspline');

% zeta_inc_fit_E=fit(time_js,zeta_inc_rE','smoothingspline');
% zeta_inc_dot_fit_E=fit(time_js,zeta_inc_dot_rE','smoothingspline');
% zeta_inc_fit_W=fit(time_js,zeta_inc_rW','smoothingspline');
% zeta_inc_dot_fit_W=fit(time_js,zeta_inc_dot_rW','smoothingspline');
%Fitting a curve to the data resulting in piecewise expressions for the
%height and velocity of the wave elevation
%Jonswap %%%%%%%%%%%%%%%%%%%%%%%%% CHANGE THIS %%%%%%%%%%%%%%%%%%%%%%
% zeta_inc_fit_E=fit(time_js,zeta_inc_jsE','smoothingspline');
% zeta_inc_dot_fit_E=fit(time_js,zeta_inc_dot_jsE','smoothingspline');
% zeta_inc_fit_W=fit(time_js,zeta_inc_jsW','smoothingspline');
% zeta_inc_dot_fit_W=fit(time_js,zeta_inc_dot_jsW','smoothingspline');
%Torsethaugen %%%%%%%%%%%%%%%%%%%%%%%%% CHANGE THIS %%%%%%%%%%%%%%%%%%%%%%
zeta_inc_fit_E=fit(time_js,zeta_inc_thE','smoothingspline');
zeta_inc_dot_fit_E=fit(time_js,zeta_inc_dot_thE','smoothingspline');
zeta_inc_fit_W=fit(time_js,zeta_inc_thW','smoothingspline');
zeta_inc_dot_fit_W=fit(time_js,zeta_inc_dot_thW','smoothingspline');
% Directional Torsethaugen %%%%%%%%%%%%%%%%%% CHANGE THIS %%%%%%%%%%%%%%%%%
% zeta_inc_fit_SE=fit(time_js,zeta_inc_SE','smoothingspline');
% zeta_inc_dot_fit_SE=fit(time_js,zeta_inc_dot_SE','smoothingspline');
% zeta_inc_fit_SW=fit(time_js,zeta_inc_SW','smoothingspline');
% zeta_inc_dot_fit_SW=fit(time_js,zeta_inc_dot_SW','smoothingspline');
% zeta_inc_fit_NE=fit(time_js,zeta_inc_NE','smoothingspline');
% zeta_inc_dot_fit_NE=fit(time_js,zeta_inc_dot_NE','smoothingspline');
% zeta_inc_fit_NW=fit(time_js,zeta_inc_NW','smoothingspline');
% zeta_inc_dot_fit_NW=fit(time_js,zeta_inc_dot_NW','smoothingspline');
% Determine which type of wave elevation to be exported to the force
%calculations
zeta_inc_main_E=zeta_inc_thE;   %Output wave elevation for eastern anchors
zeta_inc_main_W=zeta_inc_thW;   %Output wave elevation for western anchors

%Plot comparison between wave realisations with unidirectional and
%directional Torsethaugen and unidirectional JONSWAP
% count=count+1;
```

```
% figure(count)
% subplot(311),
% plot(time_js,zeta_inc_thE);
% title('Realizations of Torsethaugen waves at East-anchors');
% xlabel('time [s]');
% ylabel('Surface elevation [m]');
% subplot(312), plot(time_js,zeta_inc_jsE);
% title('Realizations of JONSWAP-spectrum at East-anchors');
% xlabel('time [s]');
% ylabel('Surface elevation [m]');
% subplot(313), plot(time_js,zeta_inc_SE);
% title(['Realizations of Directional-Torsethaugen-spectrum'...
%     ' at Southeast-anchor']);
% xlabel('time [s]');
% ylabel('Surface elevation [m]');
%Plot realisations together
% count=count+1;
% figure(count)
% plot(time_js,zeta_inc_SE,time_js,zeta_inc_thE,time_js,zeta_inc_jsE);
% set(gca,'FontSize',30);
% title('Comparison of wave realizations versus time');
% legend('Short crested-Torsethaugen','Long crested Torsethaugen',...
%     'JONSWAP');
% xlabel('Time [s]');
% ylabel('S [m^{2}s]');
% count=count+1;
% figure(count)
% plot(time_js,zeta_inc_thE,time_js,zeta_inc_jsE);
% % set(gca,'FontSize',30);
% title('Comparison of long crested wave realizations versus time');
% legend('Torsethaugen',...
%     ' JONSWAP');
% xlabel('Time [s]');
% ylabel('S [m^{2}s]');
% count=count+1;
% figure(count)
% plot(omega_js1,S_js,'LineWidth',3); set(gca,'FontSize',15);
% title('Jonswap spectrum');
% xlabel('\omega [rad/s]');
% ylabel('S [m^{2}s]');
end
```

Published with MATLAB® R2013a

G.6 Calculation of dynamic air cushion pressure

odesolvernew.m Calculation of the dynamic air cushion pressure

```
%for four suction anchors
% This functions use input for the vertical motion of the suction anchors
% and wave elevations at each location for calculating the dynamic air
% cushion pressure inside each suction anchor.
function [y_SE,y_NE,y_SW,y_NW] = odesolvernew()

global time_tot g H Ac Al Patm gamma_a rho_a rho_w...
zeta_inc_fit_E zeta_inc_dot_fit_E zeta_inc_fit_W zeta_inc_dot_fit_W...
s3_fitSE s3_fitNE s3_fitSW s3_fitNW vel_fitted C

y0=0;                                       %Initial value for the dyn pressure
% myoptions=odeset('RelTol',0.0001);          %Defining tolerance level for the
                                            %solution of the dynamic pressure
% tic;    %Time-starter for the ode-function
%Calling the function which evaluates the right side of the equation for
%the dynamic air cushion pressure
[~,y_SE] = ode45(@solveSE,time_tot,y0);%,myoptions);
[~,y_NE] = ode45(@solveNE,time_tot,y0);%,myoptions);
[~,y_SW] = ode45(@solveSW,time_tot,y0);%,myoptions);
[~,y_NW] = ode45(@solveNW,time_tot,y0);%,myoptions);
% save('ySE.mat','y_SE');   %Save for checking the values of \mu afterwards
% save('yNE.mat','y_NE');   %Save for checking the values of \mu afterwards
% save('ySW.mat','y_SW');   %Save for checking the values of \mu afterwards
% save('yNW.mat','y_NW');   %Save for checking the values of \mu afterwards
% toc;

% count=count+1;
% figure(count)
% plot(t_SE,y_SE,t_NE,y_NE,t_SW,y_SW,t_NW,y_NW);
% title(['Calculating \mu with ode23tb in Matlab']);
% xlabel('Time [s]'); ylabel('Pressure [Pa]');
% legend('SE','NE','SW','NW');
% count=count+1;
% figure(count)
% plot(t,zeta_inc_eval); title('Wave elevation');
% count=count+1;
% figure(count)
% plot(t,dsub_eval); title('Vertical motion');
% count=count+1;
% figure(count)
% plot(t,vel_eval); title('Vertical motion');
% figure(2)
% plot(omega_js1,S_js,'LineWidth',3); set(gca,'FontSize',15);
% title('Jonswap spectrum');
% xlabel('\omega [rad/s]');
% ylabel('S [m^{2}s]')

function dydt = solveSE(time_t,u)
```

```
%Evaluating the fitted and saved values for the submergence level,
%total vertical velocity of the suction anchors and wave elevation/velocity
vel_eval=feval(vel_fitted,time_t);     %Total vertical velocity

dsub_eval=feval(s3_fitSE,time_t);        %Subm. level(heave motion)
%Evaluates the wave elevation
zeta_inc_eval=feval(zeta_inc_fit_E,time_t);  %Wave elevation
%Velocity of wave elevation
zeta_inc_dot_eval=feval(zeta_inc_dot_fit_E,time_t);  %Wave velocity

%Defining the right hand side of the derivative of the dynamic air cushion
%pressure which will be solved for each time instant during lowering

dydt=((zeta_inc_dot_eval-vel_eval-C*(Al/Ac)*sign(u)*sqrt(2*abs(u)/...
    rho_a))/(1/(gamma_a*Patm)*(1+((u)/Patm))^(-1)*(H+dsub_eval+((u)/...
    (rho_w*g))-zeta_inc_eval)+(1/(rho_w*g))));
end

function dydt = solveNE(time_t,u)

%Evaluating the saved values for the submergence level and total vertical
%velocity of the suction anchors
vel_eval=feval(vel_fitted,time_t);     %Total vertical velocity

dsub_eval=feval(s3_fitNE,time_t);        %Subm. level(heave motion)

zeta_inc_eval=feval(zeta_inc_fit_E,time_t);  %Wave elevation
%Velocity of wave elevation
zeta_inc_dot_eval=feval(zeta_inc_dot_fit_E,time_t);  %Wave velocity

%Defining the right hand side of the derivative of the dynamic air cushion
%pressure which will be solved for each time instant during lowering

dydt=((zeta_inc_dot_eval-vel_eval-C*(Al/Ac)*sign(u)*sqrt(2*abs(u)/...
    rho_a))/(1/(gamma_a*Patm)*(1+((u)/Patm))^(-1)*(H+dsub_eval+((u)/...
    (rho_w*g))-zeta_inc_eval)+(1/(rho_w*g))));
end

function dydt = solveSW(time_t,u)

%Evaluating the saved values for the submergence level and total vertical
%velocity of the suction anchors
vel_eval=feval(vel_fitted,time_t);     %Total vertical velocity

dsub_eval=feval(s3_fitSW,time_t);        %Subm. level(heave motion)

zeta_inc_eval=feval(zeta_inc_fit_W,time_t);  %Wave elevation
%Velocity of wave elevation
zeta_inc_dot_eval=feval(zeta_inc_dot_fit_W,time_t);  %Wave velocity

%Defining the right hand side of the derivative of the dynamic air cushion
%pressure which will be solved for each time instant during lowering
```

```
dydt=((zeta_inc_dot_eval-vel_eval-C*(Al/Ac)*sign(u)*sqrt(2*abs(u)/...
    rho_a))/(1/(gamma_a*Patm)*(1+((u)/Patm))^(-1)*(H+dsub_eval+((u)/...
    (rho_w*g))-zeta_inc_eval)+(1/(rho_w*g))));
end

function dydt = solveNW(time_t,u)

%Evaluating the saved values for the submergence level and total vertical
%velocity of the suction anchors
vel_eval=feval(vel_fitted,time_t);     %Total vertical velocity

dsub_eval=feval(s3_fitNW,time_t);        %Subm. level(heave motion)

zeta_inc_eval=feval(zeta_inc_fit_W,time_t);  %Wave elevation
%Velocity of wave elevation
zeta_inc_dot_eval=feval(zeta_inc_dot_fit_W,time_t);   %Wave velocity

%Defining the right hand side of the derivative of the dynamic air cushion
%pressure which will be solved for each time instant during lowering
% h=mupad('ump.mn');
dydt=((zeta_inc_dot_eval-vel_eval-C*(Al/Ac)*sign(u)*sqrt(2*abs(u)/rho_a...
   ))/(1/(gamma_a*Patm)*(1+((u)/Patm))^(-1)*(H+dsub_eval+((u)/(rho_w*g))...
    -zeta_inc_eval)+(1/(rho_w*g))));
end
end
```

Published with MATLAB® R2013a

G.7 Calculation of buoyancy and slamming forces

slam_func.m calculate buoyancy and slamming forces on suction anchors

including slamming with Wagner's approach for a wedge in addition to two approaches with different slamming coefficients

```
function [F_buoy_SE,F_buoy_NE,F_buoy_SW,F_buoy_NW]=...
    slam_func(mu_SE,mu_NE,mu_SW,mu_NW)

%Last updated at 09.06.2014, 10:08.
%Call global parameters defined in the Main script
global zeta_inc_main_E zeta_inc_main_W s3_SANE s3_SASE s3_SASW s3_SANW g...
     eta3_SE eta3_NE eta3_SW eta3_NW v_water_E v_water_W D ...
     time_tot H Ac rho_w count gamma_a Patm

%%%%%%%%%%%%%%%%%%%%%%%%%%%%%%%%%%%%%%%%%%%%%%%%%%%%%%%%%%%%%%%%%%%%%%%%%%%%
% For calculating the slamming load on the suction anchor top Wagner's
% approach for a wedge in addition to two different approaches with
%slamming coefficients will be used
%%%%%%%%%%%%%%%%%%%%%%%%%%%%%%%%%%%%%%%%%%%%%%%%%%%%%%%%%%%%%%%%%%%%%%%%%%%%
%%%%%%%%%%%%%%%%%%%%%%%%%%%%%%%%%%%%%%%%%%%%%%%%%%%%%%%%%%%%%%%%%%%%%%%%%%%%
%Ochi's criterion
v_ochi=0.093*sqrt(g*D);
%%%%%%%%%%%%%%%%%%%%%%%%%%%%%%%%%%%%%%%%%%%%%%%%%%%%%%%%%%%%%%%%%%%%%%%%%%%%
%Define Buoyancy force for the different suction anchors
F_buoy_SE=zeros(1,length(time_tot));
F_buoy_NE=zeros(1,length(time_tot));
F_buoy_SW=zeros(1,length(time_tot));
F_buoy_NW=zeros(1,length(time_tot));
%Define slamming forces for the different suction anchors
F_slam_SE=zeros(1,length(time_tot));
F_slam_NE=zeros(1,length(time_tot));
F_slam_SW=zeros(1,length(time_tot));
F_slam_NW=zeros(1,length(time_tot));
%Define slamming forces calculated with RP-H103 with for all anchors
% F_slam_SErp=zeros(1,length(time_tot));
% F_slam_NErp=zeros(1,length(time_tot));
% F_slam_SWrp=zeros(1,length(time_tot));
% F_slam_NWrp=zeros(1,length(time_tot));
%Define slamming pressures for the different suction anchors
P_slam_SE=zeros(1,length(time_tot));
P_slam_NE=zeros(1,length(time_tot));
P_slam_SW=zeros(1,length(time_tot));
P_slam_NW=zeros(1,length(time_tot));
%Define hydrodynamic pressures for the different suction anchors
P_hyd_SE=zeros(1,length(time_tot));
P_hyd_NE=zeros(1,length(time_tot));
P_hyd_SW=zeros(1,length(time_tot));
P_hyd_NW=zeros(1,length(time_tot));
%Define vertical motion and of inner surface of each suction anchor
zeta_iSE=zeros(1,length(time_tot));
```

```
zeta_iNE=zeros(1,length(time_tot));
zeta_iSW=zeros(1,length(time_tot));
zeta_iNW=zeros(1,length(time_tot));
%Define relative motion of inner surface for each suction anchor
wsurf_iNE=zeros(1,length(time_tot));
wsurf_iNW=zeros(1,length(time_tot));
wsurf_iSE=zeros(1,length(time_tot));
wsurf_iSW=zeros(1,length(time_tot));
%Relative velocity to be used in slamming calculations
v_slam_SE=zeros(1,length(time_tot));
v_slam_NE=zeros(1,length(time_tot));
v_slam_SW=zeros(1,length(time_tot));
v_slam_NW=zeros(1,length(time_tot));
%Counters for determining delay between the immersion of the different
%suction anchors
NW_delay=1.2;
SE_delay=6.6;
SW_delay=7.0;
%Starting counters that ensure that time delay between the different
%suction anchors are performed
c_NE=1;
c_SE=1;
c_SW=1;
c_NW=1;
%Counters for determining how many impacts that shall be included in the
%slamming calculations
NE_count=0;
NW_count=0;
SE_count=0;
SW_count=0;
%Counters used for saving the zero up-crossing values
k_NE=1;
k_NW=1;
k_SE=1;
k_SW=1;
for i=1:length(time_tot)

    zeta_iNE(i)=(zeta_inc_main_E(i)-mu_NE(i)/(rho_w*g));
    wsurf_iNE(i)=s3_SANE(i)-(zeta_iNE(i));  %Defined as negative
    %Define i >=2 to compare neighbouring values
    if i >=2
        %Save first zero down crossing-value
    if (wsurf_iNE(i-1)+H)*(wsurf_iNE(i)+H) <=0
        NE_count=NE_count+1;
        save_NEi(NE_count)=(i);
        %Terminate loop if the succeeding impact is included
        if NE_count == 2
            break
        end

    end
    %Save first zero up-crossing-value
    if NE_count >=1 && NE_count <= 2
        save_NE1(k_NE)=wsurf_iNE(i);
```

```
        k_NE=k_NE+1;
    end
    c_NE=c_NE+1;
    end
end
%Northwestern suction anchor
for i=1:length(time_tot)
    if time_tot(i) >= NW_delay
        zeta_iNW(i)=(zeta_inc_main_W(c_NW)-mu_NW(c_NW)/(rho_w*g));
        wsurf_iNW(i)=s3_SANW(c_NW)-(zeta_iNW(i));  %Defined as negative
    %Save first zero down crossing
    if i>=2
        if (wsurf_iNW(i-1)+H)*(wsurf_iNW(i)+H) <=0
            NW_count=NW_count+1;
            save_NWi(NW_count)=(i);
            %Terminate loop if the succeeding impact is included
            if NW_count == 2
                break
            end

        end
        %Save first zero up-crossing
        if NW_count >=1 && NW_count <= 2
            save_NW1(k_NW)=wsurf_iNW(i);
            k_NW=k_NW+1;
        end

    c_NW=c_NW+1;
    end
    end
end
%Southeastern suction anchor
for i=1:length(time_tot)
    if time_tot(i) >=SE_delay
    zeta_iSE(i)=(zeta_inc_main_E(c_SE)-mu_SE(c_SE)/(rho_w*g));
    wsurf_iSE(i)=s3_SASE(c_SE)-(zeta_iSE(i));  %Defined as negative
    if i>=2
        %Save first 0 down- and up-crossing
    if (wsurf_iSE(i-1)+H)*(wsurf_iSE(i)+H) <=0
        SE_count=SE_count+1;
        save_SEi(SE_count)=(i);

        if SE_count == 2
            break
        end
    end
        if SE_count >=1 && SE_count <= 2
            save_SE1(k_SE)=wsurf_iSE(i);
            k_SE=k_SE+1;
        end
    c_SE=c_SE+1;
    end
    end
```

```
end
%Southwestern suction anchor
for i=1:length(time_tot)
    if time_tot(i) >= SW_delay
        zeta_iSW(i)=(zeta_inc_main_W(c_SW)-mu_SW(c_SW)/(rho_w*g));
        wsurf_iSW(i)=s3_SASW(c_SW)-(zeta_iSW(i));  %Defined as negative
    if i>=2
    if (wsurf_iSW(i-1)+H)*(wsurf_iSW(i)+H) <=0
        %Save first zero down-crossing in first column
            SW_count=SW_count+1;
            save_SWi(SW_count)=(i);

        if SW_count == 2
            break
        end
    end
    %Save first zero up-crossing in first column
        if SW_count >=1 && SW_count <= 2
            save_SW1(k_SW)=wsurf_iSW(i);
            k_SW=k_SW+1;
        end
    c_SW=c_SW+1;
    end
    end

end
%Counter for immersion of succeding suction anchors
i_NW=1;
i_SW=1;
i_SE=1;
%Index to be used for slamming-time calculations
slam_NE=1;
slam_NW=1;
slam_SE=1;
slam_SW=1;
%Deadrise angle in radians
beta=[5 10 17.5]*pi/180;
Cs=2*pi;                          %Slamming coefficient from Wagner
Vol_c=zeros(1,length(time_tot));
T_wn2=zeros(1,length(time_tot));
if length(save_NEi)==2
for i=1:length(time_tot)
    F_buoy_NE(i)=mu_NE(i)*Ac;
    %Relative velocity before impact positive downwards
    v_slam_NE(i)=(eta3_NE(i)-v_water_E(i));
    %Local hydrostatic pressure
    P_hyd_NE(i)=rho_w*g*zeta_iNE(i);
    zeta_iNE(i)=(zeta_inc_main_E(i)-mu_NE(i)/(rho_w*g));
    wsurf_iNE(i)=s3_SANE(i)-(zeta_iNE(i));

    if  (i) >= (save_NEi(1)) && (i) <= (save_NEi(2))
        t_slam_NE(slam_NE)=time_tot(slam_NE);
%%%%%%%%%%%%%%%%%%%%%%%%%%%%%%%%%%%%%%%%%%%%%%%%%%%%%%%%%%%%%%%%%%%%%%%%%%%%%%%%
            %Slamming force NE-anchor with slamming coefficient:
```

```
%     Cs_var_NE(i)=2*pi/(1+(1.5*v_slam_NE(i)*t_slam_NE(slam_NE)/(D/2)));
%     F_slam_NE(i)=0.5*Cs_var_NE(i)*rho_w*Ac*v_slam_NE(i)^2;
%     F_slam_NErp(i)=0.5*Cs*rho_w*Ac*v_slam_NE(i)^2;
%%%%%%%%%%%%%%%%%%%%%%%%%%%%%%%%%%%%%%%%%%%%%%%%%%%%%%%%%%%%%%%%%%%%%%%%%%%%
        %Slamming force with wedge-approximation
        F_slam_NE(i)=rho_w*(pi*2)*v_slam_NE(i)^4*...
            t_slam_NE(slam_NE)^2/(tan(beta(3)))^3;
        %Set dynamic air cushion pressure to zero
%         mu_NE(i)=0;
        F_buoy_NE(i)=F_slam_NE(i);
        P_slam_NE(i)=F_slam_NE(i)/Ac;
        %Set the slamming load to zero if the pressure after impact drops a
        %certain percentage
        if abs(v_slam_NE(i)) <= 0.8*v_ochi && P_slam_NE(i)...
                <= 1.2*abs(P_hyd_NE(i))
        %Another slamming criterion could be to say that if the pressure
        %reduce a certain percentage from the value at impact the slamming
        %can be considered finished
            F_slam_NE(i)=0;
            F_buoy_NE(i)=mu_NE(i)*Ac;
            break

        end
        slam_NE=slam_NE+1;
    end
end
end
    %If there is no oscillation in and out out water during slamming
    %occurence, use contemporary satisfaction criteria only.
if length(save_NEi)~=2
    for i=1:length(time_tot)
         F_buoy_NE(i)=mu_NE(i)*Ac;
    %Relative velocity before impact positive downwards
    v_slam_NE(i)=(eta3_NE(i)-v_water_E(i));
    %Local hydrostatic pressure
    P_hyd_NE(i)=rho_w*g*zeta_iNE(i);
    zeta_iNE(i)=(zeta_inc_main_E(i)-mu_NE(i)/(rho_w*g));
    wsurf_iNE(i)=s3_SANE(i)-(zeta_iNE(i));
    if wsurf_iNE(i) <= -H
        t_slam_NE(slam_NE)=time_tot(slam_NE);
 %%%%%%%%%%%%%%%%%%%%%%%%%%%%%%%%%%%%%%%%%%%%%%%%%%%%%%%%%%%%%%%%%%%%%%%%%%%%
            %Slamming force NE-anchor with slamming coefficient:
%     Cs_var_NE(i)=2*pi/(1+(1.5*v_slam_NE(i)*t_slam_NE(slam_NE)/(D/2)));
%     F_slam_NE(i)=0.5*Cs_var_NE(i)*rho_w*Ac*v_slam_NE(i)^2;
%     F_slam_NErp(i)=0.5*Cs*rho_w*Ac*v_slam_NE(i)^2;
%%%%%%%%%%%%%%%%%%%%%%%%%%%%%%%%%%%%%%%%%%%%%%%%%%%%%%%%%%%%%%%%%%%%%%%%%%%%
        F_slam_NE(i)=rho_w*(pi*2)*v_slam_NE(i)^4*...
            t_slam_NE(slam_NE)^2/(tan(beta(3)))^3;

%         mu_NE(i)=0;
        F_buoy_NE(i)=F_slam_NE(i);
        P_slam_NE(i)=F_slam_NE(i)/Ac;
        %Set the slamming load to zero if the pressure after impact drops a
        %certain percentage
```

```
            if abs(v_slam_NE(i)) <= 0.8*v_ochi && P_slam_NE(i)...
                    <= 1.2*abs(P_hyd_NE(i))
            %Another slamming criterion could be to say that if the pressure
            %reduce a certain percentage from the value at impact the slamming
            %can be considered finished
                F_slam_NE(i)=0;
                F_buoy_NE(i)=mu_NE(i)*Ac;
                break
            end
            slam_NE=slam_NE+1;

        end

        end
    end
        %Immersion of NW Suction anchor delayed by 1.2 [s]
    if length(save_NWi)==2
    for i = 1:length(time_tot)
        if time_tot(i) >= NW_delay
            zeta_iNW(i)=(zeta_inc_main_W(i_NW)-mu_NW(i_NW)/(rho_w*g));
            wsurf_iNW(i)=s3_SANW(i_NW)-(zeta_iNW(i));  %Defined as negative
            F_buoy_NW(i)=mu_NW(i_NW)*Ac;
            v_slam_NW(i)=(eta3_NW(i_NW)-v_water_W(i_NW));
            P_hyd_NW(i)=rho_w*g*zeta_iNW(i);

            %Slamming criteria NW-anchor if the top is oscillating in and
            %out of water
             if (i) >= (save_NWi(1)) && (i) <= (save_NWi(2))
                %Define starting time to be used in slamming calculations
                t_slam_NW(slam_NW)=time_tot(slam_NW);
    %%%%%%%%%%%%%%%%%%%%%%%%%%%%%%%%%%%%%%%%%%%%%%%%%%%%%%%%%%%%%%%%%%%%%%%%%%%
            %Slamming force with DNV-RP-H103 NW-anchor:
    %         Cs_var_NW(i)=2*pi/(1+(1.5*v_slam_NW(i)*t_slam_NW(slam_NW)/(D/2)));
    %          F_slam_NW(i)=0.5*Cs_var_NW(i)*rho_w*Ac*v_slam_NW(i)^2;
    %          F_slam_NWrp(i)=0.5*Cs*rho_w*Ac*v_slam_NW(i)^2;
    %%%%%%%%%%%%%%%%%%%%%%%%%%%%%%%%%%%%%%%%%%%%%%%%%%%%%%%%%%%%%%%%%%%%%%%%%%%
            %Slamming force with wedge-approximation
             F_slam_NW(i)=rho_w*(pi*2)*v_slam_NW(i)^4*...
                t_slam_NW(slam_NW)^2/(tan(beta(3)))^3;
    %%%%%%%%%%%%%%%%%%%%%%%%%%%%%%%%%%%%%%%%%%%%%%%%%%%%%%%%%%%%%%%%%%%%%%%%%%%

    %             mu_NW(i)=0;
                F_buoy_NW(i)=F_slam_NW(i);
                P_slam_NW(i)=F_slam_NW(i)/Ac;
                 %Stop slamming if contemporary satisfaction criteria is met
                if abs(v_slam_NW(i)) <= 0.8*v_ochi && P_slam_NW(i)...
                        <= 1.2*abs(P_hyd_NW(i))

                    F_slam_NW(i)=0;
                    F_buoy_NW(i)=mu_NW(i)*Ac;
                    break
                end
                slam_NW=slam_NW+1;
             end
```

```
            i_NW=i_NW+1;
        end
    end
    end
     %Contemporary satisfaction criteria only
    if length(save_NWi)~=2
        for i=1:length(time_tot)
            if time_tot(i) >=NW_delay
            zeta_iNW(i)=(zeta_inc_main_W(i_NW)-mu_NW(i_NW)/(rho_w*g));
            wsurf_iNW(i)=s3_SANW(i_NW)-(zeta_iNW(i));  %Defined as negative
            F_buoy_NW(i)=mu_NW(i_NW)*Ac;
            v_slam_NW(i)=(eta3_NW(i_NW)-v_water_W(i_NW));
            P_hyd_NW(i)=rho_w*g*zeta_iNW(i);
            if wsurf_iNW(i) <= -H
                %Define starting time to be used in slamming calculations
                t_slam_NW(slam_NW)=time_tot(slam_NW);
    %%%%%%%%%%%%%%%%%%%%%%%%%%%%%%%%%%%%%%%%%%%%%%%%%%%%%%%%%%%%%%%%%%%%%%%%%%%%
            %Slamming force with DNV-RP-H103 NW-anchor:
    %         Cs_var_NW(i)=2*pi/(1+(1.5*v_slam_NW(i)*t_slam_NW(slam_NW)/(D/2)));
    %          F_slam_NW(i)=0.5*Cs_var_NW(i)*rho_w*Ac*v_slam_NW(i)^2;
    %          F_slam_NWrp(i)=0.5*Cs*rho_w*Ac*v_slam_NW(i)^2;
    %%%%%%%%%%%%%%%%%%%%%%%%%%%%%%%%%%%%%%%%%%%%%%%%%%%%%%%%%%%%%%%%%%%%%%%%%%%%
    %Slamming force with wedge-approximation
            F_slam_NW(i)=rho_w*(pi*2)*v_slam_NW(i)^4*...
                t_slam_NW(slam_NW)^2/(tan(beta(3)))^3;
    %%%%%%%%%%%%%%%%%%%%%%%%%%%%%%%%%%%%%%%%%%%%%%%%%%%%%%%%%%%%%%%%%%%%%%%%%%%%
    %             mu_NW(i)=0;
                F_buoy_NW(i)=F_slam_NW(i);
                P_slam_NW(i)=F_slam_NW(i)/Ac;
                 %Stop slamming if contemporary satisfaction criteria is met
                if abs(v_slam_NW(i)) <= 0.8*v_ochi && P_slam_NW(i)...
                        <= 1.2*abs(P_hyd_NW(i))

                    F_slam_NW(i)=0;
                    F_buoy_NW(i)=mu_NW(i)*Ac;
                    break
                end
                slam_NW=slam_NW+1;
            end
            i_NW=i_NW+1;
            end
        end

    end

    if length(save_SEi)==2
    for i=1:length(time_tot)
            %Immersion of SE Suction anchor delayed by 8.5 [s]
        if time_tot(i) >= SE_delay

            F_buoy_SE(i)=mu_SE(i_SE)*Ac;
            v_slam_SE(i)=(eta3_SE(i_SE)-v_water_E(i_SE));
            %Hydrostat pressure
            P_hyd_SE(i)=rho_w*g*zeta_iSE(i_SE);
```

```
    zeta_iSE(i)=(zeta_inc_main_E(i_SE)-mu_SE(i_SE)/(rho_w*g));
     wsurf_iSE(i)=s3_SASE(i_SE)-(zeta_iSE(i));  %Defined as negative
         %Slamming criteria SE-anchor
          if (i) >= (save_SEi(1)) && (i) <= (save_SEi(2))
             t_slam_SE(slam_SE)=time_tot(slam_SE);
%%%%%%%%%%%%%%%%%%%%%%%%%%%%%%%%%%%%%%%%%%%%%%%%%%%%%%%%%%%%%%%%%%%%%%%%%%%%%%%
         %Slamming force with DNV-RP-H103 SE-anchor:
%         Cs_var_SE(i)=2*pi/(1+(1.5*v_slam_SE(i)*t_slam_SE(slam_SE)/(D/2)));
%                 F_slam_SE(i)=0.5*Cs_var_SE(i)*rho_w*Ac*v_slam_SE(i)^2;
%                 F_slam_SErp(i)=0.5*Cs*rho_w*Ac*v_slam_SE(i)^2;
%%%%%%%%%%%%%%%%%%%%%%%%%%%%%%%%%%%%%%%%%%%%%%%%%%%%%%%%%%%%%%%%%%%%%%%%%%%%%%%
%Slamming force with wedge-approximation
         F_slam_SE(i)=rho_w*(pi*2)*v_slam_SE(i)^4*...
             t_slam_SE(slam_SE)^2/(tan(beta(3)))^3;
%              mu_SE(i)=0;
             F_buoy_SE(i)=F_slam_SE(i);
             P_slam_SE(i)=F_slam_SE(i)/Ac;
         %Set the slamming load to zero if the pressure after impact drops a
         %certain percentage
             if abs(v_slam_SE(i)) <= 0.8*v_ochi && P_slam_SE(i)...
                     <= 1.2*abs(P_hyd_SE(i))
                 F_slam_SE(i)=0;
                 F_buoy_SE(i)=mu_SE(i)*Ac;
                 break
             end
             slam_SE=slam_SE+1;
          end
          i_SE=i_SE+1;
     end
end
end

         %Contemporary satisfaction criteria for slamming duration only
if length(save_SEi) ~=2
     for i=1:length(time_tot)
         if time_tot(i) >= SE_delay
         F_buoy_SE(i)=mu_SE(i_SE)*Ac;
         v_slam_SE(i)=(eta3_SE(i_SE)-v_water_E(i_SE));
         %Hydrostat pressure
         P_hyd_SE(i)=rho_w*g*zeta_iSE(i_SE);
         zeta_iSE(i)=(zeta_inc_main_E(i_SE)-mu_SE(i_SE)/(rho_w*g));
     wsurf_iSE(i)=s3_SASE(i_SE)-(zeta_iSE(i));  %Defined as negative
         if wsurf_iSE(i) <= -H
             t_slam_SE(slam_SE)=time_tot(slam_SE);
%%%%%%%%%%%%%%%%%%%%%%%%%%%%%%%%%%%%%%%%%%%%%%%%%%%%%%%%%%%%%%%%%%%%%%%%%%%%%%%
         %Slamming force with DNV-RP-H103 SE-anchor:
%         Cs_var_SE(i)=2*pi/(1+(1.5*v_slam_SE(i)*t_slam_SE(slam_SE)/(D/2)));
%                 F_slam_SE(i)=0.5*Cs_var_SE(i)*rho_w*Ac*v_slam_SE(i)^2;
%                 F_slam_SErp(i)=0.5*Cs*rho_w*Ac*v_slam_SE(i)^2;
%%%%%%%%%%%%%%%%%%%%%%%%%%%%%%%%%%%%%%%%%%%%%%%%%%%%%%%%%%%%%%%%%%%%%%%%%%%%%%%
         %Slamming force with wedge-approximation
         F_slam_SE(i)=rho_w*(pi*2)*v_slam_SE(i)^4*...
             t_slam_SE(slam_SE)^2/(tan(beta(3)))^3;
%              mu_SE(i)=0;
```

```
                F_buoy_SE(i)=F_slam_SE(i);
                P_slam_SE(i)=F_slam_SE(i)/Ac;
            %Set the slamming load to zero if the pressure after impact drops a
            %certain percentage
                if abs(v_slam_SE(i)) <= 0.8*v_ochi && P_slam_SE(i)...
                        <= 1.2*abs(P_hyd_SE(i))
                    F_slam_SE(i)=0;
                    F_buoy_SE(i)=mu_SE(i)*Ac;
                    break
                end
                slam_SE=slam_SE+1;
            end

            i_SE=i_SE+1;
            end
        end

    end
    %Slamming criteria SW-anchor if the top is oscillating in and out of water
    if length(save_SWi)==2
        %Immersion of SW Suction anchor delayed by 1.7 [s]
    for i=1:length(time_tot)
        if time_tot(i) >= SW_delay

            F_buoy_SW(i)=mu_SW(i_SW)*Ac;
            v_slam_SW(i)=eta3_SW(i_SW)-v_water_W(i_SW);
            %Hydrostat pressure SW-anchor:
            P_hyd_SW(i)=rho_w*g*zeta_iSW(i);
            zeta_iSW(i)=(zeta_inc_main_W(i_SW)-mu_SW(i_SW)/(rho_w*g));
            wsurf_iSW(i)=s3_SASW(i_SW)-(zeta_iSW(i));  %Defined as negative

             if (i) >= (save_SWi(1)) && (i) <= (save_SWi(2))
                t_slam_SW(slam_SW)=time_tot(slam_SW);
    %%%%%%%%%%%%%%%%%%%%%%%%%%%%%%%%%%%%%%%%%%%%%%%%%%%%%%%%%%%%%%%%%%%%%%%%%%%%
            %Slamming force with DNV-RP-H103 SE-anchor:
    %        Cs_var_SW(i)=2*pi/(1+(1.5*v_slam_SW(i)*t_slam_SW(slam_SW)/(D/2)));
    %                F_slam_SW(i)=0.5*Cs_var_SW(i)*rho_w*Ac*v_slam_SW(i)^2;
    %                F_slam_SWrp(i)=0.5*Cs*rho_w*Ac*v_slam_SW(i)^2;
    %%%%%%%%%%%%%%%%%%%%%%%%%%%%%%%%%%%%%%%%%%%%%%%%%%%%%%%%%%%%%%%%%%%%%%%%%%%%
            %Slamming force with wedge-approximation
             F_slam_SW(i)=rho_w*(pi*2)*v_slam_SW(i)^4*...
                 t_slam_SW(slam_SW)^2/(tan(beta(3)))^3;
    %             mu_SW(i)=0;
                F_buoy_SW(i)=F_slam_SW(i);
                P_slam_SW(i)=F_slam_SW(i)/Ac;
                %Time-duration critera
                if abs(v_slam_SW(i)) <= 0.8*v_ochi && P_slam_SW(i)...
                        <= 1.2*abs(P_hyd_SW(i))
                    F_slam_SW(i)=0;
                    F_buoy_SW(i)=mu_SW(i)*Ac;
                break
                end
                slam_SW=slam_SW+1;
             end
```

```
            i_SW=i_SW+1;
        end
    end
    end

            %Contemporary satisfaction criteria only
    if length(save_SWi) ~=2
        for i=1:length(time_tot)
            if time_tot(i) >= SW_delay
            F_buoy_SW(i)=mu_SW(i_SW)*Ac;
            v_slam_SW(i)=eta3_SW(i_SW)-v_water_W(i_SW);
            %Hydrostat pressure SW-anchor:
            P_hyd_SW(i)=rho_w*g*zeta_iSW(i);
            zeta_iSW(i)=(zeta_inc_main_W(i_SW)-mu_SW(i_SW)/(rho_w*g));
            wsurf_iSW(i)=s3_SASW(i_SW)-(zeta_iSW(i));  %Defined as negative

            if wsurf_iSW(i) <= -H
                t_slam_SW(slam_SW)=time_tot(slam_SW);
    %%%%%%%%%%%%%%%%%%%%%%%%%%%%%%%%%%%%%%%%%%%%%%%%%%%%%%%%%%%%%%%%%%%%%%%%%%%%
            %Slamming force with DNV-RP-H103 SE-anchor:
    %        Cs_var_SW(i)=2*pi/(1+(1.5*v_slam_SW(i)*t_slam_SW(slam_SW)/(D/2)));
    %                F_slam_SW(i)=0.5*Cs_var_SW(i)*rho_w*Ac*v_slam_SW(i)^2;
    %                F_slam_SWrp(i)=0.5*Cs*rho_w*Ac*v_slam_SW(i)^2;
    %%%%%%%%%%%%%%%%%%%%%%%%%%%%%%%%%%%%%%%%%%%%%%%%%%%%%%%%%%%%%%%%%%%%%%%%%%%%
            %Slamming force with wedge-approximation
             F_slam_SW(i)=rho_w*(pi*2)*v_slam_SW(i)^4*...
                 t_slam_SW(slam_SW)^2/(tan(beta(3)))^3;

    %             mu_SW(i)=0;
                F_buoy_SW(i)=F_slam_SW(i);
                P_slam_SW(i)=F_slam_SW(i)/Ac;
                %Time-duration critera
                if abs(v_slam_SW(i)) <= 0.8*v_ochi && P_slam_SW(i)...
                        <= 1.2*abs(P_hyd_SW(i))
                    F_slam_SW(i)=0;
                    F_buoy_SW(i)=mu_SW(i)*Ac;
                break
                end
                slam_SW=slam_SW+1;
            end
            i_SW=i_SW+1;
            end
        end

    end
    %Loop for calculation natural period in NE-SA
    % omega_wn1=zeros(1,length(time_tot));
    % omega_wn2=zeros(1,length(time_tot));
    % T_wn1=zeros(1,length(time_tot));
    % T_wn2=zeros(1,length(time_tot));
    % for i=1:length(time_tot)
    %     zeta_iNE(i)=(zeta_inc_main_W(i)-mu_NE(i)/(rho_w*g));
    %     wsurf_iNE(i)=s3_SANE(i)-(zeta_iNE(i));
    %     %Volume of air cushion
```

```
%     Vol_c(i)=Ac*(H-zeta_iNE(i)+s3_SANW(i));
%     if Vol_c(i) >= -0.1
%     omega_wn1(i)=sqrt((g+(Ac*gamma_a*(Patm+abs(mu_NW(i))))/...
%         (rho_w*Vol_c(i)))/((4*D)/(3*pi)+abs(wsurf_iNW(i))));
%     T_wn1(i)=2*pi/omega_wn1(i);  %Natural period of water and air coupled
%     omega_wn2(i)=sqrt(g/((4*D)/(3*pi)+abs(wsurf_iNW(i))));
%     %Defining the natural frequency of the oscillating water with the
%     %atmospheric pressure as the upper boundary (uncoupled)
%     T_wn2(i)=2*pi/omega_wn2(i);   %Natural period of water uncoupled
%     end
% end
% save('omega_coupled.mat','omega_wn1')

% Plot time instants used in slamming calculations
% count=count+1;
% plot(time_tot,v_slam_SE,time_tot,v_slam_NE,...
%     time_tot,v_slam_SW,time_tot,v_slam_NW);
% title('Duration of slamming [s]')
% legend('Southeast-anchor','Northeast',...
%     ' Southwest','Northwest');
%Plot dynamic air cushion pressure
% count=count+1;
% figure(count)
% plot(time_tot,mu_SE,time_tot,mu_NE,time_tot,mu_SW,time_tot,mu_NW);
% title('Dynamic air cushion pressure');
% legend('\mu Southeast','\mu Northeast',...
%     '\mu Southwest ','\mu Northwest');
% xlabel('Time [s]');
% ylabel('[Pa]');
%Plot natural period according to Miles'
% count=count+1;
% figure(count)
% plot(time_tot,T_wn1,time_tot,T_wn2);
% title('Natural period coupled vs uncopled in NE-SA vs time');
% % legend('Coupled','Uncoupled');
% xlabel('Time [s]');
% ylabel('[s]');
% %Plot air cushion volume
% count=count+1;
% figure(count)
% plot(time_tot,Vol_c);
% title('Air-cushion volume in NE-SA vs time');
% % legend('Coupled','Uncoupled');
% xlabel('Time [s]');
% ylabel('[s]');
%Plot force in lifting wire
% count=count+1;
% figure(count)
% plot(time_tot,c_interp,time_tot,F_wire);...
%     title('Force in lifting wire vs time');
% % axes([])
% legend('Measured wire force','Calculated wire force');
% xlabel('Time [s]');
% ylabel('Force [N]');
```

```
% % Plot inner surface
% count=count+1;
% figure(count)
% plot(time_tot,wsurf_iSE,time_tot,wsurf_iNE,...
%     time_tot,wsurf_iSW,time_tot,wsurf_iNW);
% title('Inner surface in suction anchors vs time');
% legend('Southeast anchor','Northeast anchor','Southwest anchor',...
%     'Northwest anchor');
% xlabel('Time [s]');
% ylabel(' [m]');
% count=count+1;
% figure(count)
% plot(time_tot,save_NEi);
% title('Inner surface in NE suction anchors vs time');
% % legend('Southeast anchor','Northeast anchor','Southwest anchor',...
% %     'Northwest anchor');
% xlabel('Time [s]');
% ylabel(' [m]');
%Plot relative velocity used in slam-calc
% count=count+1;
% figure(count)
% % % subplot(211),
% plot(time_tot,v_slam_SE,time_tot,v_slam_NE,...
%     time_tot,v_slam_SW,time_tot,v_slam_NW);
% title('Slamming velocity');
% legend('Rel vel Northeast','Rel vel Northwest',...
%     'Rel vel Southwest','Rel vel Southeast');
% xlabel('Time [s]');
% ylabel('[m/s]');
% Plot velocity of fluid particles
% count=count+1;
% figure(count)
% plot(time_tot,v_water_E,time_tot,v_water_W);
% title('Fluid velocity');
% xlabel('Time [s]');
% ylabel('[m/s]');
% legend('Wave velocity east','Wave velocity west');
%Plot slamming force
count=count+1;
figure(count)
plot(time_tot,F_slam_SE,time_tot,F_slam_NE,time_tot,...
    F_slam_SW,time_tot,F_slam_NW);
title(['Slamming force on suction anchors with Wagners model']);
legend('Southeast slamming','Northeast slamming',...
    'Southwest slamming','Northwest slamming');
axis([0 max(time_tot) 0 2.6*10^6]);
xlabel('Time [s]');
ylabel('Force [Pa]');
% subplot(212);
% plot(time_tot,F_slam_SErp,time_tot,F_slam_NErp,time_tot,...
%     F_slam_SWrp,time_tot,F_slam_NWrp);
% title('Slamming force on suction anchors with constant Cs');
% legend('Southeast slamming','Northeast slamming',...
%     'Southwest slamming','Northwest slamming');
```

```
% axis([0 max(time_tot) 0 2.6*10^6]);
% xlabel('Time [s]');
% ylabel('Force [Pa]');
% % subplot(313);
% plot(time_tot,F_slam_SErp1,time_tot,F_slam_NErp1,time_tot,...
%     F_slam_SWrp1,time_tot,F_slam_NWrp1);
% title('Slamming force on suction anchors with \beta=5 [deg]');
% legend('Southeast slamming','Northeast slamming',...
%     'Southwest slamming','Northwest slamming');
% axis([0 max(time_tot) 0 2.6*10^6]);
% xlabel('Time [s]');
% ylabel('Force [Pa]');
%Plot slamming pressure
% count=count+1;
% figure(count)
% plot(time_tot,P_slam_SE,time_tot,P_slam_NE,time_tot,...
%     P_slam_SW,time_tot,P_slam_NW);
% title('Slamming pressure on suction anchors vs time');
% legend('Southeast slamming','Northeast slamming',...
%     'Southwest slamming','Northwest slamming');
% % axis([0 max(time_tot) 0 2.3*10^6]);
% xlabel('Time [s]');
% ylabel('Force [Pa]');
end
```

Published with MATLAB® R2013a